For Reference

NOT TO BE TAKEN FROM THIS ROOM

Ex libris
universitatis
albertaensis

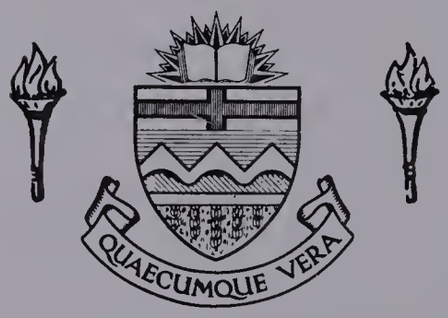

THE UNIVERSITY OF ALBERTA

SPIN POLARIZED ELECTRON TUNNELING IN MANGANESE ALLOYS

by

© PATRICK CHARLES SULLIVAN

A THESIS

SUBMITTED TO THE FACULTY OF GRADUATE STUDIES AND RESEARCH

IN PARTIAL FULFILMENT OF THE REQUIREMENTS FOR THE DEGREE

OF DOCTOR OF PHILOSOPHY in PHYSICS

DEPARTMENT OF PHYSICS

EDMONTON, ALBERTA

FALL, 1983

ABSTRACT

In the past few years the magnetic field splitting of the quasiparticle energy states in superconducting aluminum films has been used to study spin-dependent states in magnetic materials. In this thesis, an experimental investigation of electrons tunneling between ferromagnetic alloys and superconducting aluminum thin films has been carried out. Detailed measurements on $Al-Al_2O_3-Mn_xSn_{1-x}$ and $Al-Al_2O_3-Mn_xSb_{1-x}$ junctions have been performed. In both cases the polarization studies produced unexpected results.

In the case of the Mn_xSb_{1-x} system it was thought that the electron spin polarization would be approximately proportional to the magnetic moment per alloy atom. The experimental results indicated that the polarization was qualitatively similar to the magnetization per Mn atom of bulk material.

The polarization behaviour of the Mn_xSn_{1-x} system was studied to see if results similar to that of Mn-Sb alloys would be obtained. Our studies indicated that binary Mn-Sn alloys, formed by simultaneous evaporation of the two metals from separate sources, were not ferromagnetic.

ACKNOWLEDGMENTS

I wish to thank my supervisor, Dr. J. S. Rogers for his guidance and encouragement throughout the course of this project.

Thanks are due to Derk Gerritsen for his able assistance and help with many difficulties encountered in the laboratory. Special acknowledgments to D. Latta and S. Rogers for supplying liquid helium and to G. Braybrook for his electron microscopy work.

The continuing interest in this project by family and friends, especially my roommates, has been greatly appreciated.

I gratefully acknowledge the financial support of the Physics Department.

Finally, I wish to extend special thanks to Mrs. Ruth Nelson for typing this thesis.

TABLE OF CONTENTS

CHAPTER		PAGE
1.	INTRODUCTION	1
	1.1 Preamble	1
	1.2 Brief Review of Electron Polarization Measurement Techniques	1
	(a) Electron Capture Spectroscopy	2
	(b) Photoemission Spectroscopy	2
	(c) Field Emission Spectroscopy	4
	(d) Spin Polarization Measurements by Tunneling	4
	1.3 Aim and Scope of this Work	5
2.	THEORETICAL CONSIDERATIONS	7
	2.1 Introduction	7
	2.2 Theory of Elastic Tunneling	8
	2.3 Normal Metal - Superconductor Tunneling	12
	2.4 Superconductor-Normal Metal Tunneling in a High Magnetic Field	16
	2.5 Superconductor-Ferromagnetic Metal Tunneling	19
	2.6 Stearns Theory of Spin Polarized Electron Tunneling	23
	2.7 Spin-orbit and Spin-flip Scattering	29
3.	EXPERIMENTAL TECHNIQUES	34
	3.1 Junction Preparation	34
	3.2 Film Thickness Determination	40
	3.3 Low Temperature Production - Adiabatic Demagnetization	44
	3.4 Conductance Measurement Techniques	51

CHAPTER		PAGE
4.	DATA ANALYSIS	56
	4.1 Analysis of the Conductance Curves - No Spin-orbit Scattering	56
	4.2 Analysis with Spin-orbit Scatter	63
5.	EXPERIMENTAL RESULTS AND DISCUSSION	72
	5.1 Early Work	72
	5.2 Mn_xSb_{1-x} System	83
	5.3 Mn_xSn_{1-x} System	96
6.	SUMMARY AND CONCLUSIONS	107
	6.1 Conclusions	107
	6.2 Suggestions for Further Work	108
BIBLIOGRAPHY		110
APPENDIX A	Tunneling Conductance Bridge	117
APPENDIX B	Spin Polarization Papers	125

LIST OF TABLES

Table	Description	Page
1.1	Polarization Values of Fe, Co, and Ni	3
3.1	Evaporation Materials	35
5.1	Polarization Values for the Mn_xSn_{1-x} System	105

LIST OF FIGURES

Figure		Page
2.1	Energy level diagram for M-I-M junction	9
2.2	Superconductor-normal-metal tunneling	14
2.3	Superconductor-normal-metal tunneling in a high magnetic field	17
2.4	Superconductor-ferromagnetic metal tunneling	21
2.5	Energy level diagram for a 3d ferromagnet	25
2.6	Effect of spin-orbit scattering	30
3.1	Tunnel junction layout	37
3.2	Quartz crystal monitor	42
3.3	Adiabatic demagnetization of a paramagnetic salt	45
3.4	Adiabatic demagnetization cryostat	48
3.5	Simplified conductance bridge	52
4.1	Analysis of the conductance curves - no spin-orbit scattering	57
4.2	Typical conductance characteristic	61
4.3	Typical conductance characteristic decomposed into spin-up and spin-down parts	66
4.4	Illustration of an incorrect basis function	68
4.5	Correct basis function	70

Figure		Page
5.1	Scanning electron micrographs a) Ni deposited at room temperature b) Ni oxidized at 350°C for one hour	74
5.2	Scanning electron micrographs a) Ni-NiO-Aℓ tunnel junction NiO formed by thermal oxidation b) Ni-NiO-Aℓ tunnel junction NiO formed by a glow discharge	76
5.3	Scanning electron micrographs of a thermally cycled Ni film	79
5.4	Typical conductance trace of a Ni-NiO-Aℓ tunnel junction	81
5.5	Phase diagram of the Mn_xSb_{1-x} system	84
5.6	a) Crystal structure of MnSb b) Crystal structure of ε phase	86
5.7	Crystal structure of Mn_2Sb	89
5.8	Spin polarization results compared to bulk magnetization data of Guillaud [33] for Mn_xSb_{1-x}	91
5.9	Phase diagram for the Mn_xSn_{1-x} system	97
5.10	a) Crystal structure of $MnSn_2$ b) Crystal structure of Mn_3Sn	100
5.11	Crystal structure of Mn_2Sn	102
A.1	Typical load line problem	119
A.2	Simplified schematic of the conductance bridge.	122

CHAPTER 1

Introduction

1.1 Preamble

Experimental and theoretical physicists have long been fascinated by the phenomenon of ferromagnetism in metals. In the past decade there has been increasing scientific interest in fundamental studies of the surfaces of magnetic metals and several techniques for magnetic surface analysis have been devised. In spite of all of this work the exact electronic behaviour which causes ferromagnetism is still uncertain.

In a more applied nature ferromagnetic materials such as Fe, Co, and Ni are widely used as commercial catalysts [67] and the investigation of the magnetic structure of surfaces of these materials is therefore needed for a theoretical understanding of such processes. This thesis reports on work done using one of these surface analysis techniques, spin polarized electron tunneling, to study some ferromagnetic materials.

1.2 Brief Survey of Electron Polarization Measurement Techniques

Spin polarized tunneling is one of many experimental methods that has been developed in the last ten years to try to understand the surface magnetic order of ferromagnetic metals by studying the electron spin polarization of

the materials. Several comprehensive reviews of the various experimental methods appear in the literature [14,32,67,70]. Feuchtwang et al. [23,24] have also compiled a detailed theoretical analysis of electron spin polarization studies. A brief description of the major experimental methods will be given below. Table 1.1 summarizes experimental results that were obtained for 3d transition metal ferromagnets using the different techniques.

1.2a Electron capture spectroscopy

Electron capture spectroscopy is a method to investigate the surfaces of magnetic single crystals under ultra-high vacuum conditions. The basic process of this method of spin spectroscopy is the capture of one or two spin polarized electrons during small angle reflection of fast deuterons at single crystalline surfaces of magnetic crystals [67]. This technique was first proposed by Zavoiskii in 1957 [92] and the first successful experiment was reported by Kaminsky in 1969 [43]. This method measures polarization of electrons at the Fermi energy [72].

1.2b Photoemission spectroscopy

In photoemission studies the absorption of a single photon by electrons in a ferromagnetic solid leads to the emission of spin polarized electrons [66]. The

TABLE 1.1 Electron Polarization Values

	Tunneling		Field Emission	Photo Emission	Electron Capture
	[80]	[68]	[17]	[4,13]	[72]
Fe	+44	+44	+78	+42	max +38 (100)
Co	+34	+40	-35	+28	max +33 ($1\bar{1}00$)
Ni	+11	+17-+25	-4 in <111>	+15	-96 (110) +17 (120)

polarization is determined using a Mott detector. The probing depth is usually about 30Å [72]. Long et al. [45] tried the first unsuccessful experiments in 1965. Busch et al. [12] performed the first successful experiments in 1969.

1.2c Field emission spectroscopy

By applying a high electric field at a tip of a ferromagnetic solid the potential barrier at the surface changes drastically, thereby leading to the emission of polarized electrons into vacuum. The main contribution to the emission current originates from electrons within 100 meV of the Fermi level [67]. The first successful field emission experiment was done in 1967 by Hofmann et al. [39].

1.2d Spin polarization measurements by tunneling.

This is the technique that was used during the course of this work and will be elaborated on in the following sections of this thesis. Table 1.1 contains spin polarization data from work done here and work done by the originators of this technique - Meservey et al. [49].

As can be seen from Table 1.1 an agreement with regard to polarization magnitude or even direction (sign) has not been obtained with the different methods. Even for the two sets of tunneling results the Ni polarization values do not agree in magnitude. Difficult preparation of samples in

some techniques or the fact that different methods may not be measuring identical properties may be part of the answer. A better theoretical understanding of the actual processes involved in each technique will be needed before these discrepancies can be explained. The original motivation of this work was to attempt a study to try to find an explanation for some of these discrepancies, using the spin polarized tunneling technique. The rest of this thesis will deal with work done using this method on ferromagnetic metals.

1.3 Scope of This Work

Meservey et al. [48] first observed the quasi-particle splitting of the density of states of a superconducting Aℓ film in 1970. In 1971 [78] they devised an impressive tunneling experiment, utilizing the spin splitting, in an effort to help in the explanation of ferromagnetism. Since that time they have published many articles on studies they have done on thin film ferromagnetic metals and alloys [48-61,63,64,78-82] using the spin polarized tunneling technique.

This thesis consists of a report on work done utilizing this tunneling technique. The early work was done on the formation of tunneling barriers to try to study the effects of crystallographic direction, on the polarization values of ferromagnetic materials. This was an attempt to

verify a theory of Stearns [74] that had been proposed to explain spin polarized tunneling results. Later work was done on binary ferromagnetic alloys. The binary alloys chosen for this work were first studied by Heusler [38] in 1903 and had attracted his interest because ferromagnetism was found in alloys made up of constituent metals, neither of which by itself was a ferromagnetic material.

The ferromagnetic systems that were studied were Mn-Sb and Mn-Sn. Experiments were done on these alloys using Al-Al_2O_3-Alloy tunnel junctions. In previous work Paraskevopoulos et al. [63,64] had found that for various Ni alloy films the polarization of the sample was approximately proportional to μ, the bulk saturation magnetic moment. This work was started to see if this property would also be true of binary alloy films where neither metal was by itself a ferromagnet.

The spin polarized tunneling technique was also used to determine a value for the spin-orbit scattering parameter of the superconducting Al films used in this work.

CHAPTER 2

Theoretical Considerations

2.1 Introduction

Tunneling is a quantum mechanical situation that has no classical analogue. From a classical point of view it is impossible for a particle to enter a region of negative kinetic energy (the particle's potential energy would be greater than its total energy). Schrödinger's wave equation predicted that there existed a finite probability that a transition of this type could take place if the potential barrier was sufficiently thin. Thus, according to quantum mechanics, a particle may tunnel through a potential barrier.

The present investigation concerns itself with the tunneling of electrons from one metal through an oxide barrier into a second metal. If the barrier is thin enough (tens of Angstroms) a measurable current will be seen when a bias voltage is applied to the junction.

Frenkel [27] in 1930 was the first to consider the possibility that electrons may tunnel between two metals separated by a vacuum. Sommerfeld and Bethe [73] in 1933 were the first to publish detailed theoretical calculations on tunneling theory. It was not until 1960 that Fisher and Giaever [25] were able to perform the first tunneling experiment using the metal-oxide-metal sandwich

(Al-Al_2O_3-Al).

2.2 Theory of Elastic Tunneling

As a consequence of Giaever's work Bardeen [5] developed a tunneling theory based on the transfer Hamiltonian model. An electron energy diagram for a metal-insulator-metal system is shown in Fig. (2.1).

At T=0 metal 1, with barrier height ϕ_1, and metal 2 with height ϕ_2, have all the states below the Fermi energies, (E_{F1}, E_{F2}), filled, while those above are empty. For tunneling to occur, from left to right, the filled states of metal 1 must be aligned with the available empty states in metal 2. This is accomplished by applying a voltage V so that the left hand metal is negatively biased. Now current flow may occur across the junction i.e. tunneling takes place.

In Harrison's work [36], he shows how to obtain a theoretical expression for the tunneling current. Fermi's Golden Rule gives the transition probability, P_{12}, per unit time, of an electron from state ψ_1 in metal 1 moving to a state ψ_2 in metal 2 as

$$P_{12} = (2\pi/\hbar) \, |M_{12}|^2 \, N_2 \, f_1 \, (1-f_2) \qquad (2.1)$$

where M_{12} is the transition matrix between states ψ_1 and ψ_2, N_2 is the density of states in metal 2, and f_1 and f_2

Fig. 2.1

The electron energy level diagram for a metal-insulator-metal junction is shown with and without an applied bias voltage V. Here, s is the barrier thickness, E_{F1} and E_{F2} are the Fermi levels of the two metals, and ϕ_1 and ϕ_2 are the barrier heights. When a bias voltage is applied, tunneling occurs in the direction indicated by the arrow.

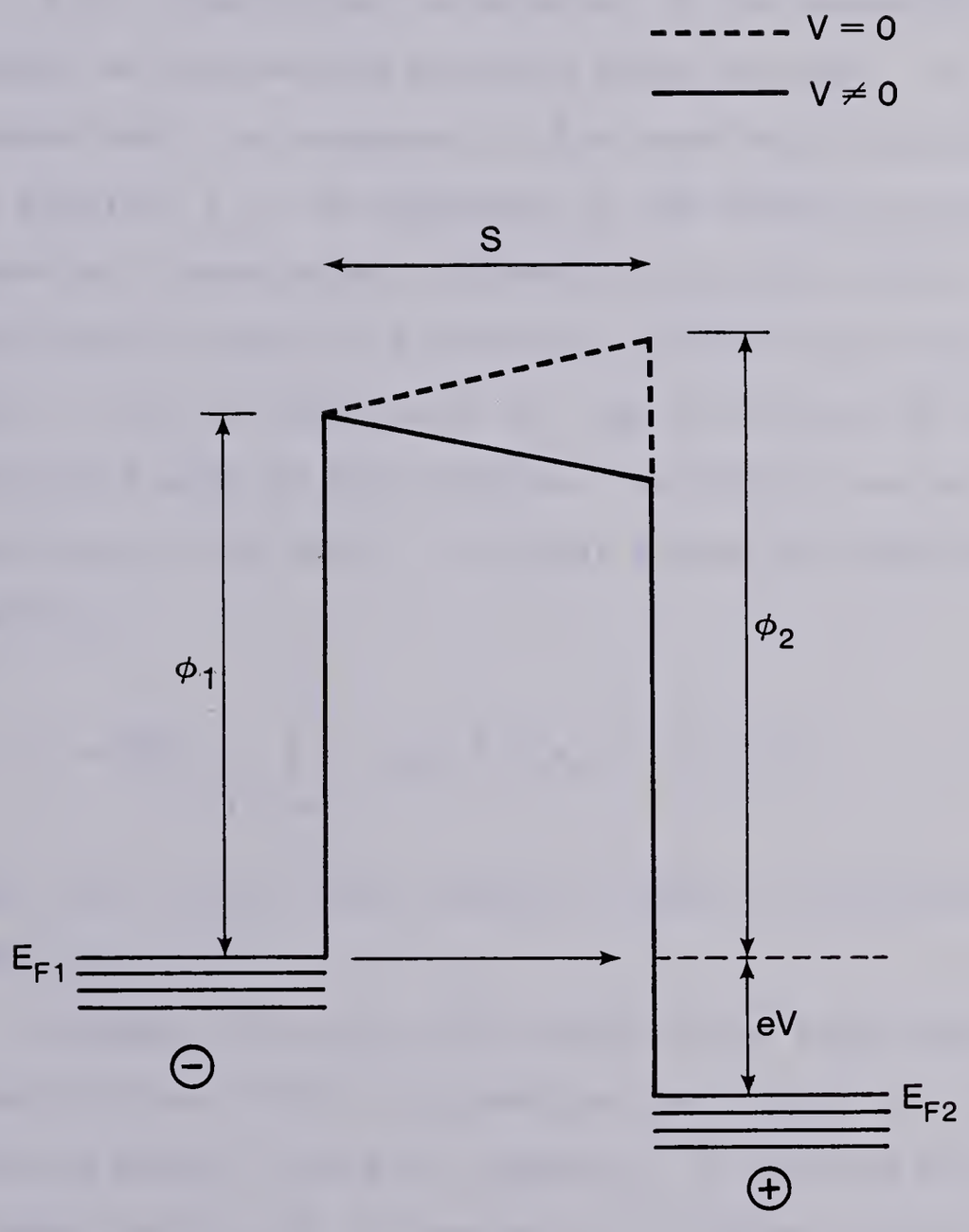
V = 0
V ≠ 0
S
ϕ_1
ϕ_2
E_{F1}
eV
E_{F2}
⊖
⊕
Metal 1
Insulator
Metal 2

are the Fermi-Dirac probabilities of occupation of states ψ_1 and ψ_2.

For a theoretical calculation of the tunneling current an independent particle model is used. It is assumed that the component of the wave vector parallel to the barrier, k_{11}, is conserved in the tunneling process (specular transmission), otherwise M_{12} will vanish. Therefore to obtain the tunneling current from metal 1 to metal 2, P_{12} is summed over k_{11} and multiplied by 2e for charge and spin of the electron. To obtain the net current, the current from metal 2 to metal 1 must be subtracted yielding

$$I = \frac{4\pi e}{\hbar} \sum_{k_{11}} \int_{-\infty}^{\infty} |M_{12}|^2 N_1 N_2 (f_1 - f_2) \, dE \qquad (2.2)$$

where the integral over energy is taken at fixed wave number k_{11}.

Bardeen [5] using a WKB method and a many particle point of view, found it plausible that $|M_{12}|^2$ is a constant over the energy values of interest. If the sum over k_{11} is taken and $|M_{12}|^2$ (a constant), is pulled outside the integral, the theory of Giaever and Megerle [29] gives the expression for the current as

$$I = \frac{4\pi e}{\hbar} |M_{12}|^2 \int_{-\infty}^{\infty} N_1 N_2 (f_1 - f_2) \, dE \qquad (2.3)$$

here $f_1 = f(E)$ and $f_2 = f(E+ev)$ where $f(E) = 1/(1+e^{E/kT})$ and E is measured from the Fermi energy.

If Eq. (2.3) is evaluated for two normal metals at T=0 and for small applied voltages

$$I_{NN} = \xi N_1(0)N_2(0)\ eV \ ; \quad \xi = \text{constant} \tag{2.4}$$

i.e. current is proportional to the voltage.

2.3 Normal Metal-Superconductor Tunneling

To calculate the tunneling current when one of the metals is in the superconducting state, the density of states from the Bardeen-Cooper-Schrieffer (BCS) [6,7] theory is used. For a BCS superconductor, with energy gap 2Δ, the superconducting density of states is $N_s(0)\rho_s$, where $N_s(E)$ is the density of states of the superconductor when in the normal state and

$$\begin{aligned} \rho_s(E) &= |E|/(E^2-\Delta^2)^{\frac{1}{2}} && |E| \geq \Delta \\ &= 0 && |E| < \Delta \end{aligned} \tag{2.5}$$

Therefore by substituting into Eq. (2.3) the current between one metal in the normal state and the other in the superconducting state can be written as

$$I_{SN} = C_N \int_{-\infty}^{\infty} \rho(E)\ [f(E) - f(E+eV)]\ dE \qquad (2.6)$$

where the constant

$$C_N = 2\pi e/\hbar\ |M_{SN}|^2\ N_N(0)\ N_S(0). \qquad (2.7)$$

The experimental quantity that is measured in a spin polarized tunneling experiment is the normalized conductance of the junction. The conductance is given by the first derivative of the current with respect to voltage, i.e. dI/dV. The normalized conductance is the conductance with one metal in the superconducting state divided by the conductance with both metals in the normal state.

$$\sigma(V) = \frac{dI_{SN}}{dV} \Big/ \frac{dI_{NN}}{dV} = \int_{-\infty}^{\infty} \rho_s(E)\ \frac{\beta\, e^{\beta(E+eV)}}{\left[1+e^{\beta(E+eV)}\right]^2}\ dE \qquad (2.8)$$

where $\beta = 1/k_B T$.

At T=0 the second factor in the integrand becomes a delta function and $\sigma(V)_{T=0} = \rho_s(eV)$. The conductance at T=0 is proportional to the superconducting density of states. For small finite temperatures, below the superconducting transition temperature T_c, the second factor in the integrand is a bell shaped function symmetrical about E=-eV. The conductance qualitatively reflects the density of states somewhat broadened by temperature. Fig. (2.2) illustrates this situation. The BSC density of

Fig. 2.2

Superconductor-normal-metal tunneling

a) BCS density of states of a superconductor as a function of voltage

b) Temperature-dependent Kernel in the integral expression for the conductance

c) Theoretical normalized conductance σ

Voltage is measured from the Fermi energy of the superconductor.

Electron energy decreases as the voltage increases.

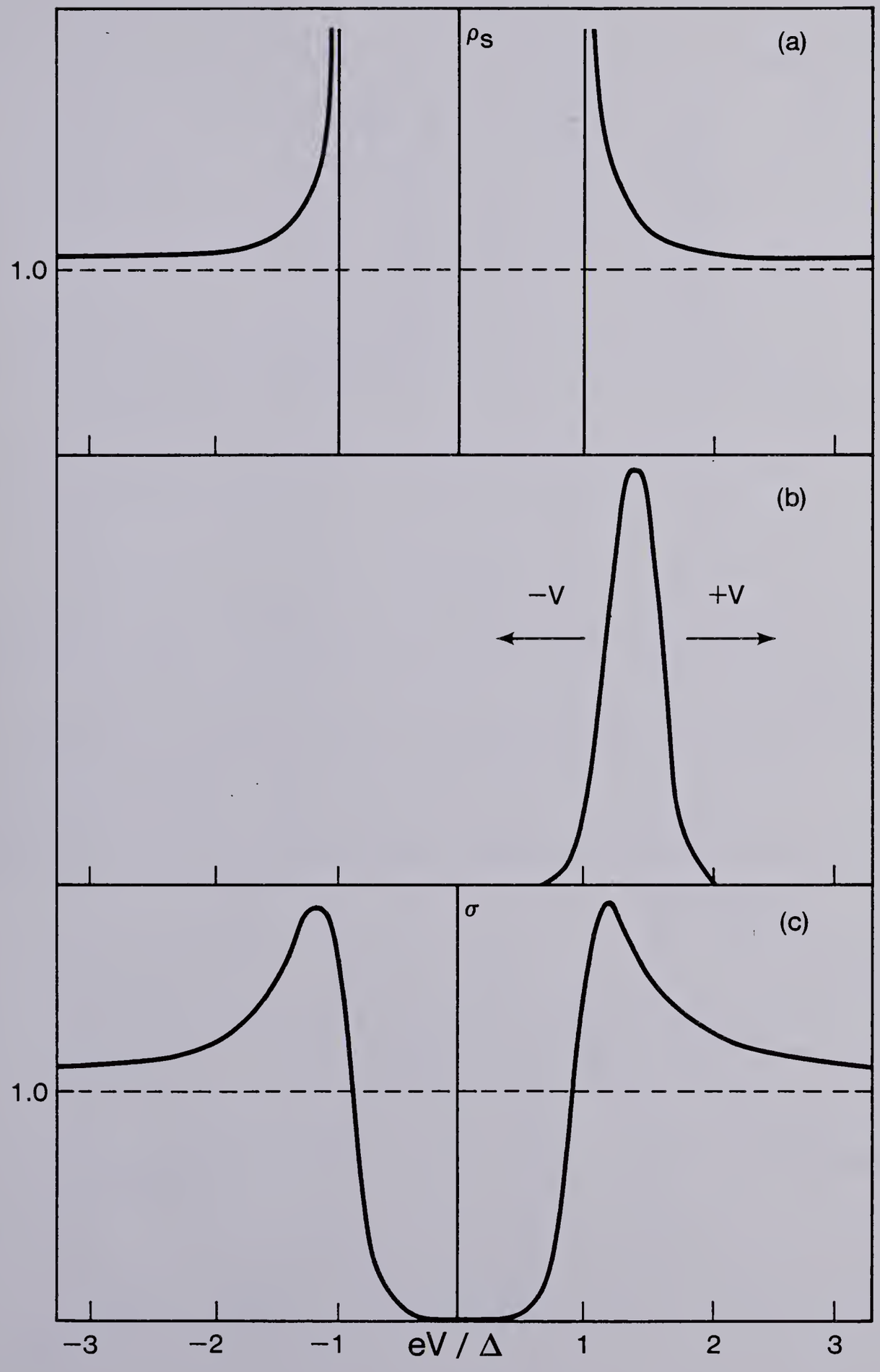
ρ_s
(a)
1.0
(b)
−V
+V
σ
(c)
1.0
−3
−2
−1
eV / Δ
1
2
3

Fig. 2.3

Superconductor-normal-metal tunneling in a high magnetic field:

(a) Magnetic field splitting of the density of states into spin-up (solid) and spin-down (dashed) densities.

(b) Spin-up and spin-down conductances add to give total conductance.

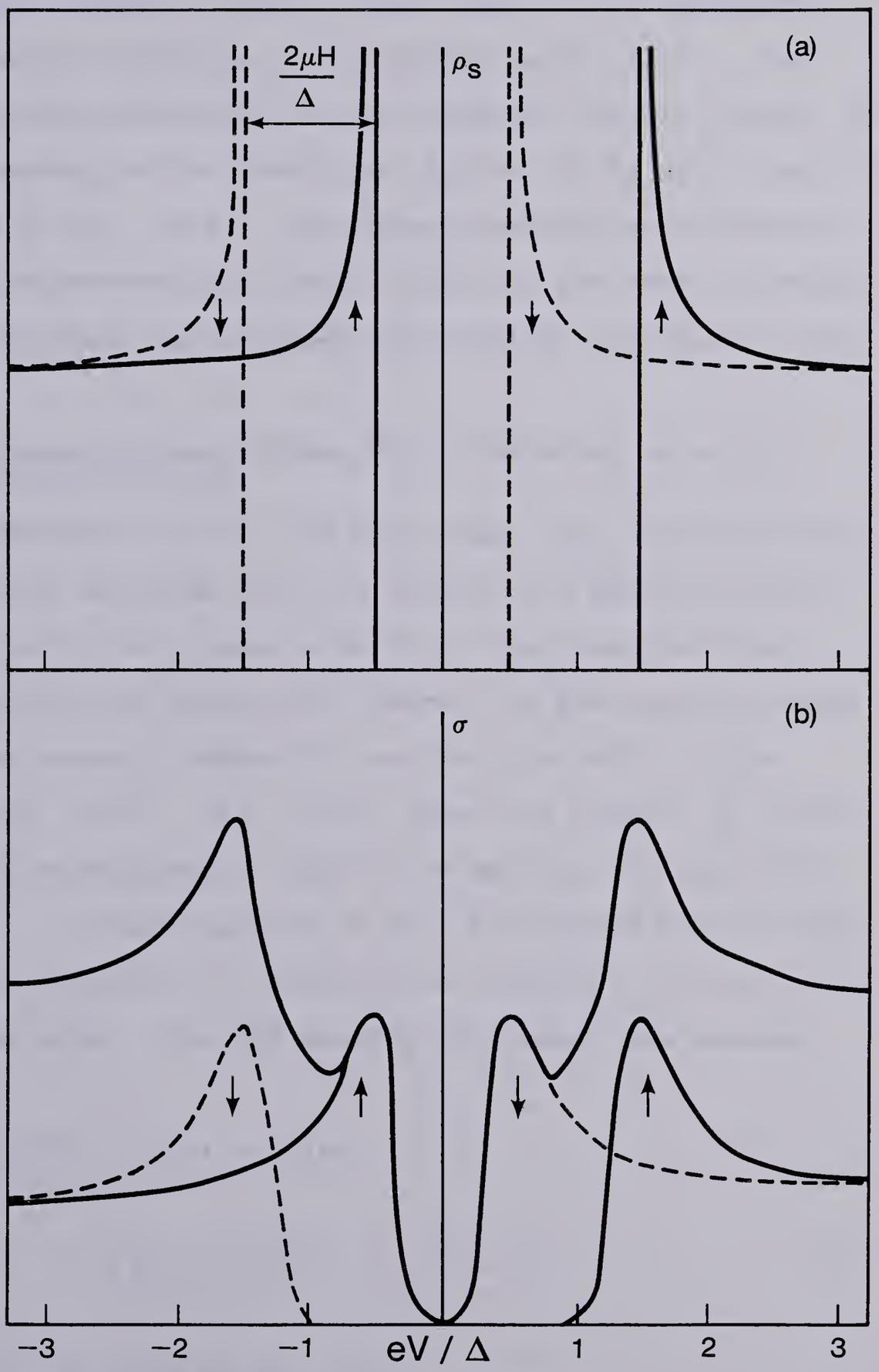
(a)
$\frac{2\mu H}{\Delta}$
ρ_s
(b)
σ
−3
−2
−1
eV / Δ
1
2
3

states is shown in Fig. (2.2a), Fig. (2.2b) represents the second factor in the integrand in Eq. (2.8). The resulting conductance is the integral, overall energy, of the product of the functions of Figs. (2.2a and b) and is shown in Fig. (2.2c). The above description of normal-metal-superconducting metal tunneling has been thoroughly demonstrated, for a review see Douglass and Falicov [20].

2.4 Superconductor-Normal Metal Tunneling in a High Magnetic Field.

Meservey et al. [48] have shown that the application of a high magnetic field to a thin film superconductor, such as $A\ell$, will cause a shift in the quasi-particle energies by an amount $\pm\mu H$. Here μ is the absolute value of the magnetic moment of the electron and H is the magnetic field. Fig. (2.3a) shows the density of states of the superconductor split into spin-up and spin-down parts. In this analysis it will be assumed that the spin of the electrons is conserved in tunneling from one metal to the other. The BCS density of states then becomes

$$\rho_s(E) = \rho\uparrow(E) + \rho\downarrow(E)$$

$$= \frac{1}{2}\left[\rho_s(E+\mu H) + \rho_s(E-\mu H)\right] \qquad (2.9)$$

when ρ_s is given by Eq. (2.5).

When the resulting conductance is calculated it is expected that the two spin states will be independent of each other and that their separate conductances will simply add. Fig. (2.3b) shows the result of applying Eqs. (2.8 and 2.9). The observed experimental results agree closely with the above theory.

2.5 Superconductor-Ferromagnetic Metal Tunneling

In ferromagnetic metals and alloys it is believed that there exists an excess population of conduction electrons of one spin direction over the other at the Fermi surface (see for example Kittel [44]). A tunneling measurement between a superconductor and a ferromagnetic metal is an attempt to measure this excess.

To do a spin polarized tunneling measurement on a tunneling sample the superconducting film is aligned so that the film plane is parallel to the field direction. The superconductor must be extremely thin (<40A) so that the critical field of the film is well above the saturation field of the ferromagnet. The large magnetic field is then applied in the plane of the tunnel barrier so that the magnetization of all the domains of the ferromagnetic metal are in the magnetic field direction. It is assumed that because the normal metal is a ferromagnet, that there will be a difference in tunneling current for each spin direction, but each spin is a constant over the energy

region of importance (within about 10^{-3} eV of the Fermi energy). Using the tunneling theory of sec. (2.3) the normalized conductance would be the sum of the conductances for the two completely independent spin directions. Eq. (2.8) would become

$$\sigma(V) = \int_{-\infty}^{\infty} a\frac{\rho_s(E+\mu H)\beta e^{(E+eV)}}{[1+e^{\beta(E+eV)}]^2}\,dE + \int_{-\infty}^{\infty}(1-a)\frac{\rho_s(E-\mu H)\beta e^{(E+eV)}}{[1+e^{\beta(E+eV)}]^2} \tag{2.10}$$

Here a accounts for the difference in tunneling current between spin-up and spin-down electrons. It is defined as the fraction of the tunneling electrons whose magnetic moment is in the direction of the magnetic field (majority electrons in the ferromagnet).

$$a \equiv \eta\uparrow / (\eta\uparrow + \eta\downarrow) \tag{2.11}$$

The electron polarization is defined as

$$P \equiv \frac{\eta\uparrow - \eta\downarrow}{\eta\uparrow + \eta\downarrow}. \tag{2.12}$$

Fig. (2.4a) shows the split density of states of the superconducting film. Fig. (2.4b) shows the second factors in the integrands of Eq. (2.10). The spin-up and spin-down parts are weighted by the factors a and (1-a). In

Fig. 2.4

Superconductor-ferromagnetic metal tunneling:

(a) BCS density of states of a superconductor as a function of voltage in a magnetic field

(b) Temperature dependent kernels for each spin direction

(c) Theoretical normalized conductance for each spin direction and the total conductance.

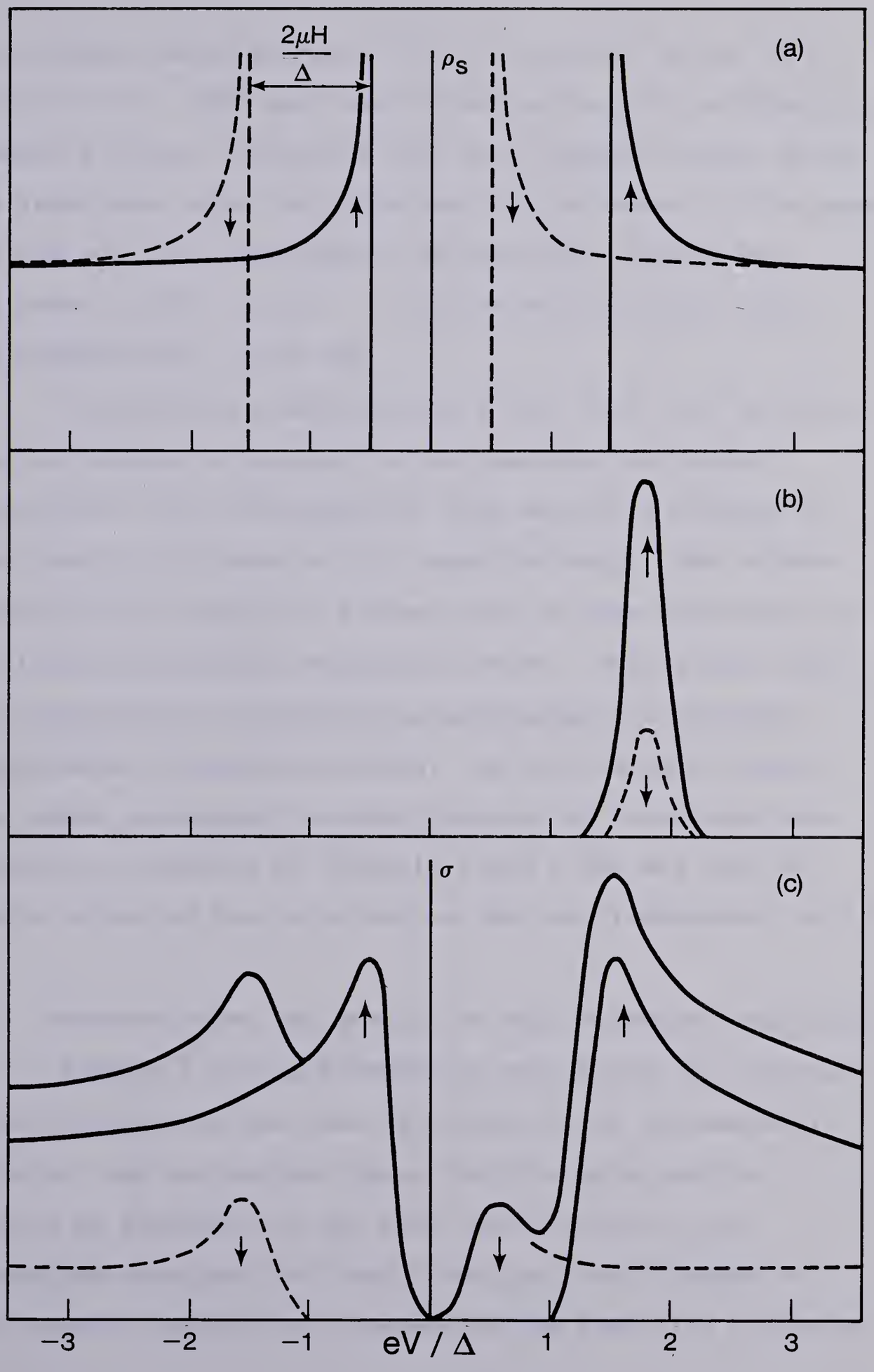
2μH
Δ
ρs
(a)
(b)
σ
(c)
−3
−2
−1
eV / Δ
1
2
3

the example shown in Fig. (2.4) a was chosen to be .25 so that P=-50%. Thus each spin direction has its own sharply peaked function, differing only by a constant factor which is associated with the difference in the number of electrons in the two spin directions. The resulting conductance is shown in Fig. (2.4c). It can be seen that the curve is asymmetrical, about V=0.

A qualitative explanation of Fig. (2.4) can be given. As the voltage is applied to the junction the peaked functions of the ferromagnetic film move with respect to the density of states of the superconductor. The corresponding spin density of states curve is then reproduced as a slightly broadened conductance curve. This simple model is justified by the success in accounting for measured experimental tunneling results. As will be shown later, the model reproduces the main features of the conductance curve as a function of magnetic field H and was able to yield values of the polarization that are independent of H.

2.6 Band-structure Explanation of Spin Polarized Tunneling.

Stearns [74] has proposed an explanation of tunneling that follows from the band structure of the ferromagnetic metals. Her explanation shows that the polarization should be dependent on the Fermi wave vector of the tunneling electrons and thus tunneling should depend on the crystallographic orientation of the tunneling electrons.

Fig. (2.5) shows an energy level diagram for a ferromagnetic-insulator-metal tunnel junction. The nonmagnetic state of Fig. (2.5) has energy E_o. Because this metal is a ferromagnet, the spin-up and spin-down parts of the energy vs k graph are split from E_o by an exchange energy Δ. When an electron leaves the ferromagnet its exchange energy is converted into kinetic energy and thus the wave vector in the metal, k_L^M is different from the wave vector just inside the barrier, $k_L^B = (2mE_o/\hbar^2)^{\frac{1}{2}}$.

Using Harrison's theory of sec. 2.2 an expression for the transition probability from left to right through the barrier B is given by P_t:

$$P_t = |M_{LB}|\ |M_{BR}|\ \rho_{LB}\ \rho_{BR}$$

where M_{LB} is the matrix element to go from L to B and ρ_{LB} is the density of states to the right of x_L. Using the WKB approximation solving for the matrix elements yields [74]

$$M_{LB} = \frac{\hbar^2 k_{x_L}}{2mt}\, e^{-\eta_L} \qquad (2.14)$$

where t is the metal thickness and

$$\eta_L = \int_{x_L}^{x_R} |(2m\phi_L/\hbar^2 + k_{11}^2)^{\frac{1}{2}}|\ dx \qquad (2.15)$$

ϕ_L is the left barrier height and k_{11} the transverse momentum. M_{BR} is similar. Because of the rapid decrease

Fig. 2.5

Energy level diagram for a 3d ferromagnet.

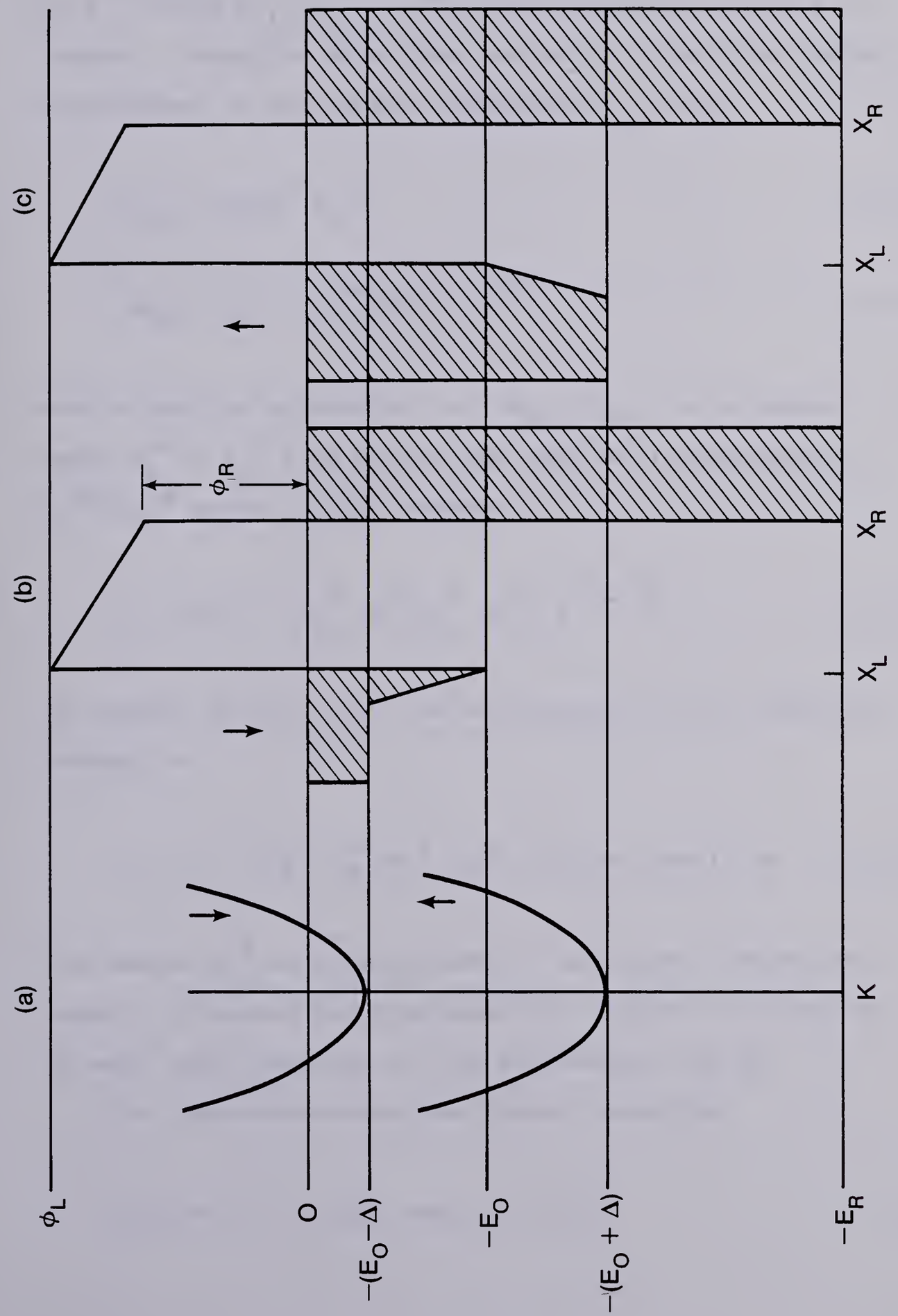
(a)
(b)
(c)
ϕ_L
ϕ_R
0
$-(E_O-\Delta)$
$-E_O$
$-(E_O+\Delta)$
$-E_R$
K
X_L
X_R
X_L
X_R

of $e^{-\eta_L}$ with k_{ll}, ρ_{LB} is the one dimensional density of states. Tunneling electrons are mainly electrons travelling normal to the barrier therefore $k_{x_L} \simeq k_L$.

$$\rho_{LB} = tm/\pi\hbar^2 \; k_L^B \tag{2.16}$$

$$|M_{LB}| \; \rho_{LB} = (k_L^M/2\pi k_L^B) \; e^{-\eta_L} \tag{2.17}$$

with a similar expression for $|M_{BR}| \; \rho_{BR}$. In a normal metal $k_L^M = k_L^B$ [36] but in the case of a ferromagnet $k_L^M \neq k_L^B$ so Eq. (2.13) becomes

$$P = (2\pi)^{-2} \; (k_L^M \; k_R^M/k_L^B \; k_R^B) \; e^{-\eta_L - \eta_R}. \tag{2.18}$$

In analogy to Eq. (2.2) the expression for the tunneling current is

$$I = \xi \int_{-\infty}^{\infty} (k_L^M \; k_R^M/k_L^B \; k_R^B) \; [f(E)-f(E+eV)] \; dE \tag{2.19}$$

The factor k_L^M is proportional to the three dimensional density of states and represents the number of electrons of each spin direction in the ferromagnet, $N_F(E)$.

For ferromagnetic-normal metal tunneling

$$N_F(E) = k^{\uparrow,\downarrow} = [2m \; (E+E_o \pm \Delta)/\hbar^2]^{\frac{1}{2}} \tag{2.20}$$

$$k_L^B = [2m\ (E_o+E)/\hbar^2]^{\frac{1}{2}} \tag{2.21}$$

$$k_R^M = k_L^M \tag{2.22}$$

$$I_{FN}^{\uparrow\downarrow} = \xi \int_{-\infty}^{\infty} (k^{\uparrow\downarrow}/k_L^B)\ [f(E)-f(E+eV)]\ dV \tag{2.23}$$

For a superconductor k_R^M represents $N_s(E)$ and

$$N_s(E) \simeq k^M\ \rho_s(E) \tag{2.24}$$

where ρ_s is the superconducting density of states factor and

$$k_R^B = k^M = [2m\ (E_R+E)/\hbar^2]^{\frac{1}{2}}. \tag{2.25}$$

Therefore for tunneling between a superconductor and a ferromagnet

$$I_{FS}^{\uparrow\downarrow} = \xi \int_{-\infty}^{\infty} \left(\frac{k^{\uparrow\downarrow}}{k_L^B}\ \rho_s(E)\ [f(E)-f(E+eV)] \right) dE \tag{2.26}$$

In a spin polarized tunneling experiment only electrons within about 1 meV of the Fermi surface are sampled, therefore $k^{\uparrow\downarrow} = k_F^{\uparrow\downarrow}$, the Fermi wave vector. Adding the currents in both spin directions in Eq. (2.26) and finding $\sigma(V)$

$$\sigma(V) = \int_{-\infty}^{\infty} \frac{k_F^{\uparrow}}{k_F^{\uparrow}+k_F^{\downarrow}} \frac{\rho_s(E+\mu H)\beta e^{(E+eV)}}{[1+e^{\beta(E+eV)}]^2} dE + \int_{-\infty}^{\infty} \frac{k_F^{\downarrow}}{k_F^{\uparrow}+k_F^{\downarrow}} \frac{\rho_s(E-\mu H)\beta e^{(E+eV)}}{[1+e^{\beta(E+eV)}]^2} dE \quad (2.27)$$

comparing this to Eq. (2.10) gives

$$a = k_F^{\uparrow}/(k_F^{\uparrow} + k_F^{\downarrow}) \quad (2.28)$$

and $p = 2a-1$ as

$$p = (k_F^{\uparrow} - k_F^{\downarrow})/(k_F^{\uparrow} + k_F^{\downarrow}) \quad (2.29)$$

Therefore the polarization should depend on the crystallographic orientation of the ferromagnetic metal that the electrons are tunneling from. From polycrystalline materials it would be expected that the polarization values would be an average of the k_F values over all directions. Calculations by Stearns [74] compared to the experimental work of Meservey [80] indicate good agreement for this model.

2.7 Spin-orbit and Spin-flip Scattering

The simplified analysis of the preceding sections has assumed that the density of states of the superconductor is as shown in Fig. (2.6a) and that spin is conserved in the tunneling process.

Maki [46] considered a thin film superconductor with

Fig. 2.6

Effect of spin-orbit scattering

(a) Spin split BCS density of states of a superconductor in a magnetic field.

(b) Spin densities of states for a superconductor with finite spin-orbit scattering.

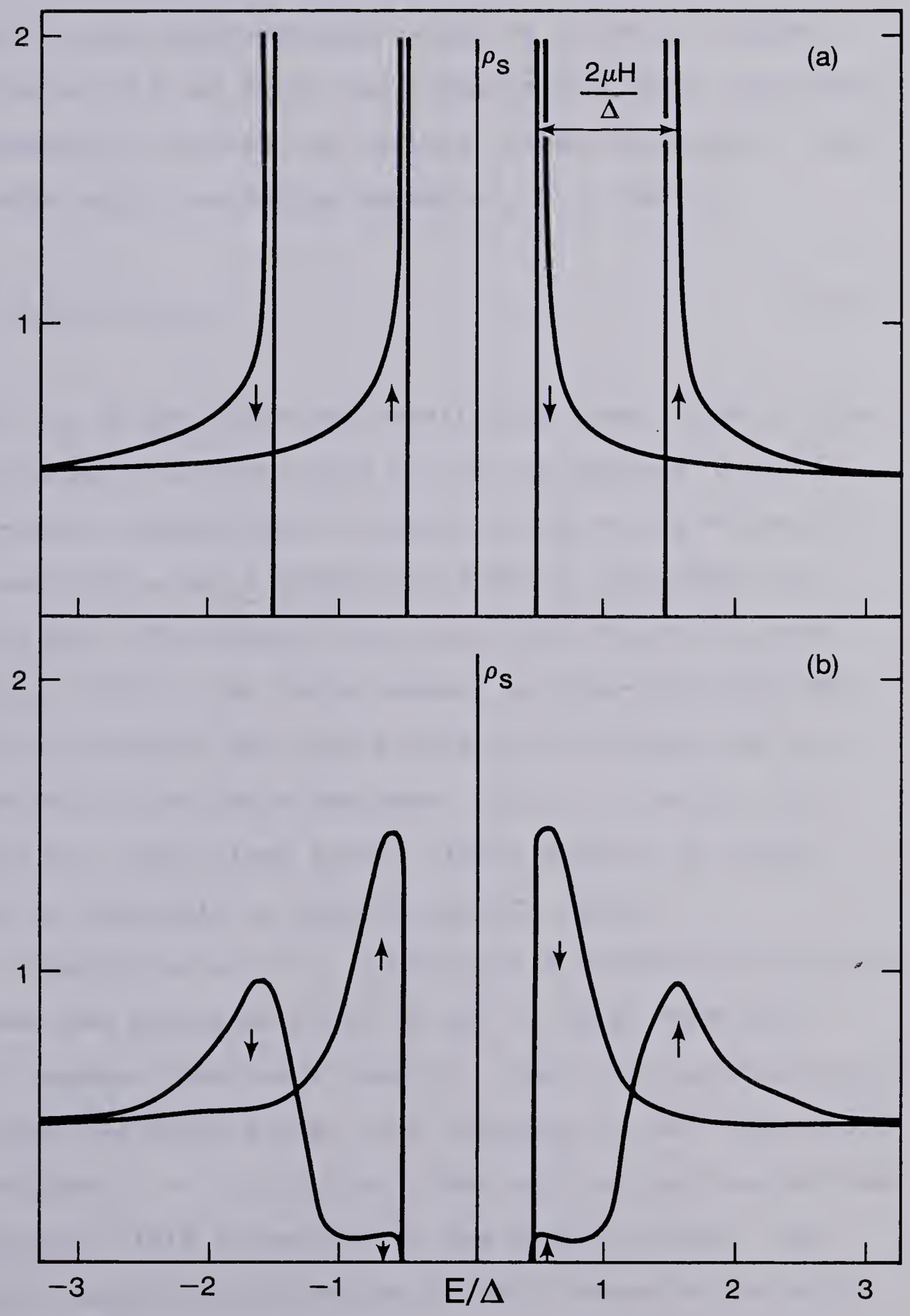
2
1
ρ_s
$\frac{2\mu H}{\Delta}$
(a)
2
1
ρ_s
(b)
−3
−2
−1
E/Δ
1
2
3

spin-orbit scattering centers and found the density of states of the superconductor would be altered. Engler and Fulde [21] and Bruno and Schwartz [11] have calculated the density of states for various values of magnetic field and spin-orbit scattering parameter, b, given by

$$b \equiv \hbar/3\ \tau_{so}\ \Delta \tag{2.30}$$

where τ_{so} is the spin-orbit scattering time. Some of the spin states at large values of $|E|$ are shifted by the spin-orbit interaction to near the peak at low values of $|E|$ and form a small spread out subpeak just above the energy gap. The result for b small and finite is shown in Fig. (2.6b). For large amounts of spin-orbit scattering the mixing of the spin states will increase and the splitting of the peaks decrease. As $b \to \infty$ the two spin states will have mixed into a single density of states which is identical to that of the BCS theory.

Meservey et al. [52,79] devised a tunneling experiment between two superconductors to see if these phenomena would produce observable results. When two superconductors are used two sharp maxima are expected in the conductance at voltages $V = \pm (\Delta_1+\Delta_2)/e$. This will be the case whether a magnetic field is applied to the sample or H=0. The overall tunneling conductance is not altered by the spin splitting that occurs in the superconductors. If spin

were not conserved in the tunneling process or if spin-orbit interaction is large enough it would be expected that each of the large peaks would split into three peaks; a smaller peak in the position of the large peak at $V = \pm(\Delta_1+\Delta_2)/e$, and two satellite peaks at $|V| = (\Delta_1+\Delta_2 \pm 2\mu H)/e$. The peak at $|V| = (\Delta_1+\Delta_2 - 2\mu H)/e$ would be the peak predicted by the spin-orbit scattering theory and a peak at $|V| = (\Delta_1+\Delta_2+2\mu H)/e$ would only be expected if the electron's spin flipped in the tunneling process and not from spin-orbit scattering in the superconductor.

Meservey has shown that for Aℓ films extra small peaks exist only at $|V| = (\Delta_1+\Delta_2-2\mu H)/e$, implying that in the spin polarized tunneling experiments with Aℓ a small amount of spin-orbit scattering exists but that spin-flip scattering is not observable. Therefore in calculating the polarization, the apparent polarization value, P_A, will have to be corrected to account for the effects of spin-orbit scattering in the superconducting Aℓ films.

Chapter 3

Experimental Techniques

3.1 Junction Preparation

A tunneling experiment requires two metals to be in close proximity but separated by an insulator. Basic tunnel junction preparation requires three steps. First a base layer metal film is deposited, a thin insulating layer is grown on the film, and finally a top cross strip metal is evaporated to complete the junction.

The preparation of the tunnel junctions was carried out in a vacuum system having an ultimate pressure of about 1×10^{-6} torr. The vacuum system consisted of a bell jar pumped on by an oil diffusion pump with a liquid nitrogen cold trap. The system was backed by a mechanical forepump that was also used for roughing out the system.

Table 3.1 shows the various filaments, boats and metals used in the course of this work. All metals used were in pellet and chunk form except for Aℓ which was in wire form. Sb and Sn metals were loaded directly onto the evaporation boats. Ni pellets were wrapped in a small amount of Ni wire to form a holder before they were placed in the boat. Mn chunks were crushed into smaller, powder-like pieces before evaporation. The Aℓ wire was first cleaned with methanol and wiped dry with kimwipe tissues. The wire was then cut into 1½" 'u' shaped pieces

TABLE 3.1

Evaporation Materials

Metal	Purity	Supplier	Evaporation Source
Aℓ	59	Terochem	F8-4X.030W coil
Mn	49	Johnson Matthey	ME 6A-.005 Ta boat
Sb	59	Cominco	ME 6A-.005 Ta boat
Sn	59	Cominco	ME 6B-AO boat
Ni	59	J.T. Baker	Me 6B-AO boat

Evaporation sources supplied by

R.D. Mathis Company.

before placement on the helical filaments.

The glasses used for substrates were 25 mm × 75 mm Canlab brand microscope slides. Each slide was then cut into 4 pieces of equal size, each piece being a substrate for a tunnel junction preparation. The slides were washed with detergent, rinsed with water and then rinsed with methanol to remove the water. The cleaned slide was then lightly flame polished over a bunsen burner before being placed in the evaporator.

The base layer required for spin polarized tunneling is an ultra-thin Aℓ film (~ 40A). To achieve such thin films the evaporation was carried out on a liquid nitrogen cooled substrate. The glass slide was greased to a backing plate which was cooled by allowing liquid nitrogen to flow through copper tubing in the system. The mask in front of the slide was also similarly cooled. The liquid nitrogen was allowed to flow through the system for approximately 20 minutes before the Aℓ evaporation took place. The shutter was arranged so that three different thicknesses of Aℓ films could be produced in one evaporation. After evaporation of the thin films was completed one shutter step was left open to evaporate thick Aℓ pads (~ 500A) at the ends of the thin films so that leads could be attached (see Fig. (3.1)).

After the Aℓ was deposited the system was allowed to warm up to room temperature for ~ 15 minutes. This was

Fig. 3.1

Tunnel junction layout

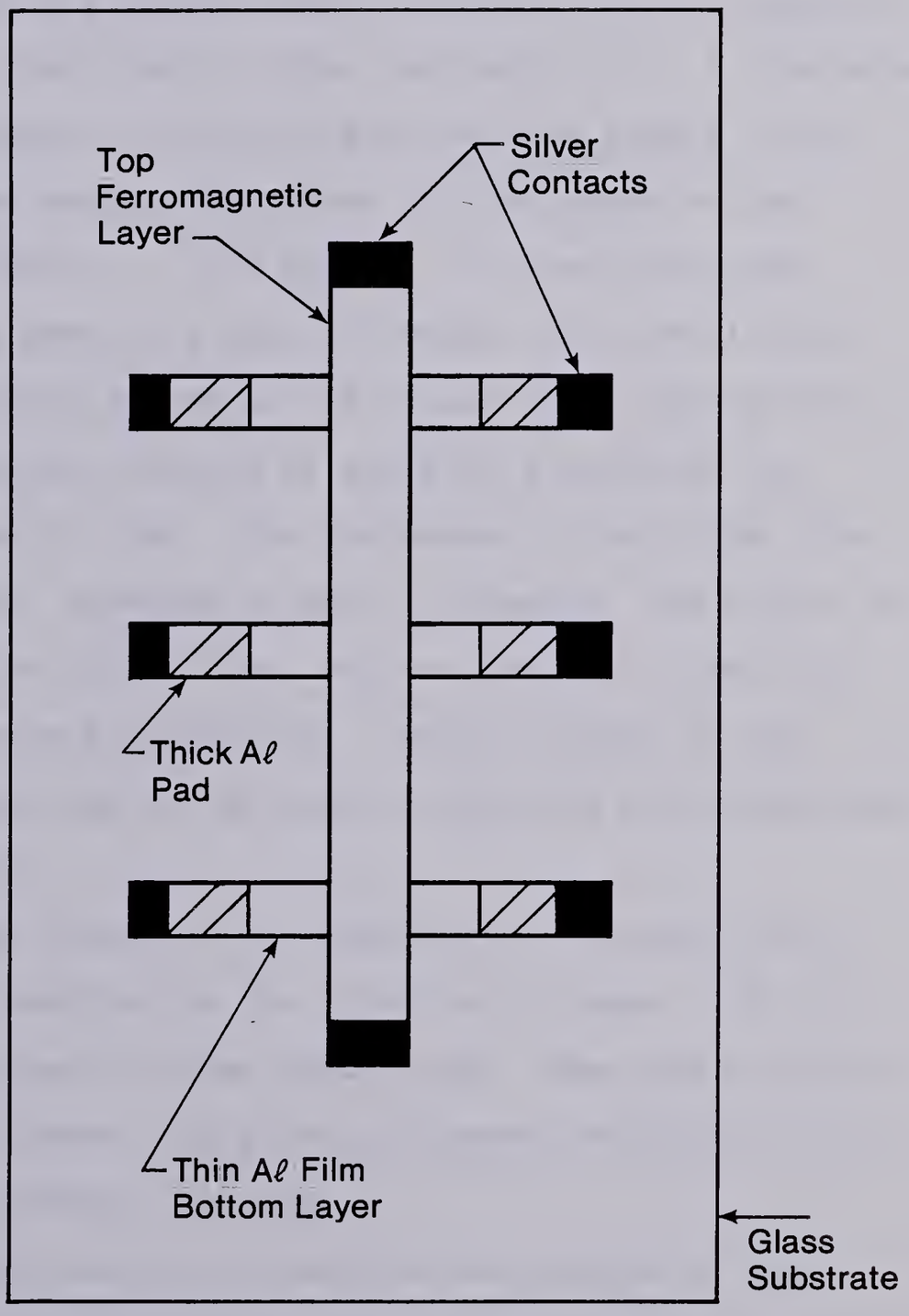
Top
Ferromagnetic
Layer
Silver
Contacts
Thick Aℓ
Pad
Thin Aℓ Film
Bottom Layer
Glass
Substrate

accomplished by forcing air through the copper tubing where the liquid nitrogen had been allowed to flow.

Oxidation was accomplished by using a glow discharge technique as described by Miles and Smith [47]. A discharge was set up between an Aℓ ring and the film sample to be oxidized. The sample was placed in the center of the ring ~ 4 cm above it. The pressure in the system was maintained at about 0.2 torr of oxygen. The metal base of the evaporator served as the ground electrode and the glow discharge was started by applying a negative dc voltage to the Aℓ ring. The thickness of the oxide film, that was grown, depended on the O_2 pressure, the amount of current flowing in the ring, and the length of time the glow discharge was maintained. Typical values of the current ranged from 1-2 mA and the glow was maintained from 100-400 seconds.

After the discharge the system was evacuated until the pressure returned to the 1×10^{-6} torr range. The top metal cover layer was then evaporated. When the top film consisted of a metal alloy, simultaneous evaporation from two separate sources was used.

After the junction preparation was completed the evaporator was vented to room air and Ag tabs were painted on the ends of each film, so that wires could be soldered on later. The electrical conductivity of each film was checked and the resistance recorded. The substrate was

then mounted in the cryostat and electrical connections were made.

In the preparation of tunnel junctions as described above, the ratio of good to bad junctions was quite high once the oxidation parameters had been determined: (O_2 pressure, glow current, duration of discharge).

3.2 Film Thickness Determination

A quartz crystal monitoring system was used to determine thickness and rate of deposition of the thin films. Sauerbrey [69] first proposed to utilize the quartz oscillator for thickness measurements. Several reviews of the subject have appeared in the literature, see for example Behrndt [8] and Steckelmacker [75].

The quartz monitor provides a simple and sensitive technique for thickness measurements. The method is based on measuring the frequency shift of a piezoelectric crystal which is proportional to the mass of material deposited on the surface of the crystal. Eshchback and Kruidhof [22] have shown that the frequency shift, Δf, caused by a variation in thickness due to an added mass, Δm, is given by

$$\Delta f = C_f \frac{\Delta m}{A} \qquad (3.1)$$

where A is the area of the quartz plate

$$C_f = f^2/N\rho \qquad (3.2)$$

f - natural frequency of the crystal

N - constant depending on the cut of the crystal

ρ - density of quartz.

Eq. (3.1) is restricted to mass deposits which are small (< 5% of the mass of the crystal itself). Film thicknesses calculated from the microbalance readings assume bulk densities and equal sticking probabilities for the deposits.

The monitor uses the thickness shear mode of a 5 megacycle AT cut crystal. The AT cut crystal is used because it has a low temperature coefficient for the resonant frequency ($\pm 5\times10^{-6}$ between -20 and 60°C).[8] The crystal is silver plated on both sides to provide electrical contact. Contact is made and the crystal secured by means of a small wire spring. The other side of the crystal is in contact with the polished surface of a water cooled copper block (see Fig. (3.2)). The outputs of the oscillators are connected to the inputs of a counter timer device (Monsanto model 100A or Fluke model 1941A).

Where alloy films were deposited two separate, but identical, quartz monitors were used. The readings from the counters were then used to determine the concentration of each of the constituent metals in the film. The accuracy of some of the concentration calculations were also verified by measuring the atomic concentrations of

Fig. 3.2

(a) Quartz crystal holder

(b) Circuit diagram of the single crystal monitor used in the present work. The integrated circuit is Motoroloa MC 1024P.

(a)

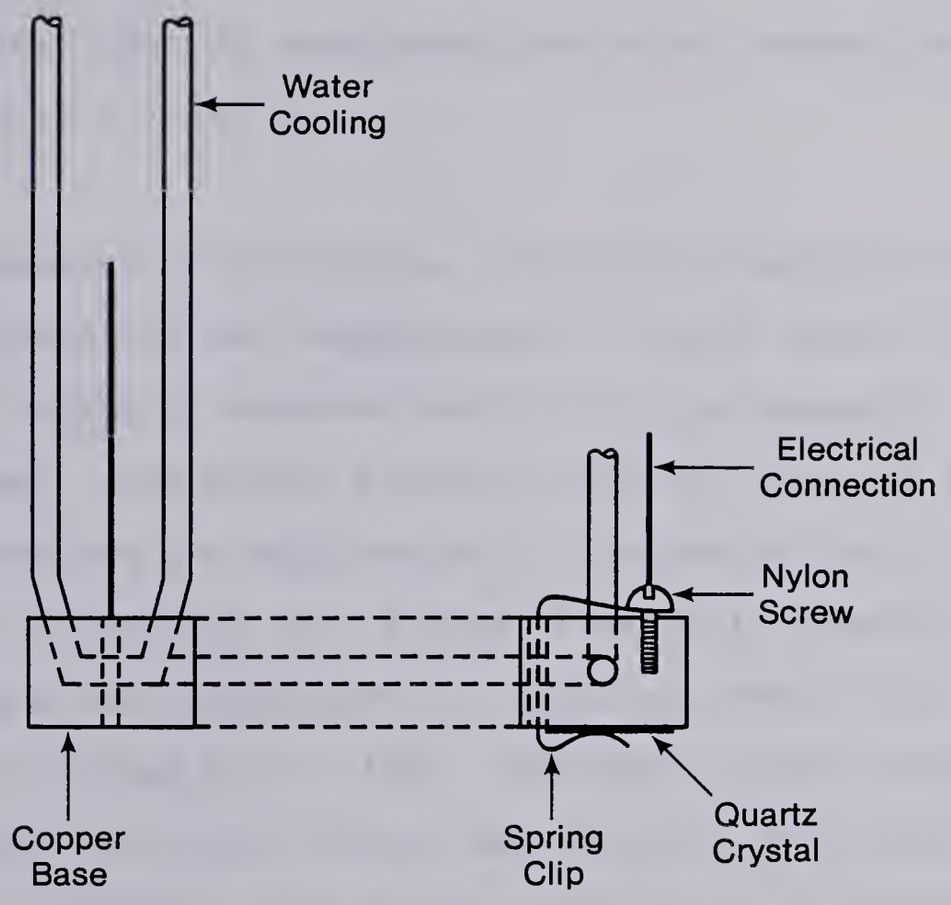
Water
Cooling
Electrical
Connection
Nylon
Screw
Copper
Base
Spring
Clip
Quartz
Crystal

(b)

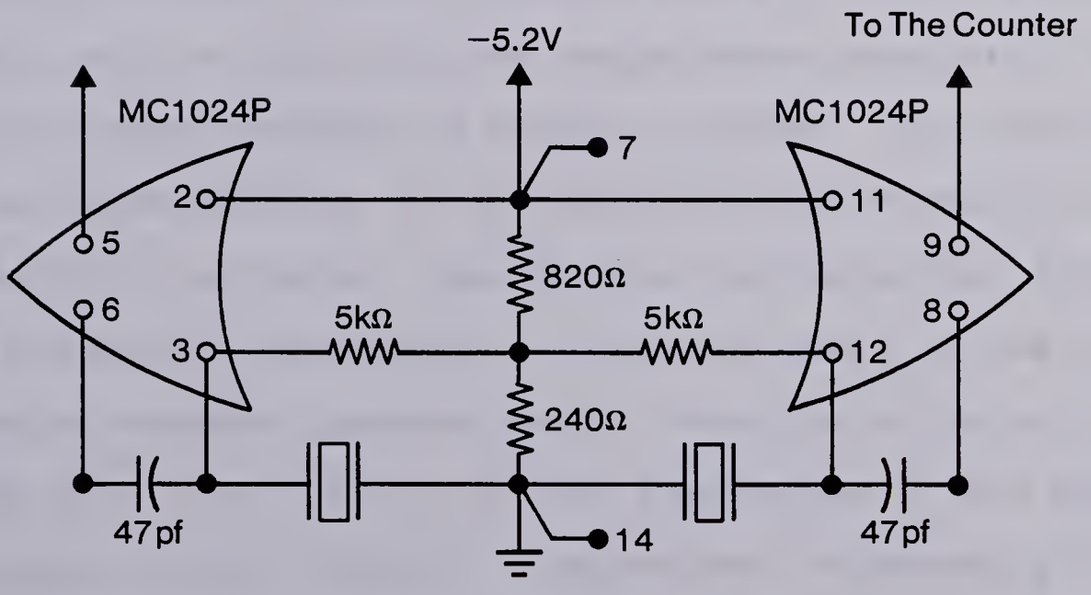
−5.2V
To The Counter
MC1024P
MC1024P
7
2
11
5
9
820Ω
6
5kΩ
5kΩ
8
3
12
240Ω
47pf
14
47pf

the thin alloy films by electron probe microanalysis. It was found that the two techniques gave alloy concentrations that agreed to ~ 1 at. %.

3.3 Low Temperature Production - Adiabatic Demagnetization

To achieve the low temperatures (~ 50 mK) used in the experiment adiabatic demagnetization of a paramagnetic salt was used. The method relies on the fact that at a fixed temperature the application of a magnetic field will lower the entropy of a system of magnetic moments. The technique was independently proposed by Debye [19] in 1926 and Giauque [31] in 1927. The first actual use of a paramagnetic salt for cooling was achieved by De Haas et al. [18] in 1933. A historical review of paramagnetic cooling has been given by Hudson [40].

The theory of paramagnetic cooling has been given by several authors, see for example Betts [9]. In a paramagnetic salt at liquid helium temperatures there still exists a disordered assembly of magnetic dipoles. The contribution to the entropy, S, of the solid from the dipoles is $R \ln(2J+1)$ per mole. Here $2J+1$ is the degeneracy (number of different orientations of the ions) and J is the total angular momentum quantum number. Starting at point X, (see Fig. (3.3)), at an initial temperature T_i and zero magnetic field, the salt is magnetized isothermally in contact with a liquid helium bath by an external magnetic

Fig. 3.3

Adiabatic demagnetization of a paramagnetic salt.

Entropy vs. temperature graph of a paramagnetic salt for $H=0$ and $H>0$. The specimen is magnetized isothermally along the path XY at an initial temperature T_i. The sample is then adiabatically demagnetized along the path YZ to a final temperature T_F.

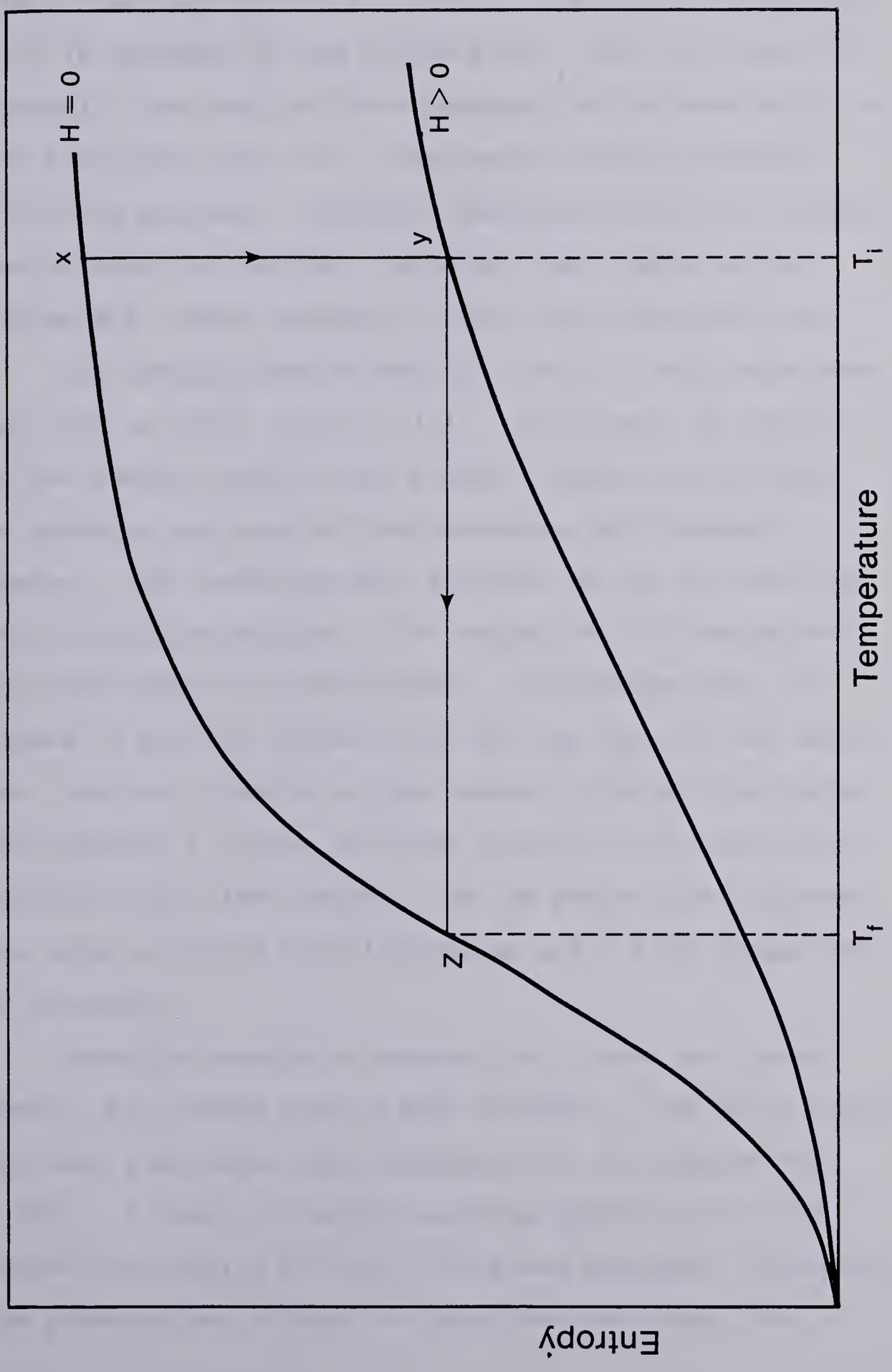
H = 0
H > 0
x
y
z
T_i
T_f
Temperature
Entropy

field (the path X→Y is followed). The heat of magnetization is absorbed by the helium bath. Next, the salt is thermally isolated and then demagnetized adiabatically to H=0 along the path Y→Z. Considerable cooling results from this process. Adiabatic demagnetization is a single cycle method of cooling. External heat leaks in the system will cause warming to start along the H=0 curve.

The demagnetization cryostat used in this experimental work is shown in Fig. (3.4). The sample is mounted to the sample platform and thermal contact is achieved by greasing the back of the substrate with Apiezon L grease. The leads are then soldered to the Ag tabs that were painted on earlier. The vacuum can is then placed over the bottom of the cryostat. The vacuum seal is formed by melting indium along the top edge of the vacuum can, cutting a groove in the indium, greasing the groove with Apiezon L grease and then attaching the can to the cryostat with eight screws. As the screws are tightened the edge is forced into the indium and a high vacuum seal is obtained.

After the sample is mounted both outer and inner dewars are filled with liquid nitrogen. The whole system was then left until the temperature of the sample was ~ 80K (~ 1 hour). The air was then pumped out of the vacuum can until a $p \sim 1 \times 10^{-5}$ torr was achieved. Typically the pressure was allowed to come down overnight, but a

Fig. 3.4

Adiabatic demagnetization cryostat

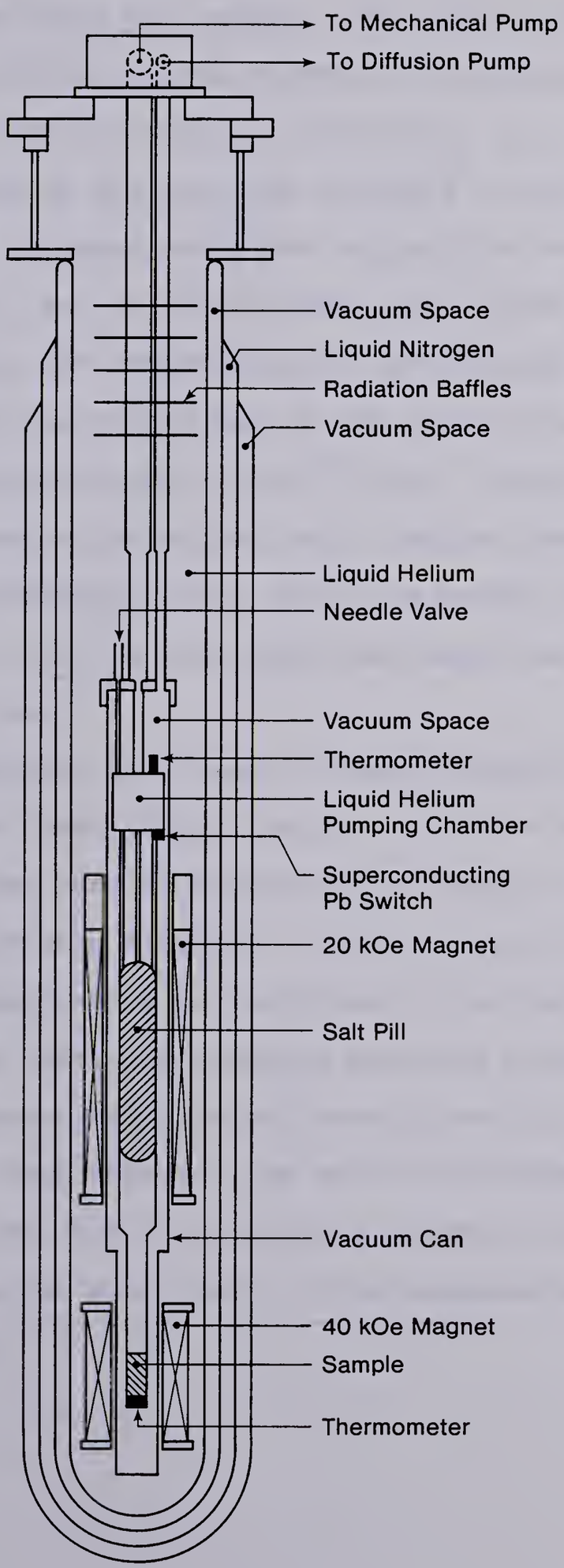
To Mechanical Pump
To Diffusion Pump
Vacuum Space
Liquid Nitrogen
Radiation Baffles
Vacuum Space
Liquid Helium
Needle Valve
Vacuum Space
Thermometer
Liquid Helium
Pumping Chamber
Superconducting
Pb Switch
20 kOe Magnet
Salt Pill
Vacuum Can
40 kOe Magnet
Sample
Thermometer

minimum of a few hours was needed. The vacuum system consisted of a diffusion pump backed by a mechanical pump which was also used to rough out the vacuum can.

Helium exchange gas was then released in the vacuum can, the liquid nitrogen was blown out of the inner dewar using helium gas, and the inner dewar was filled with liquid He^4. When the temperature had stabilized at ~ 4.2K the exchange gas was pumped out of the vacuum can. When a good vacuum was achieved (~ 5×10^{-6} torr) liquid helium was allowed to enter the helium pot. The pot was then pumped on by a mechanical pump until the sample reached a temperature of ~ 1K. At this point the magnetization of the salt took place.

The paramagnetic salt used in this cryostat is ferric ammonium sulfate ($FeNH_4(SO_4)_2\cdot12H_2O$). A 25 kOe superconducting magnet was used to magnetize the sample, typically this took about twenty minutes. In this stage of cooling the heat of magnetization is conducted to the helium pot. The salt pill is thermally isolated from its surroundings or placed in contact with the He^4 bath by use of a Pb superconducting heat switch. The salt is then demagnetized adiabatically. The final temperature reached is about 50 mK and the sample will stay in this temperature range for ~ 20 minutes.

3.4 Measurement of Junction Characteristics

The study of the tunnel junction specimens involved the measurement of their dI/dV vs V characteristics. To do this the use of an ac modulation technique was used. In this method a small ac signal of frequency ω is applied to the junction, along with the dc bias. The first derivative, dI/dV, is then obtained by synchronous detection of the signal at ω. It is then possible to plot continuously on an X-Y recorder dI/dV vs V. This method was first applied to tunneling by Giaever et al. [30]

A simplified bridge circuit is shown in Fig. (3.5) and will be used to explain how plots of dI/dV are obtained.

Here the tunnel junction is represented by the four terminal element R_T which is assumed to be non-linear and passive. R_T must see an effectively constant voltage source and for this condition to hold the series resistance R and the impedances of the dc and ac voltage sources must be small compared to R_T, i.e. Z_o, Z, and $R \ll R_T$. The voltage across the junction then becomes an independent variable and the current will be a function of this voltage, i.e. $I = I(V)$. By Taylor's expansion this may be written as

$$I(V) = I_o + \left(\frac{dI}{dV}\right)_{V_o} (V-V_o) + \frac{1}{2}\left(\frac{d^2I}{dV^2}\right)_{V_o} (V-V_o)^2 + \ldots \tag{3.3}$$

Fig. 3.5

Simplified conductance bridge

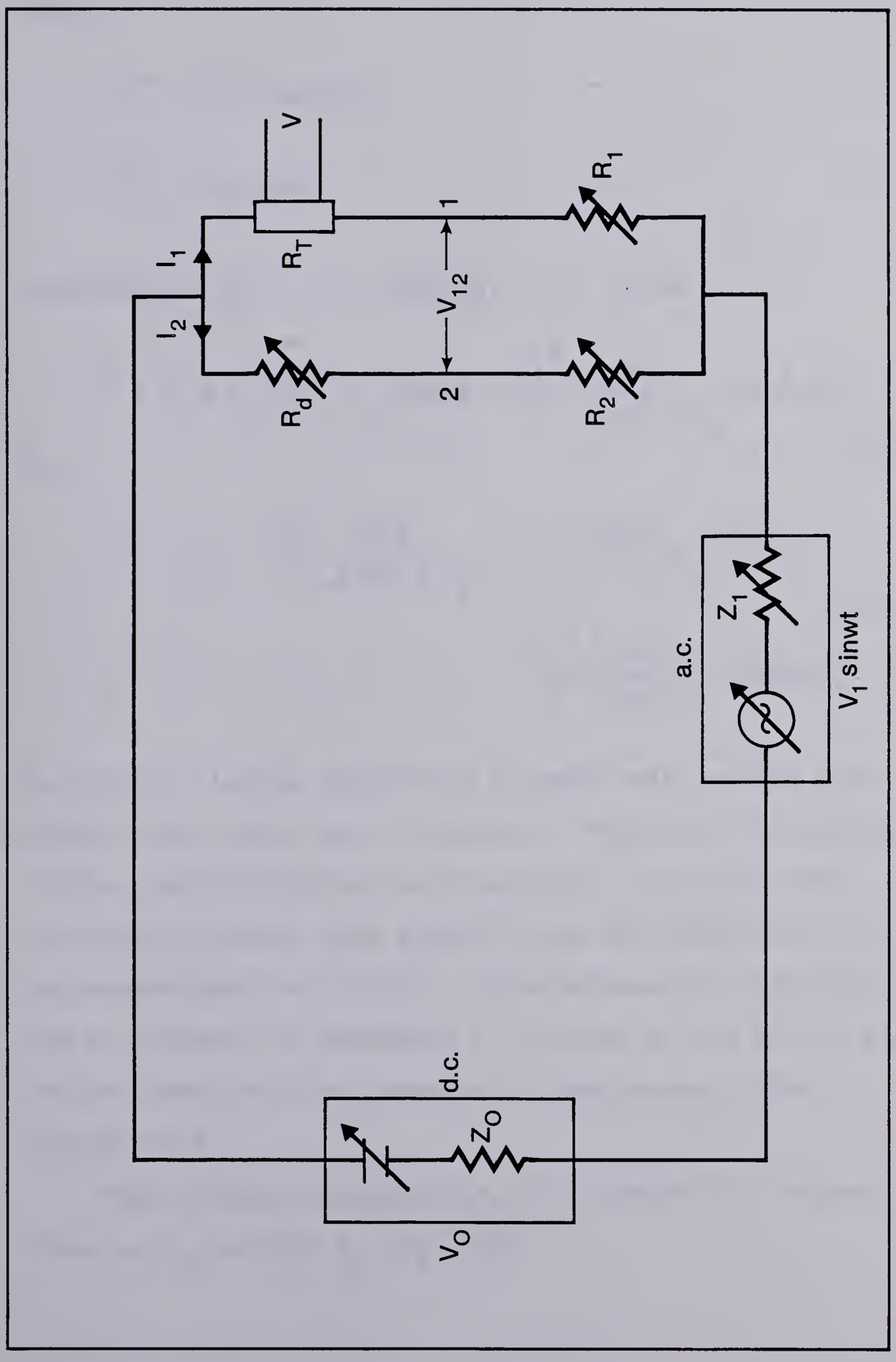
V
R_T
I_1
I_2
1
2
V_{12}
R_1
R_2
R_d
a.c.
Z_1
V_1 sinwt
d.c.
Z_O
V_O

where

$$I_o = (V_o/R_T)_{static} \tag{3.4}$$

$$V-V_o = V_1 \sin\omega t \tag{3.5}$$

substituting Eq. (3.5) into Eq. (3.3) gives

$$I = I_o + V_1\left(\frac{dI}{dV}\right)_{V_o} \sin\omega t + \frac{V_1^2}{2}\left(\frac{d^2I}{dV^2}\right)_{V_o} \sin^2\omega t + \ldots \tag{3.6}$$

or

$$I \simeq \left[I_o + \frac{V_1^2}{4}\left(\frac{d^2I}{dV^2}\right)_{V_o}\right] + V_1\left(\frac{dI}{dV}\right)_{V_o} \sin\omega t - \frac{V_1^2}{4}\left(\frac{d^2I}{dV^2}\right)_{V_o} \cos 2\omega t \tag{3.7}$$

In practice the ac modulation is kept small enough that higher level terms may be ignored. Therefore the component of the junction current at frequency ω is proportional to dI/dV at the dc bias level V_o and the component at 2ω is proportional to d^2I/dV^2. By simultaneously measuring the ac current, at frequency ω, through R_1 and the dc bias on the junction it is possible to continuously plot (dI/dV) vs V.

The variable resistance R_d is adjusted to a value close to R_T so that $R_d >> R_2$, then

$$I_2 = (V_o + V_1 \sin\omega t)/R_d \tag{3.8}$$

The voltage V_{12} is of interest and its component at frequency f is given by

$$V_{12}(\omega) \simeq R[I(\omega) - I_2(\omega)] \tag{3.9}$$

substituting from Eq. (3.7) this becomes

$$V_{12}(\omega) \simeq RV_1 \sin\omega t\left[\left(\frac{dI}{dV}\right)V_o - \frac{1}{R_d}\right] \tag{3.10}$$

R_d is adjusted to make $V_{12}(\omega)$ very small and then when the dc bias voltage, V_o, is changed, small variations in dI/dV become large variations in $V_{12}(\omega)$ and the sensitivity of the system is greatly increased.

CHAPTER 4

Data Analysis

4.1 Analysis of the Conductance Curves - No Spin-Orbit Scattering

In the first analysis of a conductance curve spin-orbit scattering in the Aℓ film and spin-flip scattering in the tunnel barrier will be neglected. Spin-orbit scattering is known to be small [79] and spin-flip scattering has been shown to be unobservable for $A\ell_2O_3$ barriers [52]. From sec. (2.6) it is assumed that the conductance curves are composed of the sum of the two conductances, for the two spin directions, displaced in energy by $\pm\mu H$. The amplitude of the conductance curves, in the two spin directions, will be different because it is assumed that the tunneling current is different (independent of energy) for each spin direction. Fig. (4.1a) demonstrates this behaviour.

If f(eV) is the original unsplit conductance curve, then af(eV+μH) and (1-a)f(eV-μH) are the conductances of the two spin states. Here a represents a constant between 0 and 1.

The solid curve F(eV) (Fig. (4.1b)) is the sum of the separate conductances, and if all assumptions are true should coincide with the measured conductance curve.

The BCS theory has predicted that the original function f(eV) is symmetric about the Fermi surface,

Fig. 4.1

a) Temperature-dependent kernels for each spin direction

b) Two conductances add to give measured curve.

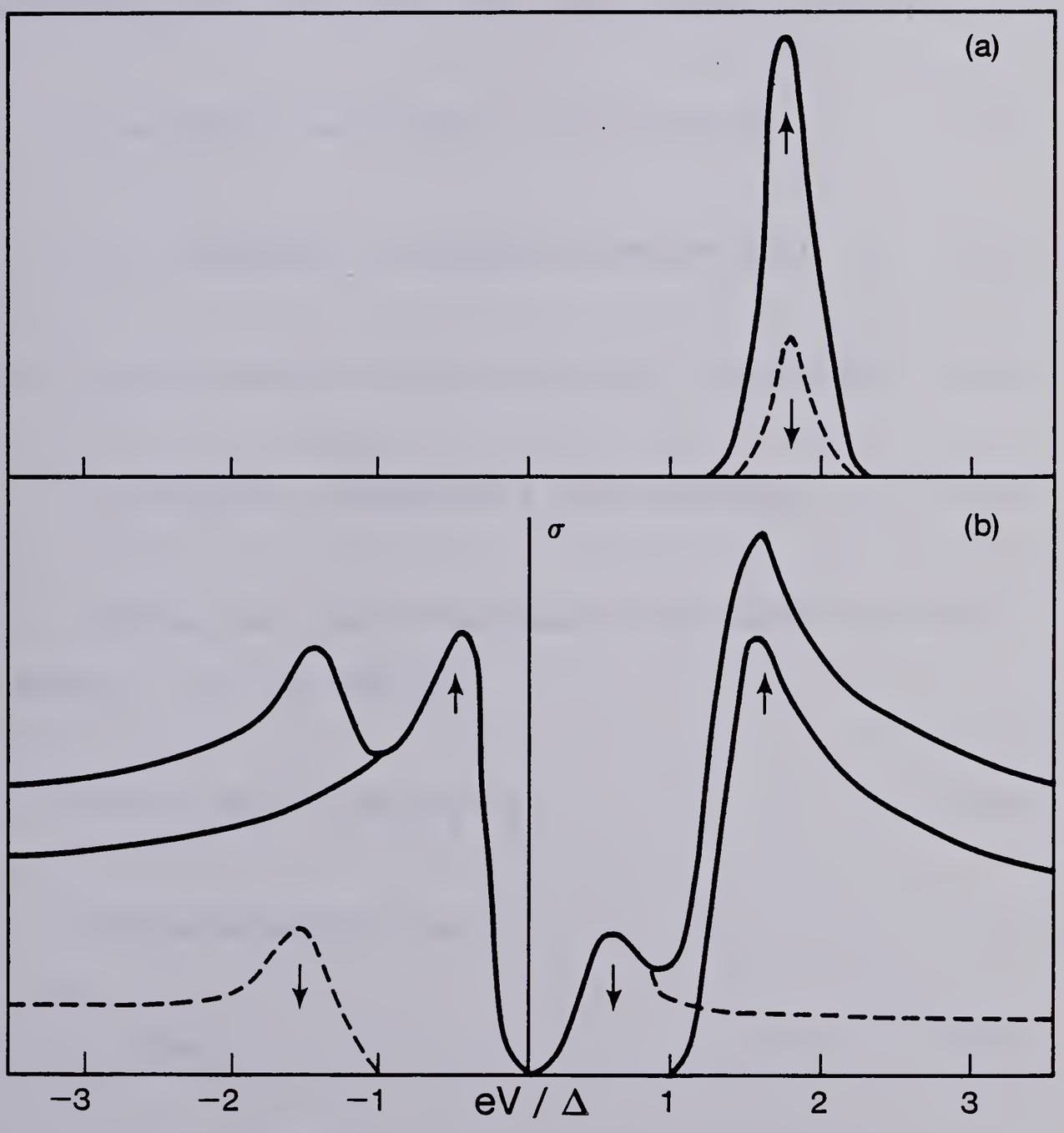
(a)
(b)
σ
−3
−2
−1
eV / Δ
1
2
3

$$f(eV) = f(-eV) \tag{4.1}$$

For any value of eV, Tedrow et al. [80] have shown that you can write four equations for the total measured conductance at the points eV, -eV, eV+2μH, -eV-2μH:

$$\sigma_1 = F(eV) = af(eV+\mu H) + (1-a)f(eV-\mu H) \tag{4.2}$$

$$\sigma_2 = F(eV+2\mu H = (1-a)f(eV+\mu H)+af(eV+3\mu H) \tag{4.3}$$

$$\sigma_3 = F(-eV-2\mu H) = (1-a)f(eV+3\mu H) + af(eV+\mu H) \tag{4.4}$$

$$\sigma_4 = F(-eV) = af(eV-\mu H) + (1-a)f(eV+\mu H). \tag{4.5}$$

Solving for a as a function of the measured conductances σ_1, σ_2, σ_3, and σ_4:

$$a = (\sigma_4-\sigma_2)/(\sigma_4-\sigma_2+\sigma_1-\sigma_3). \tag{4.6}$$

The polarization P is

$$P \equiv 2a-1 \tag{4.7}$$

Eqs. (4.2-4.6) allow the original function to be obtained in terms of a and the measured curve F(eV).

$$f(eV+\mu H) = \frac{aF(eV)-(1-a)F(-eV)}{2a-1} \qquad (4.8)$$

The above equations imply that any arbitrary value of voltage and magnetic field could be used to obtain a value for the polarization. In actual practice this is not the case. If the value of H is too low, the fringing fields of the incompletely saturated ferromagnetic film act to change the density of states of the Aℓ [64]. For large values of H, close to the critical field of Aℓ, the depairing of the Aℓ will broaden the density of states and obscure the effects of the magnetic field splitting. Values of the voltage are chosen so that σ_1, σ_2, σ_3, and σ_4 are close to the maxima of the conductance curves. In other areas the slopes of the conductance curves are too large and the results more sensitive to random errors.

Fig. (4.2) is a typical conductance trace for a ferromagnetic alloy sample. Two traces are shown in this figure. The first is for H=0 and shows the superconducting energy gap for the Aℓ film. The second curve is taken when H=30 kOe and is the trace used to calculate the polarization value. The junction used here was an Aℓ-$Aℓ_2O_3$-Mn_xSb_{1-x} tunnel junction where the ferromagnetic alloy is 40 at. % Mn (x=0.4). Using Eq. (4.6) and Eq. (4.7) the polarization of the sample is then

$$P = \frac{(\sigma_4-\sigma_2) - (\sigma_1 - \sigma_3)}{(\sigma_4-\sigma_2) + (\sigma_1 - \sigma_3)} \qquad (4.9)$$

Fig. 4.2

Typical conductance characteristic for an Al-Al_2O_3-Mn_xSb_{1-x} tunnel junction.
(The arrows indicate a separation of $2\mu H/e$).

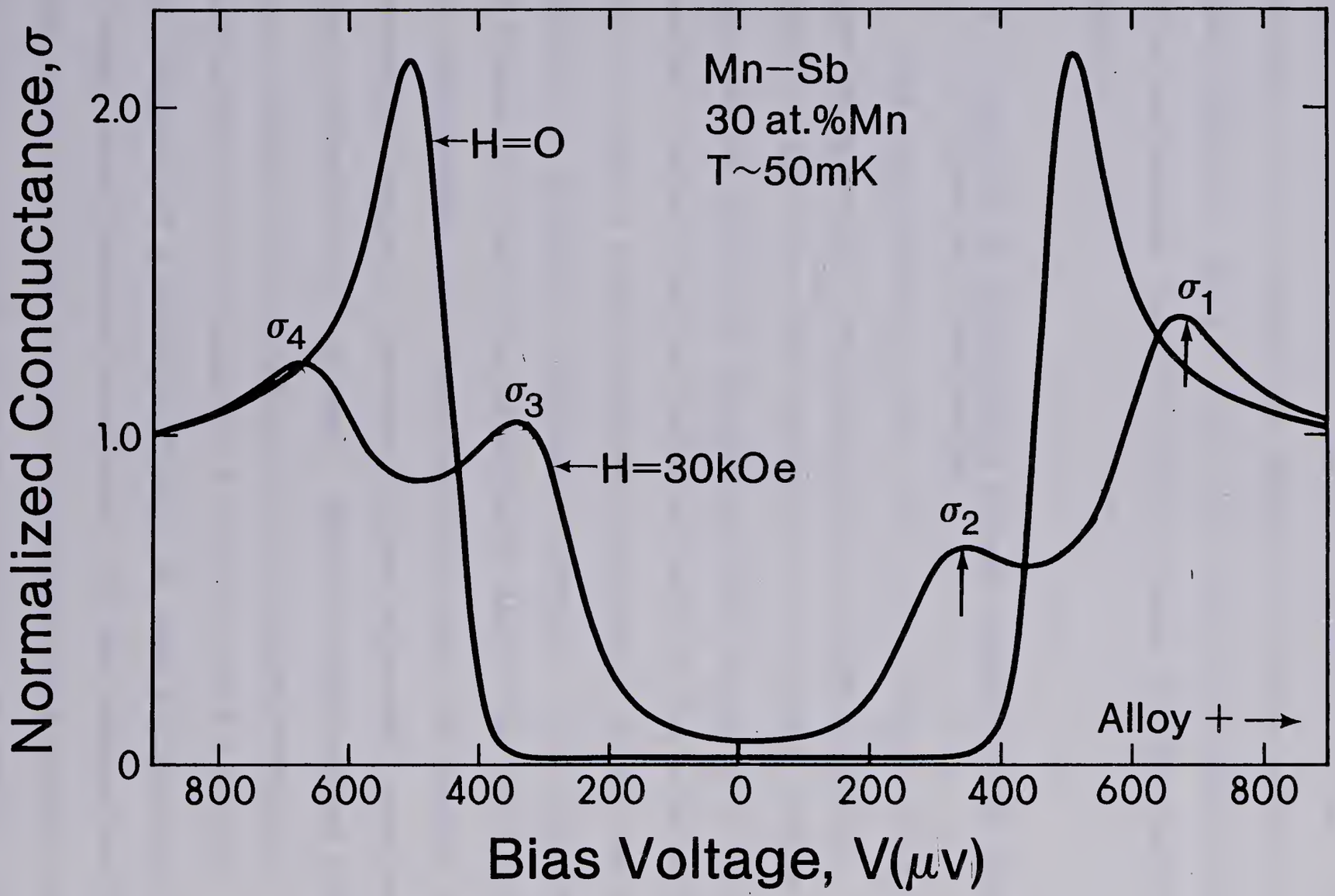
Normalized Conductance, σ
2.0
1.0
0
Mn–Sb
30 at.%Mn
T~50mK
←H=O
←H=30kOe
σ4
σ3
σ2
σ1
Alloy + →
800
600
400
200
0
200
400
600
800
Bias Voltage, V(μv)

In the sample shown P = 27.3%.

This sample also shows a confirmation of the simple theory of spin polarized tunneling described in sec. (2.6). According to the theory the energy difference between the peaks should be $2\mu H/e$. Fig. (4.2) shows the separation $2\mu H/e$ corresponds closely with the peaks in the conductance curve.

4.2. Analysis of Conductance Curves Including the Effects of Spin-Orbit Scattering

The explanation of sec. (4.1) is no longer valid if there is spin-orbit scattering in the superconductor. The effect of the spin-orbit scatter is to slightly reduce the polarization values by multiplying the values of P by a constant factor that is characteristic of the superconductor. In such a case the density of states of the two spin states are different functions of energy. The total density of states will still be symmetrical about the Fermi energy but the separate spin densities will not. To analyse a conductance curve to account for the spin-orbit scatter a single function B(V) is used. What is being called B(V) is in reality the spin-up part of the superconducting modification of the density of states in the Aℓ film, in the presence of a magnetic field, as seen by tunneling with a normal metal counter-electrode. At the temperature of this experiment B(V) should be qualitatively similar to the density of states function calculated by Engler and

Fulde [21] (see Fig. (2.6)).

The normalized sample conductance can be written in terms of B(V) as

$$\sigma(V) = (1+P)B(V) + (1-P)B(-V) \qquad (4.10)$$

where B(V) is taken to have an amplitude of 0.5 at high bias voltage and P is the true polarization index of the sample when the spin-orbit scatter is accounted for. (In this section P_a will be the apparent polarization index and is as defined in Eq. (4.9)).

If Eq. (4.10) is solved for B(V) the result is

$$B(V) = \frac{(1+P)}{4P}\sigma(V) - \frac{(1-P)}{4P}\sigma(-V) \qquad (4.11)$$

while any value of P (other than P=0) will generate a function B(V) through this equation, only a very limited range of P values will generate a result which is in qualitative agreement with the theory of Engler and Fulde [21] as discussed in sec. (2.7). With reference to the theoretical curves of Fig. (2.6), the main effect of spin-orbit scattering is to transfer spin states from the high energy main peak into a small, spread out subpeak just above the energy gap.

The experimental arrangement used analog electronics to present sample conductance, as a function of bias voltage, on an X-Y recorder as described in sec. (3.4). The

conductance record was then manually digitized and the results fed into a computer for analysis. For analysis the $A\ell$-$A\ell_2O_3$-Fe sample of Fig. (4.3) is used. For this sample $P_a = 0.437 \pm .005$. If $P=P_a$ is substituted into Eq. (4.1) a function B(V) is generated (see Fig. (4.4)) that is not in qualitative agreement with theory. The two main peaks which result are of equal amplitude and two subpeaks P_1 and P_2 are generated. The function B(V) of Fig. (4.4) is shown folded over on itself and the (+) and (-) signs refer to the bias voltage polarities of Fig. (4.3).

To agree with theory the true polarization of the sample is taken to be that value of P which causes the subpeak P_2 of Fig. (4.4) to vanish. Fig. (4.5) is an illustration of this. The value of P used to generate this curve was $P = .380 \pm .005$.

This result gives a polarization ratio $P/P_a = 0.87$. The model calculations of Paraskevopoulos et al. [64] indicate that this polarization ratio corresponds to a spin-orbit scattering parameter b=0.08.

Fig. 4.3

Typical conductance trace of a spin polarized tunneling result for an Al-Al_2O_3-Fe sample (solid line). This trace is shown decomposed into spin-up and spin-down parts (dashed lines).

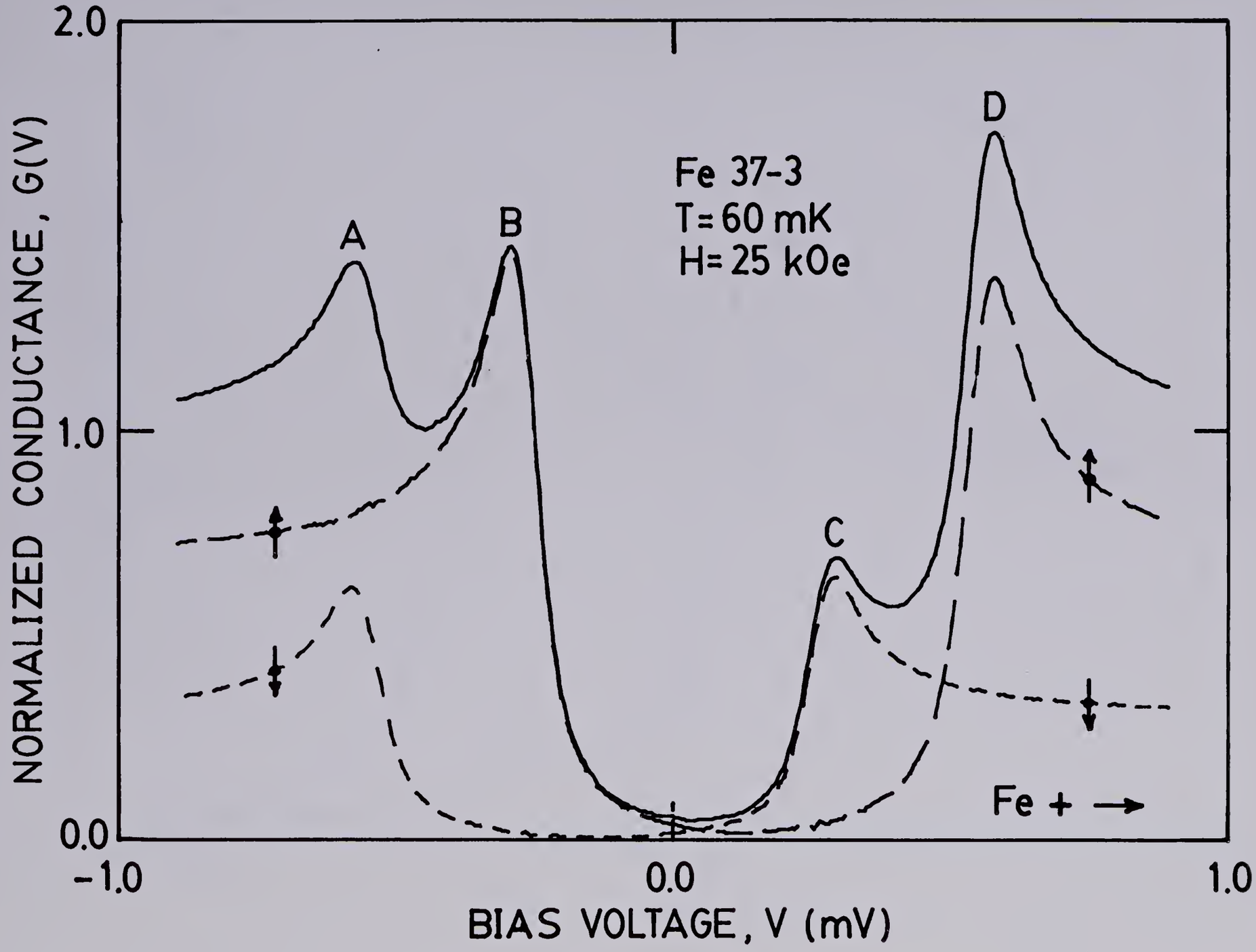
2.0
1.0
0.0
-1.0
0.0
1.0
NORMALIZED CONDUCTANCE, G(V)
BIAS VOLTAGE, V (mV)
A
B
C
D
Fe 37-3
T = 60 mK
H = 25 kOe
Fe + →

Fig. 4.4

Illustration of an incorrect basis function.

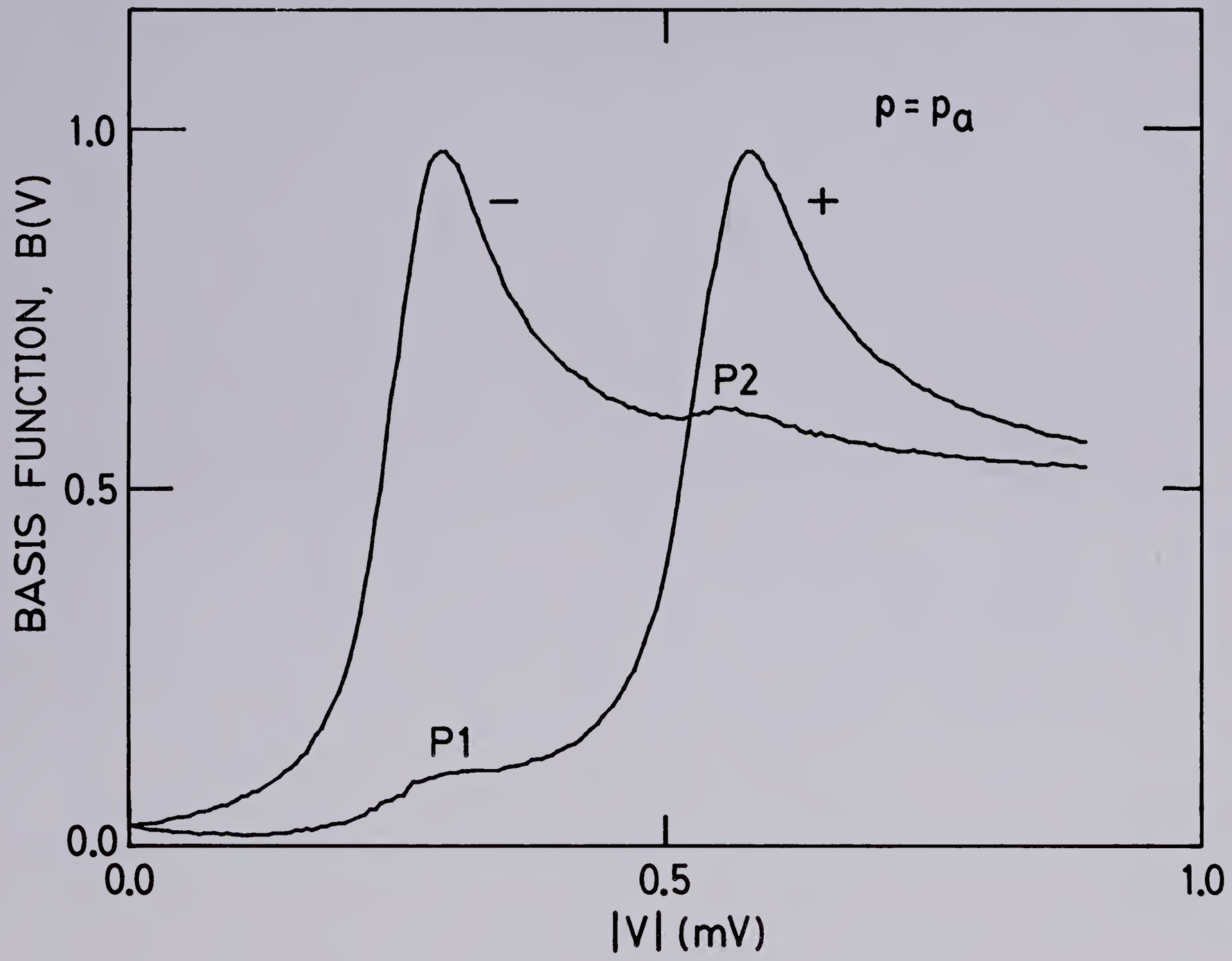
p = pa
1.0
0.5
0.0
BASIS FUNCTION, B(V)
−
+
P2
P1
0.0
0.5
1.0
|V| (mV)

Fig. 4.5

Correct basis function for the tunneling result of Fig. (4.3)

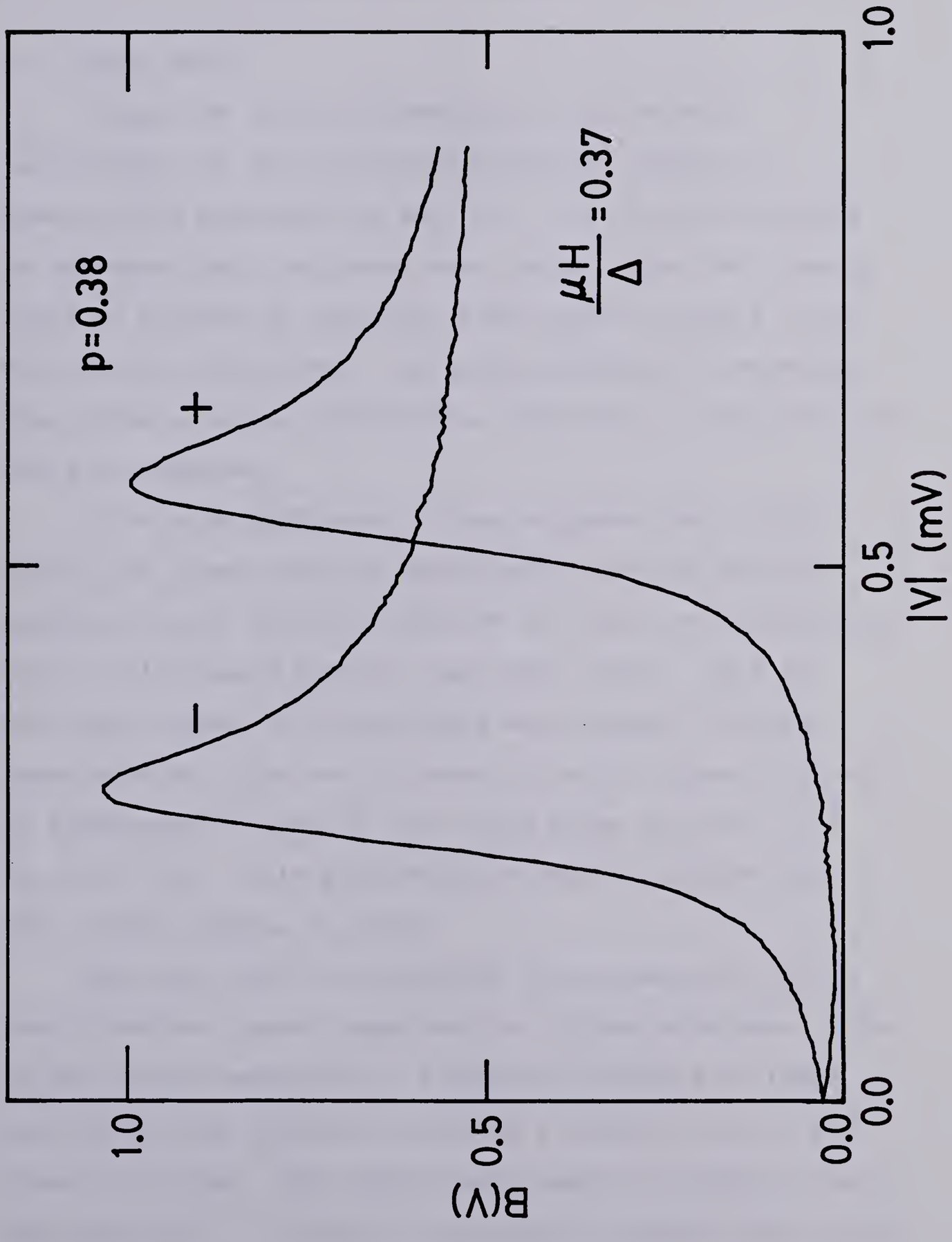
p=0.38
+
−
$\frac{\mu H}{\Delta}$ =0.37
B(V)
1.0
0.5
0.0
0.0
0.5
1.0
|V| (mV)

CHAPTER 5.

EXPERIMENTAL RESULTS

5.1 Early Work

It was the initial intention of this work to investigate the spin polarized tunneling theory of Stearns [74] described in sec. 2.6. If the polarization is dependent upon the Fermi wave vector, then this theory could be studied by tunneling from single crystals of Ni with known orientations. By using different Ni crystals the crystallographic directional dependence of polarization would be examined.

To do this experiment it was proposed that single crystal Ni films would be epitaxially grown on Si substrates, the Ni would be oxidized and then the superconducting Aℓ film would form the top cover layer. Work by Wray and Prutton [87] and Charig and Skinner [15] has shown that Ni films can be grown by vapour deposition onto Si substrates so that Ni (110) face grows parallel to Si (111) face. This step would be used to produce the thin single crystal Ni films.

The first step to accomplish this experiment was to grow Ni-NiO-Aℓ tunnel junctions on a glass substrate. The Ni was vapour deposited to a typical thickness of 1000A and the NiO was thermally grown in a furnace with O_2 gas flowing through. The temperatures used for oxidation were from 100-350°C. It was not possible to produce good tunnel

junctions using this procedure.

Fig. (5.1a) shows a scanning electron micrograph of a Ni film deposited on a glass substrate. The Ni surface is extremely smooth. The rough area in the upper half of the picture is a dust grain on the film surface. Fig. (5.1b) shows a Ni film on a glass substrate that has been oxidized at 350°C for one hour. The film is no longer smooth but contains many whiskers and hillocks. Chaudhari and others [16,28,41,42,65] using different metals have found that thermal cycling can lead to hillock growth in films.

Fig. (5.2a) shows a tunnel junction formed using the sequence Ni-NiO-Aℓ. It can be seen that the hillocks and whiskers that grow due to the heating of the Ni film are large enough that they pierce the oxide and the Aℓ cover layer making these films unsuitable for tunneling work.

The oxidation procedure was then changed so that no thermal cycling would occur. The NiO was formed using a glow discharge as described in sec. (3.1). Fig. (5.2b) shows a Ni-NiO-Aℓ junction where the NiO was formed using the glow discharge technique. It can be seen that there is some structure in the photograph but these bumps and scratches are from the thin vapour deposited films conforming to the contours of the glass substrate and not from hillock growth.

The next step to obtain spin polarized tunneling

Fig. 5.1

Scanning electron micrographs:

a) Ni film deposited on a glass substrate at room temperature (rough area in the upper half of the picture is a dust grain).

b) Ni film deposited on a glass substrate that has been oxidized at 350°C for one hour.

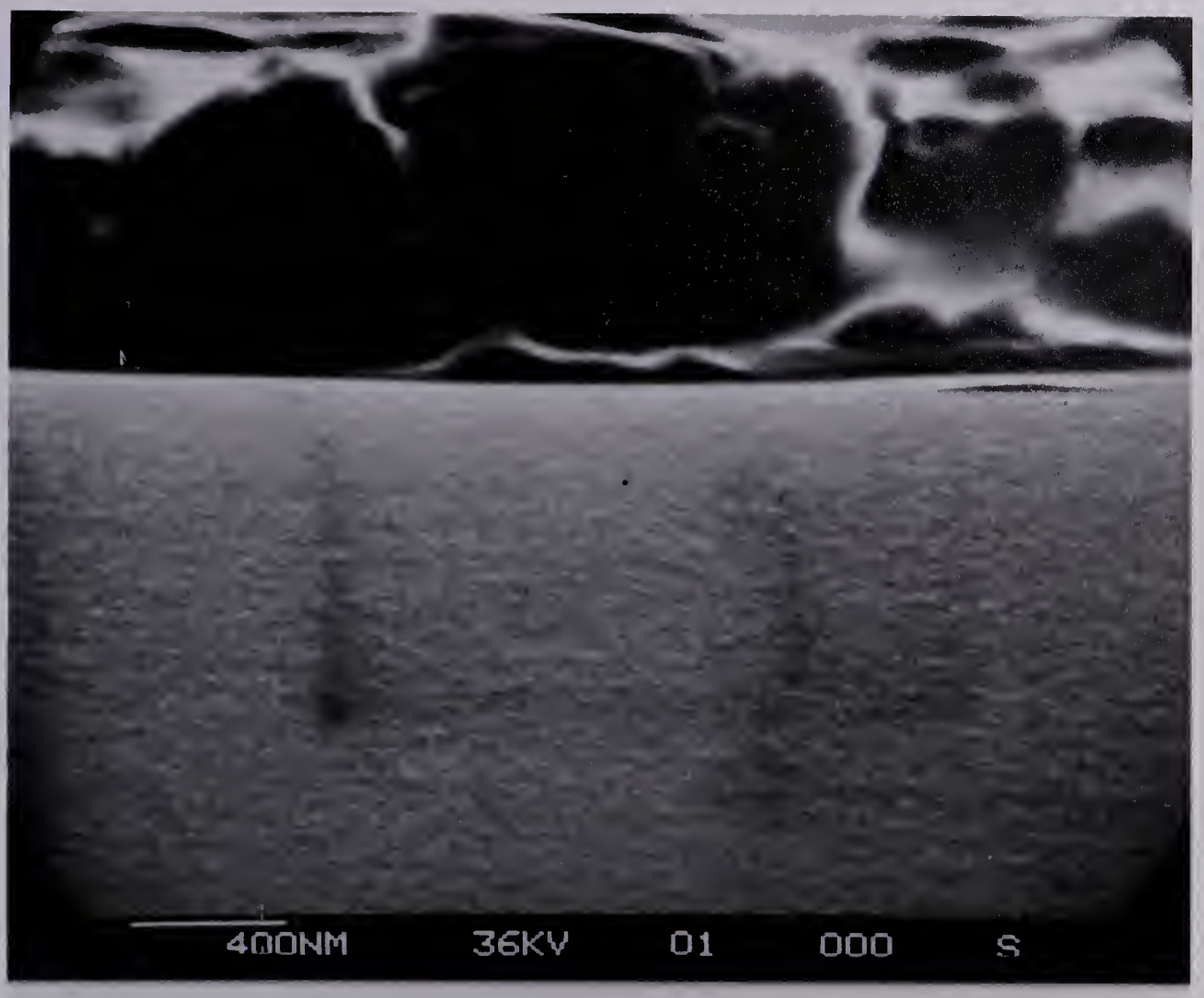
400NM 36KV 01 000 S

2UM 36KV 02 006 S

Fig. 5.2

Scanning electron micrographs

a) Ni-NiO-Aℓ tunnel junction NiO formed by thermal oxidation

b) Ni-NiO-Aℓ tunnel junction NiO formed by a glow discharge.

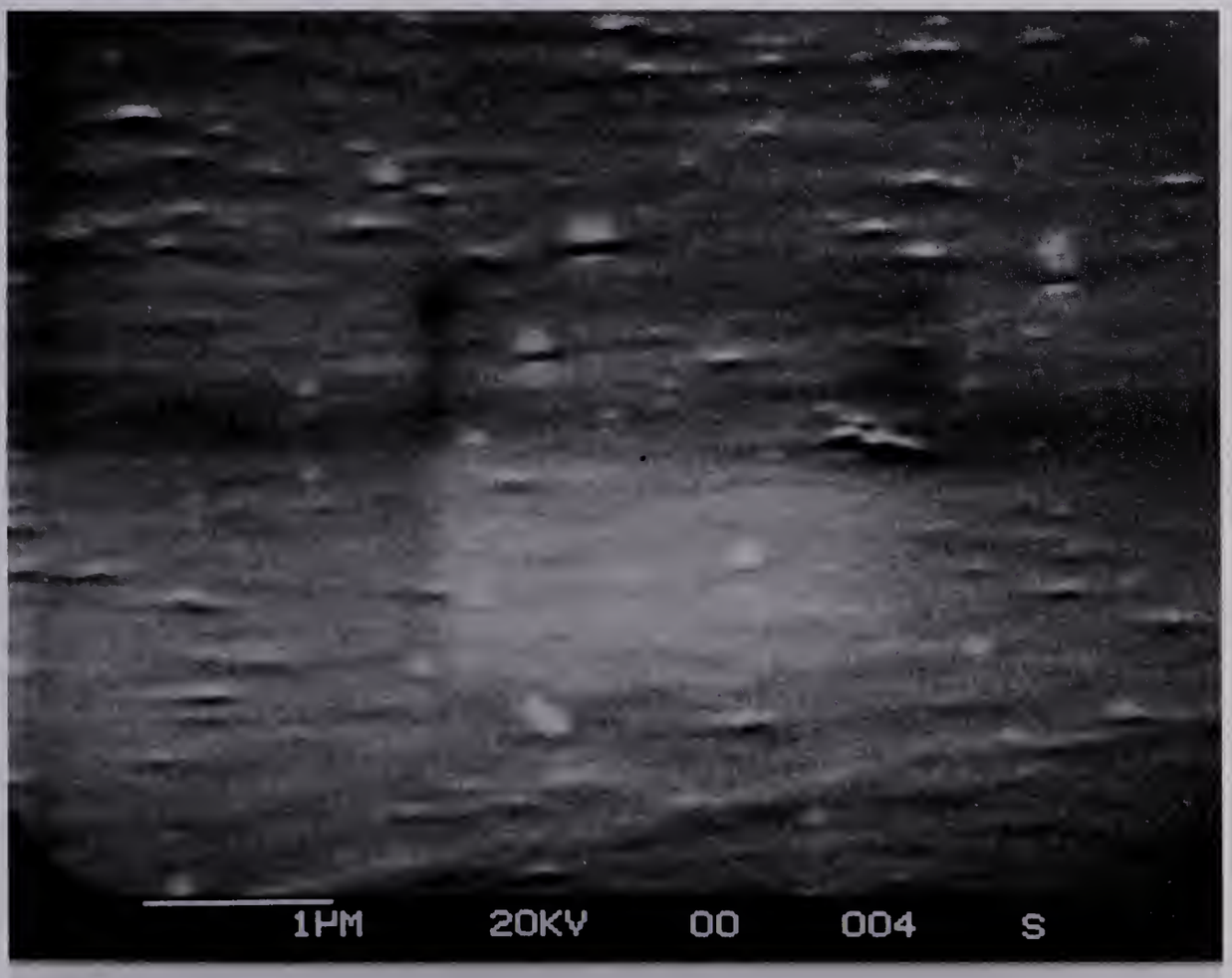
1μM 20KV 00 004 S

400NM 20KV 28 001 S

results was to replace the Aℓ film (~300A) with an ultra-thin Aℓ film (~40A). To do this the glass substrate must be cooled to liquid nitrogen temperatures. Again it was found that good junctions could not be made. Fig. (5.3) shows a Ni film that has been cycled from room temperature, to liquid nitrogen temperatures to deposit the Aℓ, and back to room temperature. The thermal cycling on the glass substrate has caused cracking of the Ni film. When a Si substrate was used instead of a glass substrate the cracking of the Ni film no longer occurred. At this stage we were able to fabricate Ni-NiO-Aℓ junctions on Si substrates, but it was found that NiO proves unsatisfactory as a barrier for this type of experiment because it drastically depairs the superconducting density of states of the Aℓ film and makes spin polarized tunneling experiments impossible. Fig. (5.4) shows a typical conductance trace (solid line) of a Ni-NiO-Aℓ tunnel junction on a Si substrate. The energy gap is drastically reduced from what is expected for an Aℓ film (broken line). This result has also been recently reported by Meservey et al. [60].

The focus of the work was then changed to try to produce an $Aℓ_2O_3$ barrier on top of the Ni electrode. The procedure that was followed was that from one to three thin, non-continuous layers of Aℓ were separately deposited and oxidized using a glow discharge, to form the $Aℓ_2O_3$ tunneling barrier. In the initial stages of this work Pb was

Fig. 5.3

Scanning electron micrographs of a Ni film that has been cycled from room temperature, to liquid nitrogen temperature, and back to room temperature.

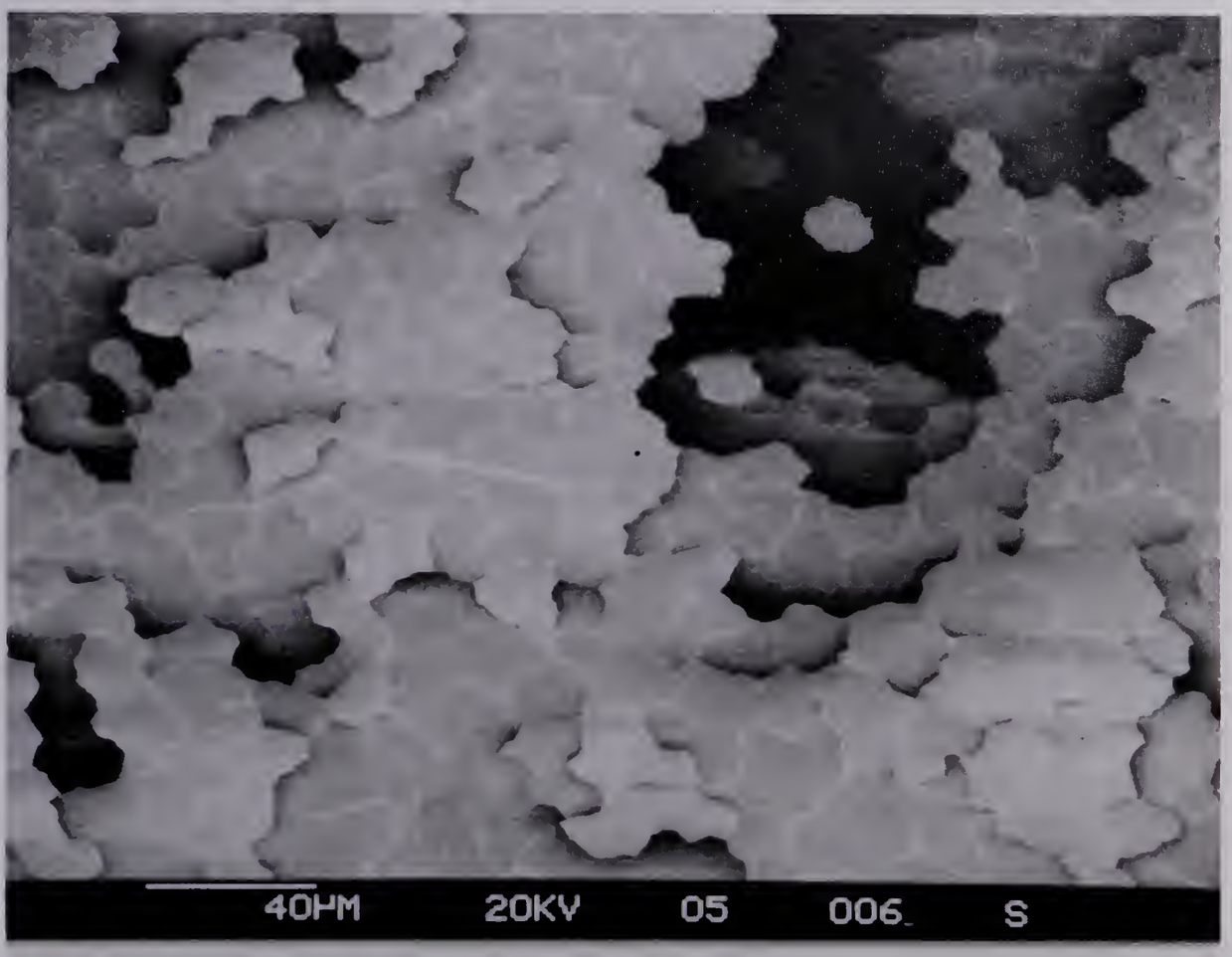
40µM 20KV 05 006 S

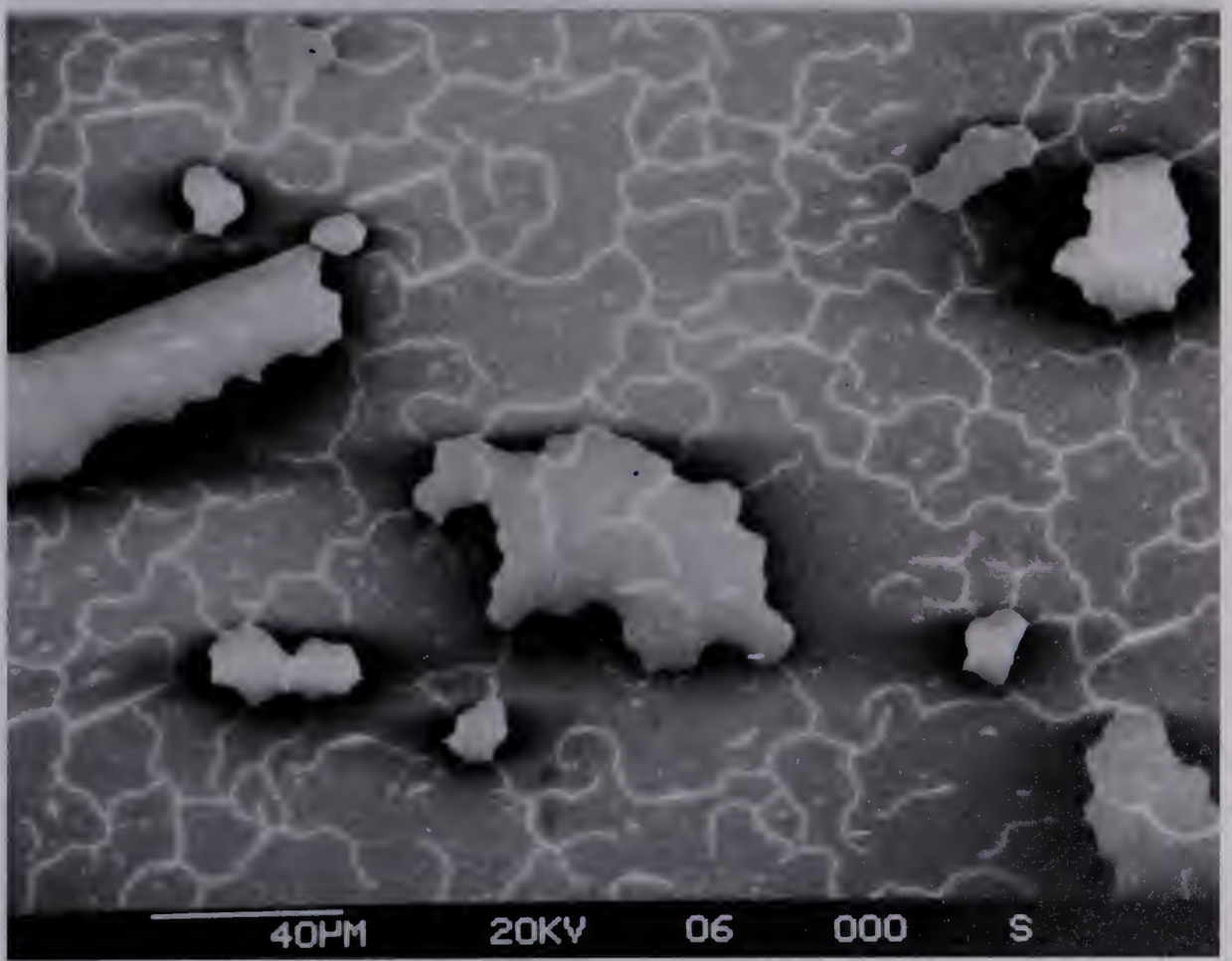
40µM 20KV 06 000 S

Fig. 5.4

A typical conductance trace (solid line) of a Ni-NiO-Aℓ tunnel junction on a Si substrate (T ~ 50 mK). The energy gap is drastically reduced from what is expected for an Aℓ film (broken line).

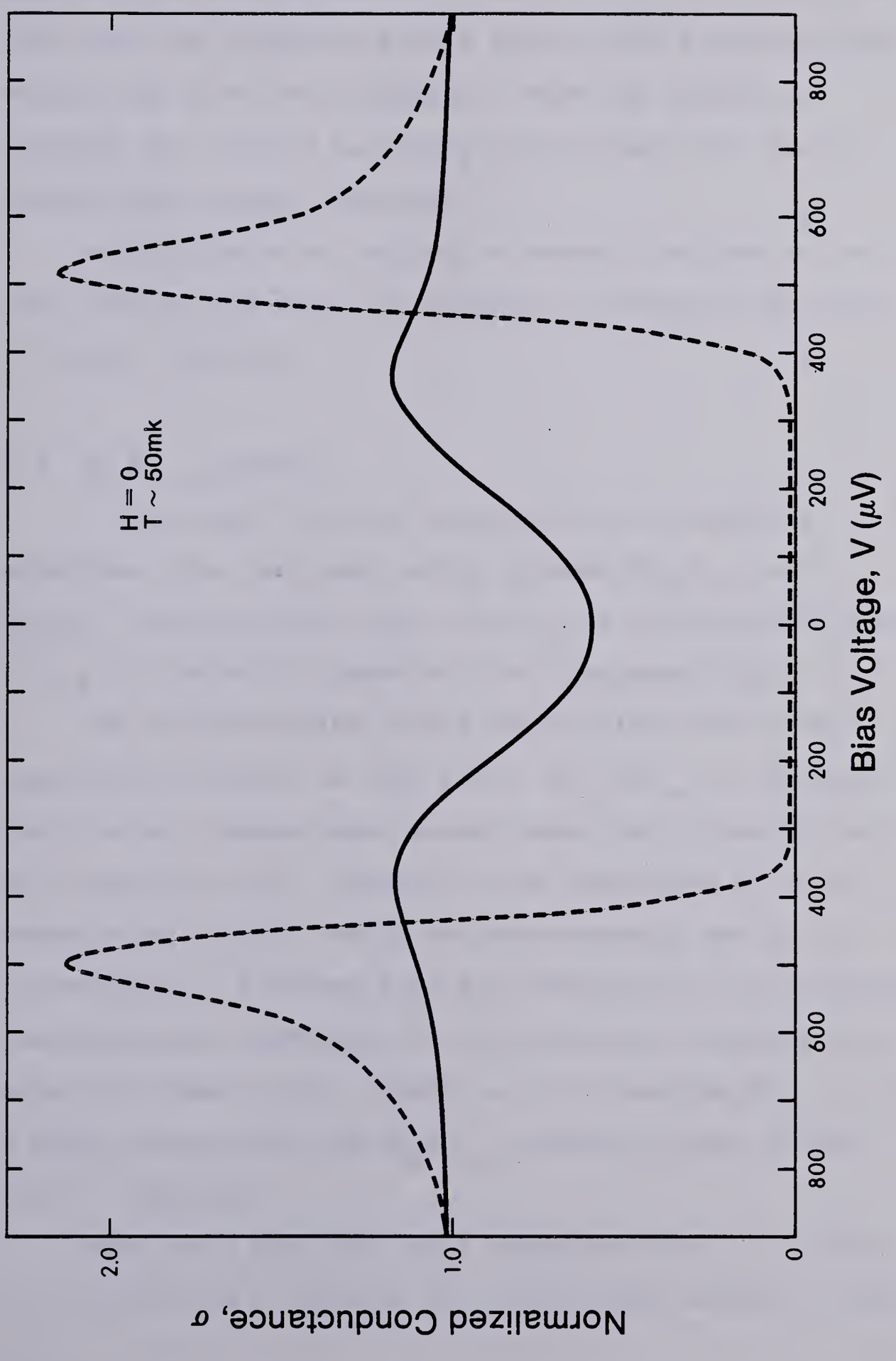
H = 0
T ~ 50mk
Normalized Conductance, σ
Bias Voltage, V (μV)
2.0
1.0
0
800
600
400
200
0
200
400
600
800

used as the cover electrode. Good Ni-$A\ell_2O_3$-Pb junctions were made and tunneling traces showing the superconducting energy gap of Pb were obtained. When the formation sequence was changed to Ni-$A\ell_2O_3$-$A\ell$ we were not able to produce good tunnel junctions.

At this point we decided to change the focus of our work, and we abandoned our efforts to produce Ni-barrier-$A\ell$ tunnel junctions.

5.2 Mn_xSb_{1-x} system

In this work the spin polarization of tunneling electrons from the binary alloy systems Mn_xSb_{1-x} and Mn_xSn_{1-x} were measured over the full Mn concentration range $0 \leq x \leq 1$. The Mn-Sb system will be discussed first.

The ferromagnetism of the Mn-Sb alloys was first reported by Heusler in 1903 [38]. $Mn_x\ Sb_{1-x}$ is ferromagnetic at all compositions except those very close to pure Mn or pure Sb [10]. Neither of the components is ferromagnetic by itself. Mn is antiferromagnetic and Sb is non-magnetic. Williams [85] and Wedekind [83] investigated the system and concluded two stoichiometric compositions exist for these alloys - MnSb ($x = 0.5$) and Mn_2Sb ($x = 0.67$). A phase diagram for the Mn_xSb_{1-x} system is shown in Fig. (5.5). [33,35].

MnSb has a NiAs (B8) type structure with a = 4.128A, c = 5.789A, c/a = 1.402 at x = 0.5 [77,86] see Fig. (5.6a).

Fig. 5.5

Phase diagram of the Mn_xSb_{1-x} system.

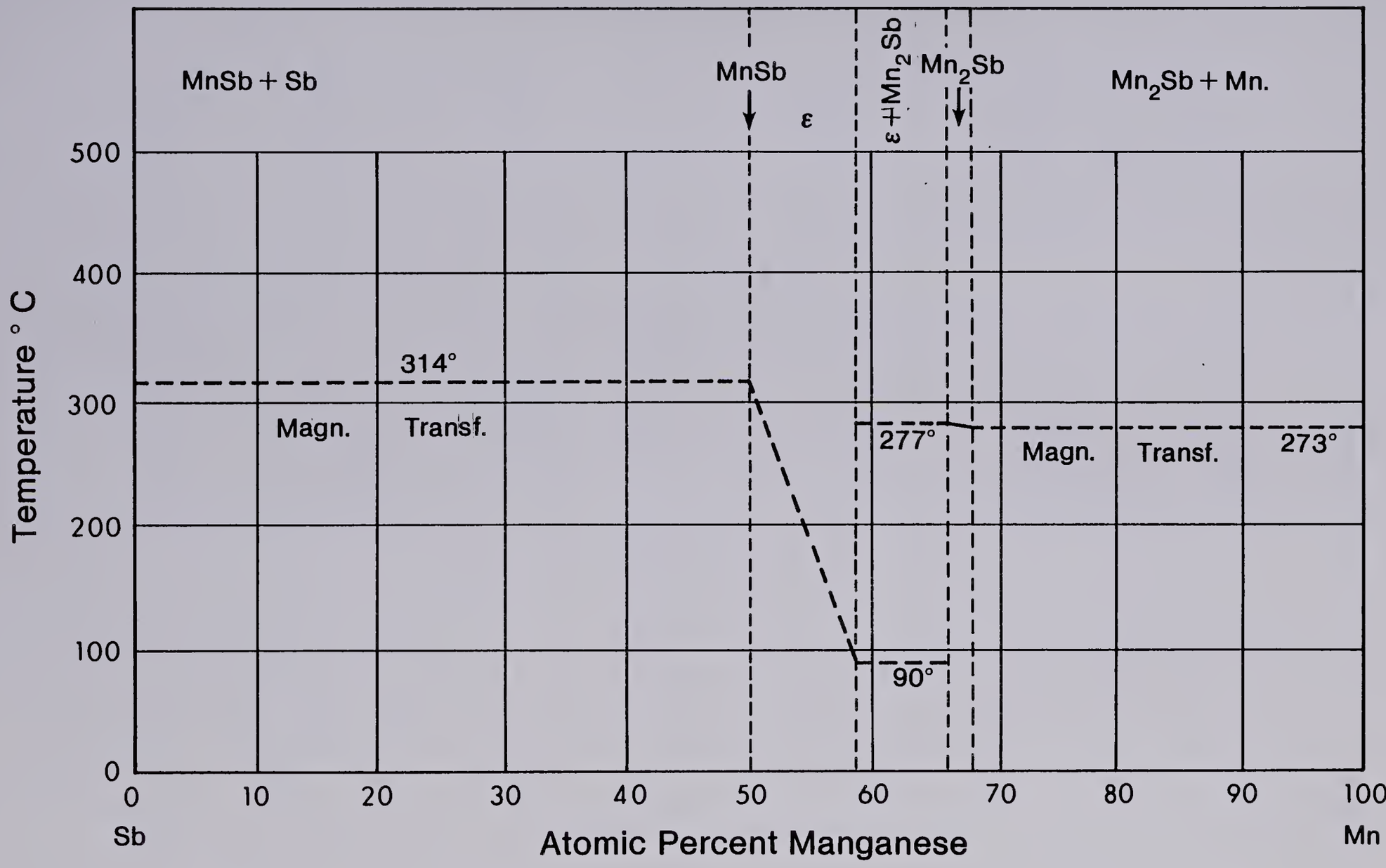
MnSb + Sb
MnSb
ε
ε + Mn2Sb
Mn2Sb
Mn2Sb + Mn.
314°
Magn.
Transf.
277°
Magn.
Transf.
273°
90°
Temperature ° C
500
400
300
200
100
0
0
10
20
30
40
50
60
70
80
90
100
Sb
Atomic Percent Manganese
Mn

Fig. 5.6

(a) Crystal structure of MnSb

(b) Crystal structure of ε phase

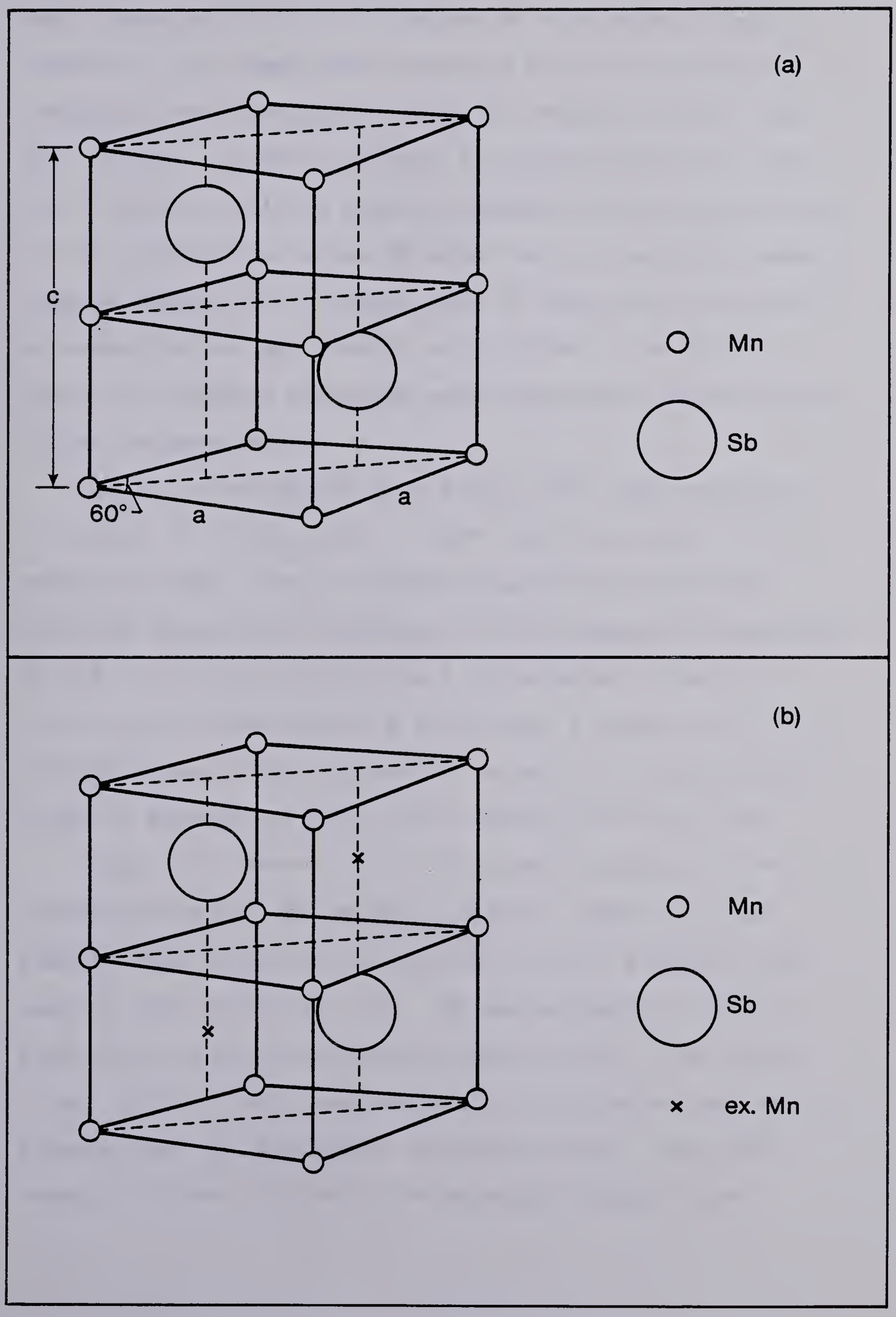
(a)
c
60°
a
a
Mn
Sb
(b)
Mn
Sb
ex. Mn

The ε phase of Fig. (5.5), on the Mn rich side of MnSb, consists of the same MnSb structure with the excess Mn occupying the interstitial sites at random ([88-90], see Fig. (5.6b)). MnSb is present in alloys from about 0-60 at. % Mn and carries a magnetic moment of 3.53 μ_B/Mn atom. In the ε phase the excess Mn atoms have no magnetic moment amongst themselves, although they do cause some reduction of magnetization per formula unit [88-90]. In this ε phase the magnetic moment/Mn atom decreases linearly with the Mn concentration.

Mn_2Sb is tetragonal with Cu_2Sb (C38) type structure, a = 4.06A, c = 6.57A, c/a = 1.606 ([34], see Fig. (5.7)). Manganese atoms occupy crystallographically different sites in this crystal resulting in ferrimagnetic behaviour. In Fig. (5.7) Mn atoms at the A sites have a moment of -3.87 μ_B and those at the B sites have a moment of 2.3 μ_B [37,84] giving a net saturation value of 0.94 μ_B/Mn atom. Mn_2Sb is present in alloys from about 60-100 at. % Mn.

Fig. (5.8) shows a plot of magneton number, n, vs. concentration for the Mn_xSb_{1-x} system. These data are adapted from Guillaud [33] and are for well annealed bulk samples from 45-75 at. % Mn. No magnetization data are available for Mn concentrations below 45 at. % or above 75 at. %, but Curie Temperature data indicate that MnSb is present down to very low Mn concentrations. The graph contains curves for both n/Mn atom and n/alloy atom.

Fig. 5.7

Crystal structure of Mn_2Sb

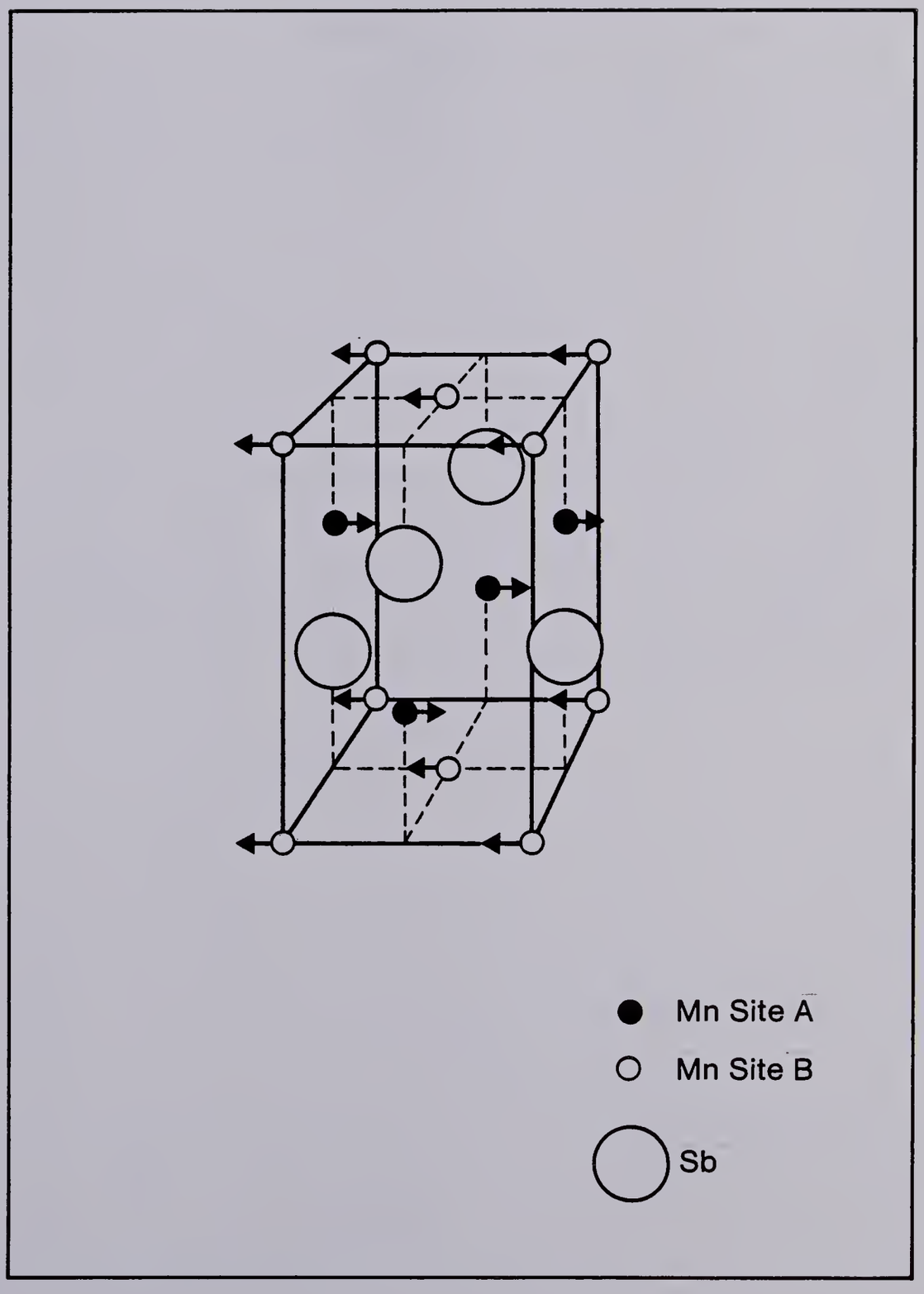
Mn Site A
Mn Site B
Sb

Fig. 5.8

Spin polarization results compared to bulk magnetization data of Guillaud [33].

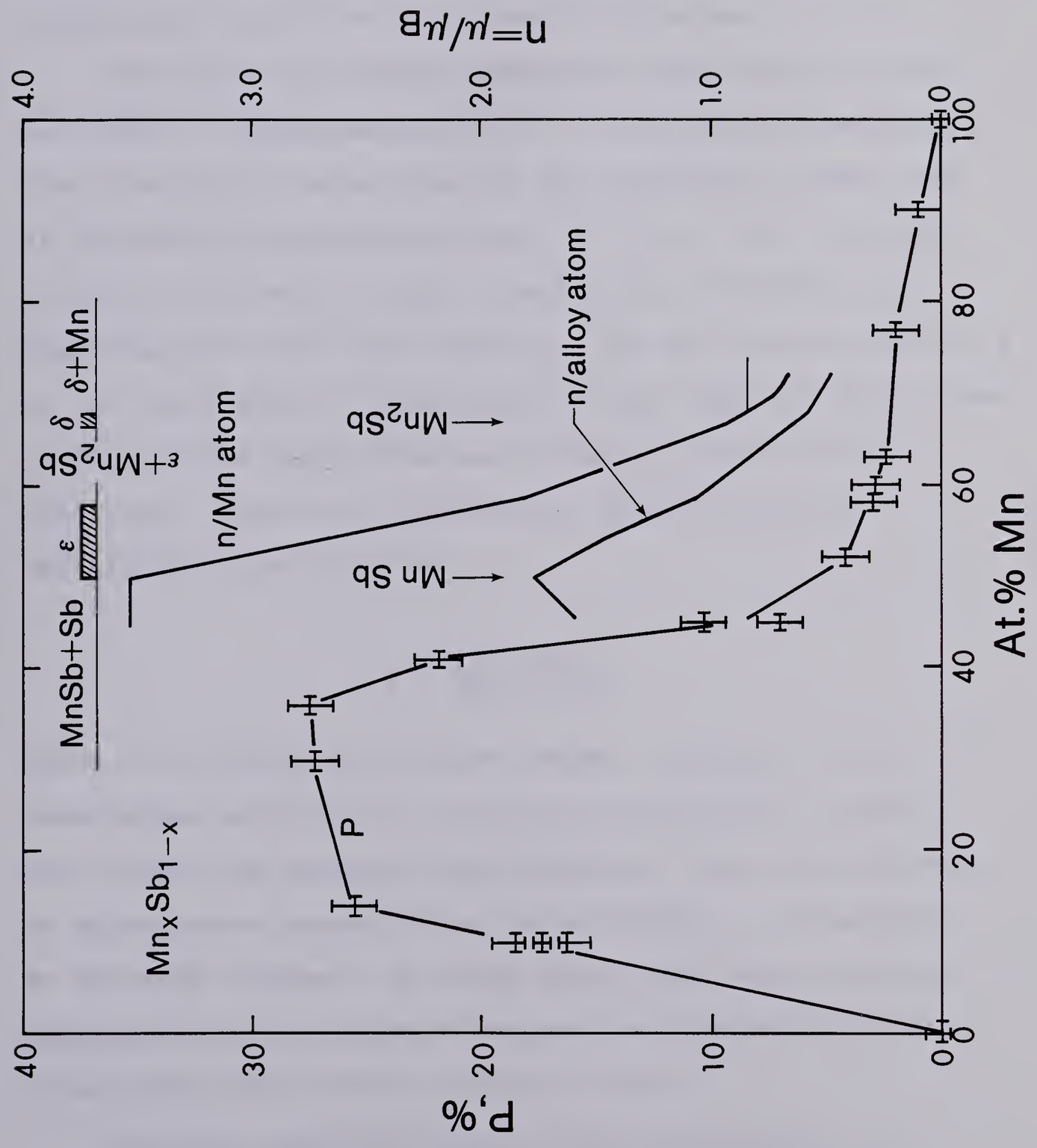
n=μ/μB
P,%
At.% Mn
n/Mn atom
n/alloy atom
Mn2Sb
Mn Sb
MnSb+Sb
ε
ε+Mn2Sb
δ δ+Mn
MnxSb1−x
P

The techniques used to measure thin film composition (Sec. 3.2) give an average composition over the entire thickness of film and would not indicate if a different composition existed at the junction interface.

The tunneling results themselves would seem to indicate that at approximately 40 at. % Mn indicated concentration, the alloy composition at the interface is MnSb, and at indicated concentrations down to 15 at. % Mn, regions of MnSb still occur at the interface and tunneling is predominately into these regions. For the region 0-15 at. % Mn the rapid drop in polarization would indicate large areas of Sb now form the predominant tunneling areas at the interface. These last conclusions follow from the definition of polarization,

$$P = \frac{(\eta\uparrow - \eta\downarrow)}{(\eta\uparrow + \eta\downarrow)} ,$$

where η is tunneling electron number. Anything which contributes unpolarized electrons to the tunnel current will reduce the measured polarization. The rapid decrease of polarization beyond 40 at. % Mn evidently corresponds to the bulk ε phase. It would appear that the interface compositions of the thin films used in this work follow closely the bulk phases of Mn-Sb alloys.

From the tunneling data the spin polarization of electrons tunneling from MnSb is approximately 25% after correcting for spin-orbit scattering in the Al film. This

yields $P/n_{mn} \simeq 7\%$ where n_{Mn} is magneton number per Mn atom. The corresponding ratio for the Fe-group elements and their alloys is $P/n \simeq 20\%$ [64], where n is per alloy atom for the alloys. For the heavy rare earth metals $P/n_{CE} \simeq 20\%$ [58], where n_{CE} is per conduction electron. In this case the atoms carry a considerable localized moment and for Gd, $P/n_{GD} \simeq 2\%$ where n is per Gd atom. MnSb appears to be somewhat intermediate between the Fe group elements and the heavy rare earth metals in its spin polarized tunneling behaviour.

One would like to draw some kind of inference or conclusion from the observed spin polarization value for MnSb. Since spin polarized tunneling is a relatively new experimental tool which is not in itself completely understood, it is not possible to say anything definitive about the present result at this time. However, it is possible to look for some degree of systematic behaviour in relation to the 3-d ferromagnets. The saturation magnetizations per alloy atom of Cr-Fe, Fe-Co, Co-Ni, and Ni-Cu alloys fall on the triangular shaped Slater-Pauling curve when plotted as a function of position in the periodic table. Mn lies between Cr and Fe, but it does not form a ferromagnetic alloy with Fe or Cr. Mn by itself is an antiferromagnet. This led Bethe [10] to suggest an interaction curve where the exchange interaction swings from negative (antiferromagnetic) to positive with increasing interatomic spacing. MnSb then becomes a ferromagnet because the Sb

atoms space the Mn atoms further apart to give a positive exchange interaction. But the alloy is not part of the Slater-Pauling sequence because Sb is too far removed in the periodic table. The Slater-Pauling curve may be understood as a filling-up process in a rigid band model. The 3d band is first split by the exchange interaction and then filled with electrons as one moves from left to right along the periodic table. It is thought that spin polarized tunneling may be sampling itinerant 3d electrons, and the early tunneling results of Meservey et al. did in fact follow the Slater-Pauling curve quite accurately, with a polarization ratio of 20% per Bohr magneton number. However, the early work was done with laboratory-air oxidized tunnel barriers. Subsequent work in the laboratory with glow discharge oxidized barriers and by Meservey's group [61] with glow discharge barriers and also with deposited alumina barriers has raised the polarization to about 40% per magneton number at the Ni end of the curve, and left the Fe end unchanged. For MnSb we have from the neutron scattering work of Yamaguchi et al. [88-90] that the Sb atoms carry no magnetic moment; the magneton number is then 3.55 per Mn atom and the polarization ratio is 7% per magneton number. This polarization ratio is considerably smaller than the values given above for the 3d ferromagnets, and it suggests that some of the moment carried by the Mn atoms may be localized. Alternately, the low polarization may be simply a dilution effect due to some tunneling of

unpolarized electrons from the Sb atoms. Ferromagnetism is like a jig-saw puzzle where many pieces have been fitted together to be suggestive of a picture, but where there are also large gaps. To fill in the gaps one needs more pieces of experimental data from experiments which must be different from those done in the past. The result from here is of that type, and hopefully it will eventually tie in with other findings to give a better picture of ferromagnetism.

5.3 Mn_xSn_{1-x} System

Heusler [38] was also the first to investigate and find ferromagnetism in the Mn-Sn system. The magnetic properties of the alloys of this system have been studied by several authors but the results are not in agreement. Early work by Williams [85], Potter [66], and Guillaud [33] pointed to the existence of 3 stoichiometric compounds in the Mn_xSn_{1-x} system: MnSn ($x = 0.5$), Mn_2Sn ($x = 0.67$), and Mn_4Sn ($x = 0.8$). Later work by Hanson [35] and Singh [71] (see Fig. (5.9)) indicated that Mn_4Sn was misidentified and the phase that forms is Mn_3Sn. Also the intermediate phase richest in Sn is $MnSn_2$, not MnSn. The three authors also disagreed on which phases are ferromagnetic. Williams concluded that all 3 phases exhibited ferromagnetism and alloys from 14-96 at. % Mn were ferromagnets. Potter thought only 2 phases were ferromagnetic

Fig. 5.9

Phase diagram of Mn_xSn_{1-x} system

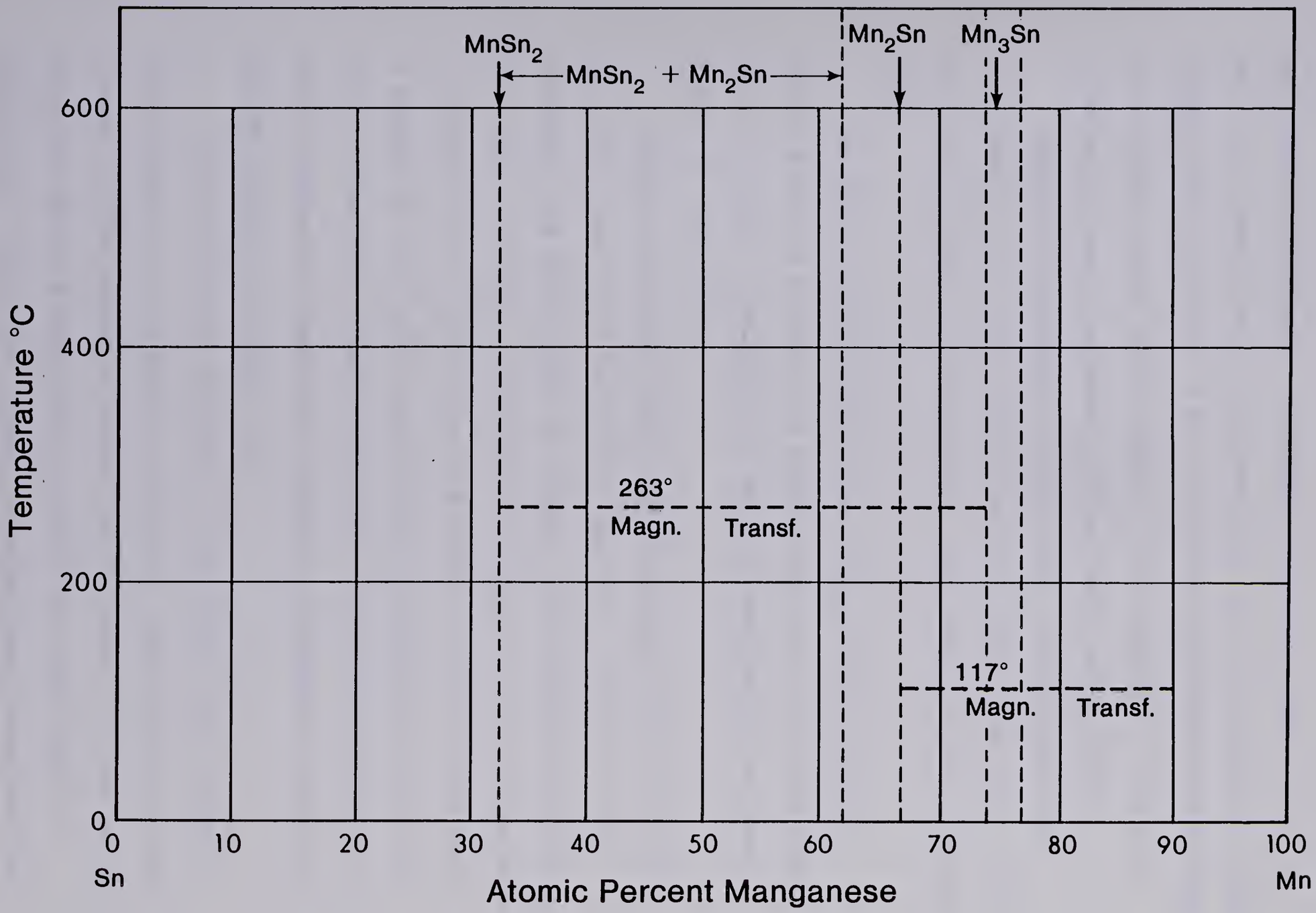
MnSn2
MnSn2 + Mn2Sn
Mn2Sn
Mn3Sn
600
400
200
0
Temperature °C
263°
Magn.
Transf.
117°
Magn.
Transf.
0
10
20
30
40
50
60
70
80
90
100
Sn
Mn
Atomic Percent Manganese

and the ferromagnetic existence region was from 35-97 at. % Mn. Guillaud's work indicates only one ferromagnetic phase exists from 12-78 at. % Mn. The vast discrepancies between the various works would appear to be connected with the effects of heat treatment on the atomic arrangement.

$MnSn_2$ is tetragonal of the $CuAl_2$ (C16) type with a = 6.659A, c = 5.436A and c/a = 0.816 [91] (see Fig. (5.10a)). Antiferromagnetic behaviour has been found in this compound [91].

Mn_3Sn is a hexagonal Ni_3Sn (DO_{19}) type structure [62,91] with a = 5.66A, c = 4.52A, and c/a = 0.79 [62] (see Fig. (5.10b)). Evidence of antiferromagnetism has been found in this alloy.

Mn_2Sn is of NiAs (B8) type structure with a = 4.37A, c = 5.47A, and c/a = 1.25 [62] (see Fig. (5.11)). This compound has been found to exhibit ferrimagnetic behaviour [2,3,91]. In Fig. (5.11) the Mn atoms at the A sites have a moment of 3.5 μ_B/Mn atom and those at the B sites have a moment of 2.2 μ_B/Mn atom but in the opposite direction [2,3]. Over the composition range from about 60-65 at. % Mn the magnetic moment per molecule decreases linearly as the Mn content increases [3].

In the previous section it was shown that the spin polarization of the Mn-Sb system was approximately proportional to the magnetic moment per Mn atom. It was expected that the Mn-Sn system would exhibit the same type of behaviour. Thin film tunneling experiments were carried

Fig. 5.10

(a) Crystal structure of $MnSn_2$

(b) Crystal structure of Mn_3Sn

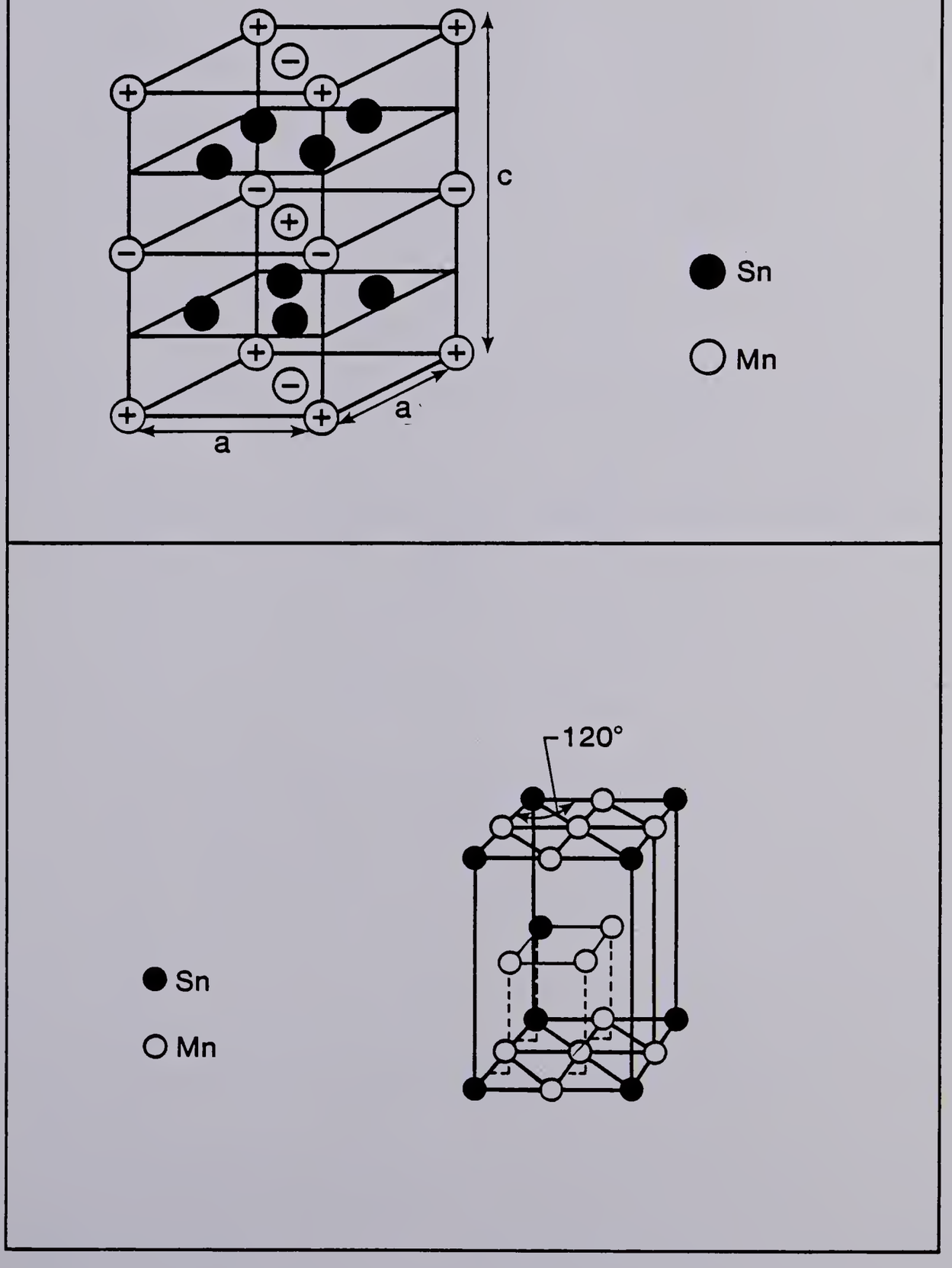
c
a
a
Sn
Mn
120°
Sn
Mn

Fig. 5.11

Crystal structure of Mn_2Sn. Mn atoms at the A sites have a moment of 3.5 μ_B.

Mn atoms at the B sites have a moment of 2.2 μ_B.

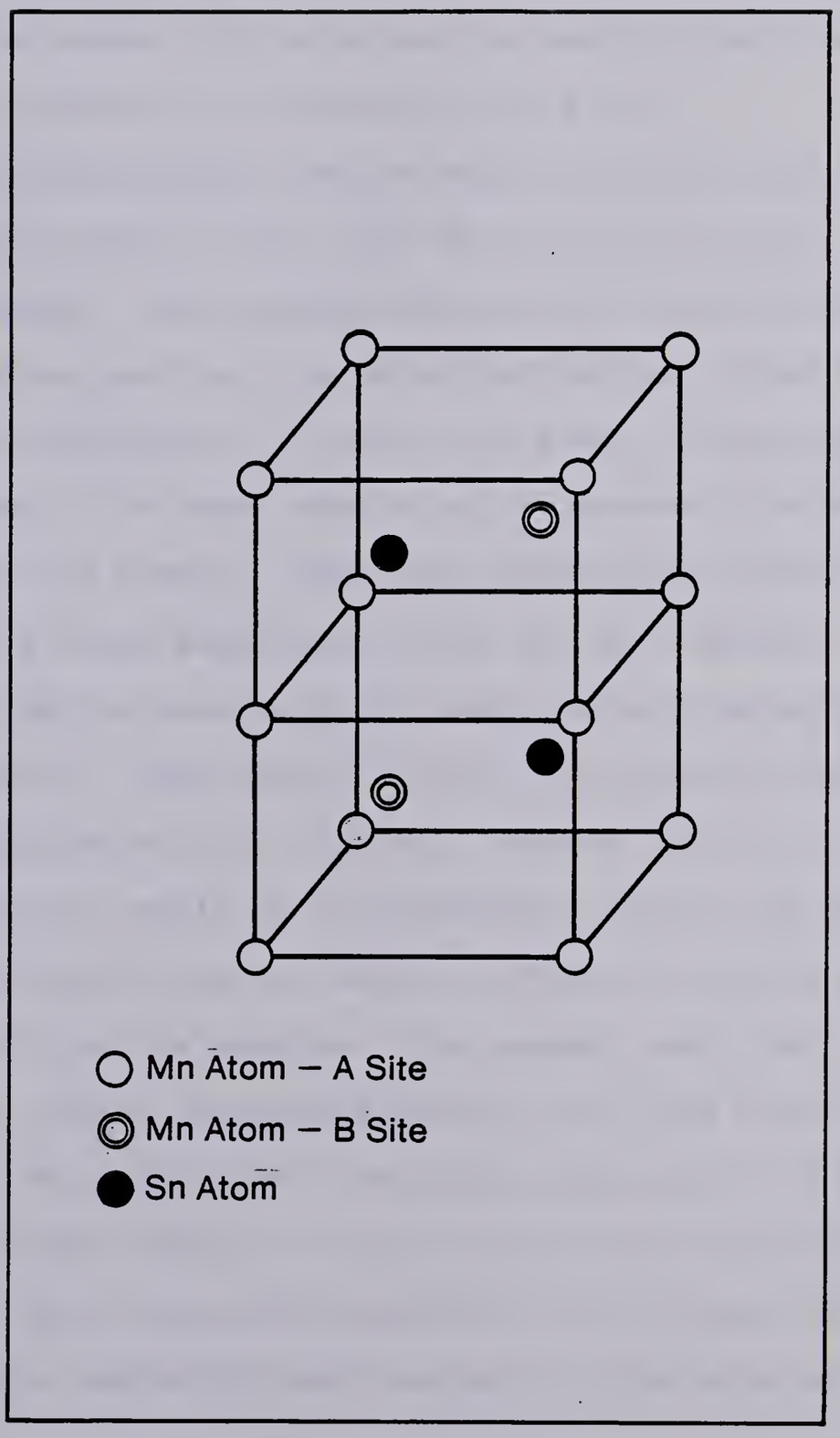
Mn Atom – A Site
Mn Atom – B Site
Sn Atom

out over the full range of compositions of the Mn-Sn system. Table (5.1) shows the results of this work. As this table shows a 0% polarization was obtained for all samples studied in the course of this work.

The polarization results would indicate that the first few atomic layers of the thin Mn-Sn films are non-ferromagnetic. Two attempts were made to see if the thin film samples used in this experiment showed other ferromagnetic properties. In the first test a vibrating-sample magnetometer [26] was used to try to measure the magnetic moment of the sample. When bulk Mn-Sn alloys were prepared by melting known quantities of Mn and Sn together, ferromagnetic metals were made and their moments detected by the magnetometer. When the thin Mn-Sn film samples were tried no ferromagnetism was detected. However, thin Ni films were also tried and again no ferromagnetic signal was detected. The magnetometer was not able to detect the small signals from the thin film samples. The second test that was used to try to detect ferromagnetism in the films involved floating the samples off the glass substrate in a dish of water and then seeing if the film would be attracted to a magnet. This test proved positive for Ni films, but again the results indicated that the Mn-Sn films were not ferromagnetic.

In summary, the magnetometer and magnet tests showed that bulk Mn-Sn alloys were ferromagnetic. The polarization results implied that the first few deposited layers of

Table 5.1

Spin Polarization Data for the Mn-Sn System

Sample	at. % Mn	Polarization %
108	0	0
563	30	0
562	50	0
527	57	0
531	60	0
528	63	0
546	64	0
559	66	0
525	74	0
526	79	0
500	100	0

the thin films were non-ferromagnetic and the magnet test confirmed this result for the bulk of the film.

Yamaguchi et al. [91] have done heat treatment experiments on the ferrimagnetic alloy Mn_2Sn. They have found that the hexagonal structure was modified in the course of the heat treatment and as the structure was modified the magnetic behaviour as indicated by the Curie temperature and the magnetic moment per molecule changed.

As mentioned above, in early work done on this system, several authors presented conflicting reports on the ferromagnetic existence region of these alloys. Their work seems to indicate that heat treatment of the samples is the factor which is responsible for the discrepancies. Our own work shows that bulk samples formed from melting the two metals together in a resistance heated boat produces ferromagnetic alloys. The thin film alloys used in this work were deposited by vacuum evaporation onto a glass substrate at room temperature. The alloys were not subjected to heat treatment. The results indicate that for ferromagnetism to occur in Mn-Sn alloys heat treatment must take place which affects the atomic arrangement and a magnetic ordering takes place.

CHAPTER 6

SUMMARY AND CONCLUSIONS

6.1 Conclusions

In this thesis we have reported on the results of spin polarized tunneling studies done on the alloys of the Mn-Sb and Mn-Sn systems. At the outset we were trying to determine if ferromagnetic alloys formed from non-ferromagnetic metals would show properties similar to the 3d ferromagnets and their alloys. We were trying to determine if the electron spin polarization of these alloys was proportional to the magnetic moment per atom of alloy.

In the Mn-Sb system we discovered that the electron spin polarization was approximately proportional to the magnetic moment per Mn atom and not the magnetic moment per alloy atom. The spin polarization of MnSb is approximately 25% and $P/n_{Mn} \simeq 7\%$.

It appears that the first few atomic layers, from which electrons tunnel in thin films of MnSb, are richer in Mn than the rest of the film. The tunneling work would also seem to indicate that thin Mn-Sb films form phases very similar to the known phase diagram for bulk material.

In the Mn-Sn system we found no evidence of a ferromagnetic thin film alloy. Our work did show that ferromagnetism existed in bulk Mn-Sn samples, but there was no proof that the thin Mn-Sn films were ferromagnetic. All work on Mn-Sn alloys seems to indicate that heat treatment of the

alloys is a requirement for the onset of ferromagnetism.

The spin polarized tunneling technique was also used to determine a value for the spin-orbit scattering parameter of the superconducting Aℓ films used in this work, $b \simeq 0.08$.

6.2 Suggestions for Further Work.

Recently Moodera et al. [61] have proposed a method to produce artificial tunnel barriers by depositing electron beam evaporated sapphire on substrates cooled to near 77 K. Using this method they were able to make Ni-$A\ell_2O_3$-Aℓ tunnel junctions. Tunnel junctions produced with this type of artificial barrier deposited over epitaxially grown single crystal films of Ni could be used to study the crystallographic dependence of electron spin polarization as predicted by the Stearns theory of sec. 2.6.

The artificial barriers could also be used to produce Mn_xSn_{1-x}-$A\ell_2O_3$-Aℓ tunnel junctions to study the effects of heat treatment on Mn-Sn films. The thin alloy films could be subjected to heat treatment before deposition of the barrier to see if such treatment would produce a ferromagnetic film.

The Mn-Sb results leave questions as to the formation of the thin alloy films by evaporation from separate sources. Work is needed on alloy film formation. The tunneling results imply a Mn rich surface region and they also offer evidence for the thin films forming phases the

same as bulk alloy samples. Experimentation is needed to confirm the phase structure of these films and analysis of the nucleation and growth processes of alloy films formed by evaporation from two separate sources is needed for a better understanding of these results.

BIBLIOGRAPHY

[1] R. Anton, M. Harsdorff, and Th. Martens. Nucleation and growth of binary alloys on substrates. Thin Solid Films 57, 233 (1979).

[2] M. Asanuma. Magnetic properties of B8 type compounds in manganese-tin system. J. Phys. Soc. Japan 16, 1265 (1961).

[3] M. Asanuma. The magnetic properties of B8 type structure compounds in transition elements-tin systems. J. Phys. Soc. Japan 17, 300 (1962).

[4] U. Bänninger, G. Busch, M. Campagna, and H.C. Siegmann. Photo-electron spin polarization and ferromagnetism of crystalline and amorphous nickel. Phys. Rev. Lett. 25, 585 (1970).

[5] J. Bardeen. Tunnelling from a many particle point of view. Phys. Rev. Lett. 6, 57 (1961).

[6] J. Bardeen, L.N. Cooper, and J.R. Schrieffer. Microscopic theory of superconductivity. Phys. Rev. 106, 162 (1957).

[7] J. Bardeen, L.N. Cooper, and J.R. Schrieffer. Theory of superconductivity. Phys. Rev. 108, 1175 (1957).

[8] K.H. Behrndt. Film-thickness and deposition-rate monitoring devices and techniques for producing films of uniform thickness in *Physics of Thin Films*. Edited by G. Haas and R.E. Thun. (Academic Press Inc., New York 1966). 3, 1 (1966).

[9] D.S. Betts. *Refrigeration and Thermometry Below One Kelvin*. (Sussex University Press, 1976) p. 75.

[10] R.M. Bozorth. Ferromagnetism, p. 334 and references therein. (Van Nostrand, New York, 1951).

[11] R.C. Bruno and B.B. Schwartz. Magnetic field splitting of the density of states of thin superconductors. Phys. Rev. B8, 3161 (1973).

[12] G. Busch, M. Campagna, P. Cotti, and H.C. Siegmann. Observation of electron polarization in photoemission. Phys. Rev. Lett. 22, 597 (1969).

[13] G. Busch, M. Campagna, and H.C. Siegmann. Spin-polarized photoelectrons from Fe, Co, and Ni. Phys. Rev. B4, 746 (1971).

[14] M. Campagna, D.T. Pierce, F. Meier, K. Sattler, and H.C. Siegmann. Emission of polarized electrons from solids in *Advances in Electronics and Electron Physics.* Edited by L. Martin (Academic Press, New York, London, 1976) p. 113.

[15] J.M. Charig and D.K. Skinner. Auger electron spectroscopy of nickel deposits on the silicon (111) surface. Surface Sci. 19, 283 (1970).

[16] P. Chaudhari. Hillock growth in thin films. J. Appl. Phys. 45, 4339 (1974).

[17] G. Chrobok, M. Hofmann, G. Regenfus, and R. Sizmann. Spin polarization of field-emitted electrons from Fe, Co, Ni, and rare-earth metals. Phys. Rev. B15, 429 (1977).

[18] W.J. De Haas, E.C. Wiersma, and H.A. Kramers. Experiments on adiabatic cooling of paramagnetic salts in magnetic fields. Physica 1, 1 (1934).

[19] P. Debye. Einge bemerkurgen zur magnetisierung bei tiefer temperatur. Ann. Phys. 81, 1154 (1926).

[20] D.H. Douglass and L.M. Falicov. The superconducting energy gap in *Progress in Low Temperature Physics.* Edited by C.J. Gorter (North-Holland, Amsterdam, 1964) 4, p. 97.

[21] H. Engler and P. Fulde. The role of spin-orbit scattering in high field superconductor tunneling. Z. Phys. 247, 1 (1971).

[22] H.L. Eschback and W.E. Kruidhof. Vacuum Microbalance Tech. 3, 207 (1965).

[23] T.E. Feuchtwang, P.H. Cutler, and J. Schmidt. Analyses of ESP in ferromagnetic metals I. Surface Sci. 75, 401 (1978).

[24] T.E. Feuchtwang, P.H. Cutler, and J. Schmidt. Analyses of ESP in ferromagnetic metals II. Surface Sci. 75, 490 (1978).

[25] J.C. Fisher and I. Giaever. Tunneling through thin insulating layers. J. Appl. Phys. 32, 172 (1961).

[26] S. Foner. Versatile and sensitive vibrating-sample magnetometer. Rev. Sci. Instr. 30, 548 (1959).

[27] J. Frenkel. On the electrical resistance of contacts between solid conductors. Phys. Rev. 36, 1604 (1930).

[28] C.Y. Fu and T. Van Duzer. Hillock growth on lead films upon cycling to cryogenic temperatures. J. Vac. Sci. Technol. 17, 752 (1980).

[29] I. Giaever and K. Megerle. Study of superconductors by electron tunneling. Phys. Rev. 122, 1101 (1961).

[30] I. Giaever, H.R. Hart, Jr., and K. Megerle. Tunneling into superconductors at temperatures below 1°K. Phys. Rev. 126, 941 (1962).

[31] W.F. Giauque. A thermodynamic treatment of certain magnetic effects. A proposed method of producing temperatures considerably below 1° absolute. J. Am. Chem. Soc. 49, 1864 (1927).

[32] U. Gradmann. Ferromagnetism near surfaces in thin films. Appl. Phys. 3, 161 (1974).

[33] C. Guillaud. Propriétés ferromagnétiques des alliages manganèse-antimoine et manganèse-arsenic. Ann. de Phys. [12], 4, 671 (1949).

[34] F. Halla and H. Nowotny. X-ray study of the system Mn-Sb. Z. Physik Chem. B34, 141 (1936).

[35] M. Hansen. *Constitution of Binary Alloys.* (McGraw-Hill Book Co., New York, 1958).

[36] W.A. Harrison. Tunneling from an independent-particle point of view. Phys. Rev. 123, 85 (1961).

[37] L. Heaton and N.S. Gingrich. The crystal structure of Mn_2Sb. Acta. Cryst. 8, 207 (1955).

[38] F. Heusler. Magnetic Mn alloys. Verhandl. deut Physik Ges. 5, 219 (1903).

[39] M. Hofmann, G. Regenfus, O. Schärpf, and P.J. Kennedy. Measurements of field emitted electrons from polycrystalline gadolinium. Phys. Lett. 25A, 270 (1967).

[40] R.P. Hudson. Proc. 1970 Ultralow Temp. Symp. U.S. Naval Research Laboratory Report No. 7133, Washington, D.C. p. 3.

[41] S.K. Lahiri. Stress relief and hillock formation in thin films. J. Appl. Phys. 41, 3172 (1970).

[42] S.K. Lahiri. Absence of hillock formation in epitaxial lead films. J. Appl. Phys. 46, 2791 (1973).

[43] M. Kaminsky. Polarization of channeled particles. Phys. Rev. Lett. 23, 819 (1969).

[44] C. Kittel. Introduction to Solid State Physics, 4th ed. (John Wiley and Sons, New York, 1971) p. 527.

[45] R.L. Long, Jr., V.W. Hughes, J.S. Greenberg, I. Ames, and R.L. Christensen. Polarization of photo-electrons from magnetized nickel. Phys. Rev. A138, 1630 (1965).

[46] K. Maki. Pauli paramagnetism and the superconducting state II. Prog. Theor. Phys. 32, 29 (1964).

[47] J.L. Miles and P.H. Smith. The formation of metal oxide films using gaseous and solid electrolytes. J. Electrochem. Soc. 119, 879 (1972).

[48] R. Meservey, P.M. Tedrow, and P. Fulde. Magnetic field splitting of the quasiparticle states in superconducting aluminum films. Phys. Rev. Lett. 25, 1270 (1970).

[49] R. Meservey and P.M. Tedrow. Spin polarization of tunneling electrons from films of Fe, Co, Ni, and Gd. Solid State Commun. 11, 333 (1972).

[50] R. Meservey and P.M. Tedrow. Spin polarization of electrons tunneling from thin ferromagnetic films, in *Low Temperature Physics-Lt 13*, edited by K.D. Timmerhaus, W.J. O'Sullivan, and E.F. Hammel. (Plenum Press, New York-London, 1974) Vol. 3, p. 345.

[51] R. Meservey. Tunneling measurements of electron spin effects in superconductors in *Low Temperature Physics-LT 13*. Edited by K.D. Timmerhaus, W.J. O'Sullivan, and E.F. Hammel (Plenum Press, New York-London, 1974). Vol. 2, p. 405.

[52] R. Meservey, P.M. Tedrow, and R.C. Bruno. Tunneling measurements on spin paired superconductors with spin-orbit scattering. Phys. Rev. B11, 4224 (1975).

[53] R. Meservey, P.M. Tedrow, and D. Paraskevopoulos. Electron spin polarization in ferromagnetic metals, in *Magnetism and Magnetic Materials - 1975 AIP Conference Proceedings No. 29*. Edited by J.J. Becker, G.H. Lander, and J.J. Rhyme. (American Institute of Physics, New York 1976). p. 276.

[54] R. Meservey, D. Paraskevopoulos, and P.M. Tedrow. Correlation between spin polarization of tunnel currents from 3d ferromagnets and their magnetic moments. Phys. Rev. Lett. 37, 858 (1976).

[55] R. Meservey, D. Paraskevopoulos, and P.M. Tedrow. Measurements of the spin polarization of electrons tunneling from ferromagnetic alloys of the 3d metals. Physica 91B, 91 (1977).

[56] R. Meservey, D. Paraskevopoulos, and P.M. Tedrow. Spin polarized tunneling in rare earth ferromagnets. J. Appl. Phys. 49, 1405 (1978).

[57] R. Meservey, P.M. Tedrow, V.R. Kalvey, and P. Paraskevopoulos. Studies of ferromagnetic metals by electron spin polarized tunneling. J. Appl. Phys. 50, 1935 (1979).

[58] R. Meservey, D. Paraskevopoulos, and P.M. Tedrow. Tunneling measurements of conduction-electron-spin polarization in heavy rare-earth metals. Phys. Rev. B22, 1331 (1980).

[59] R. Meservey, P.M. Tedrow, and J.S. Brooks. Tunneling characteristics of amorphous Si barriers. J. Appl. Phys. 53, 1563 (1982).

[60] R. Meservey, P.M. Tedrow, M.S. Jagadeesh, and J.S. Brooks. Spin polarized tunneling from ferromagnetic metals. Nat. Mag. Lab. Annual Report, 1981, p. 43.

[61] J.S. Moodera, R. Meservey, and P.M. Tedrow. Artificial tunnel barriers produced by cryogenically deposited Al_2O_3. Appl. Phys. Lett. 41, 488 (1982).

[62] H. Nowotny and K. Schubert. System Mn (Fe)-Sn. Z. Metallkunde 37, 17 (1946).

[63] D. Paraskevopoulos, R. Meservey, and P.M. Tedrow. Electron spin polarization in ferromagnetic alloys. Physica 86-88A, 1201 (1977).

[64] D. Paraskevopoulos, R. Meservey, and P.M. Tedrow. Spin polarization of electrons tunneling from 3d ferromagnetic metals and alloys. Phys. Rev. B16, 4907 (1977).

[65] A.E.B. Presland, G.L. Pierce, and D.L. Trimm. Hillock formation by surface diffusion on thin silver films. Surface Sci. 29, 424 (1972).

[66] H.H. Potter. Some magnetic alloys and their properties. Phil. Mag. [7] 12, 255 (1931).

[67] C. Rau. Electron spin polarization ESP at surfaces of ferromagnetic metals. J. Magn. Magn. Mater.30, 141 (1982).

[68] J.S. Rogers and P.C. Sullivan. Analysis of spin polarized tunneling results. Solid State Commun. 28, 397 (1978).

[69] G. Sauerbrey. Phys. Verhandl. 8, 113 (1957).

[70] H.C. Siegmann. Emission of polarized electrons from magnetic materials. Phys. Rept. 17C, 37 (1975).

[71] U.P. Singh, A.K. Pal, L. Chandrasekaran, and K.P. Gupta, Study of the manganese-rich end of Mn-Sn. Trans. Metallurgical Soc. of AIME, 242, 1661 (1968).

[72] R. Sizmann. Investigation of electron spin polarization in ferromagnets. Nuclear Instruments and Methods 132, 523 (1976).

[73] A. Sommerfeld and H. Bethe. *Handbuck der Physik*, Verlag Julius Springer (Von Geiger und Scheel, Berlin, 1933) p. 450.

[74] M.B. Stearns. Simple explanation of tunneling spin-polarization of Fe, Co, Ni, and its alloys. J. Magn. Magn. Mater. 5, 167 (1977).

[75] W. Steckelmacker. *Thin Film Microbalance.* Edited by L. Holland. (John Wiley and Sons, Inc., New York, 1965).

[76] P.C. Sullivan and J.S. Rogers. Spin polarization for electrons tunneling from $Mn_x Sb_{1-x}$. Solid State Commun. 45, 977 (1983).

[77] I. Teramuto and A.M.J.G. Van Run. The existence region and the magnetic and elctrical properties of MnSb. J. Phys. Chem. Solids 29, 347 (1968).

[78] P.M. Tedrow and R. Meservey. Spin-dependent tunneling into ferromagnetic nickel. Phys. Rev. Lett. 26, 192 (1971).

[79] P.M. Tedrow and R. Meservey. Direct observation of spin-state mixing in superconductors. Phys. Rev. Lett. 27, 919 (1971).

[80] P.M. Tedrow and R. Meservey. Spin polarization of electrons tunneling from films of Fe, Co, Ni, and Gd. Phys. Rev. B7, 318 (1973).

[81] P.M. Tedrow and R. Meservey. Critical thickness for ferromagnetism and the range of spin-polarized electrons tunneling into Co. Solid State Commun. 16, 71 (1975).

[82] P.M. Tedrow and R. Meservey. Spin-dependent electron tunneling in superconducting vanadium and vanadium-titanium thin films. Phys. Lett. 69A, 285 (1978).

[83] E. Wedekind. Magnetic compounds of non-magnetic elements. Z. Physik Chem. 66, 614 (1909).

[84] M.K. Wilkinson, N.S. Gingrich, and C.G. Shull. The magnetic structure of Mn_2Sb. J. Phys. Chem. Solids 2, 289 (1957).

[85] R.S. Williams. Alloys of Sb with Mn, Cr, Si, and Sn; of Bi with Cr and Si; Mn with Sn and Pb. Z. Anorg. Allgem. Chem. 55, 1 (1907).

[86] B.T.M. Wills and H.P. Rooksby. Magnetic transitions and structural changes in hexagonal manganese compounds. Proc. Phys. Soc. (London) 67B, 290 (1954).

[87] L. Wray and M. Prutton. The structure of nickel and cobalt films on the (111) surface of n-type silicon. Thin Solid Films 15, 173 (1973).

[88] Y. Yamaguchi, H. Watanabe, and T. Suzuki. Magnetic moment of excess Mn in $Mn_{1+\delta}Sb$. J. Phys. Soc. Japan 41, 703 (1976).

[89] Y. Yamaguchi and H. Watanabe. Magnetic and crystallographic study on the electronic state of interstitial cations in MnSb. J. Phys. Soc. Japan 46, 1138 (1979).

[90] Y. Yamaguchi and H. Watanabe. Magnetic disturbance around the interstitial site Mn in MnSb. J. Phys. Soc. Japan 48, 435 (1979).

[91] K. Yasakochi and F. Kanematsa. Magnetic properties of intermetallic compounds in manganese-tin system: $Mn_{3.67}Sn$, $Mn_{1.77}Sn$, and $MnSn_2$. J. Phys. Soc. Japan 16, 1123 (1961).

[92] E.K. Zovioskii. Concerning a possible method for the polarization of a proton beam. Sov. Phys. JETP 5, 338 (1957).

APPENDIX A

Tunneling Conductance Bridge

APPENDIX A

TUNNELING CONDUCTANCE BRIDGE

A number of conductance measuring systems suitable for thin film electron tunneling are available from the literature. A simple system has been described in the main body of this thesis (sec. 3.4) as an illustration of small modulation techniques. The measuring system which was actually used for the work reported here was developed by J.S. Rogers and is somewhat more specialized towards spin polarized tunneling measurements than was an earlier published circuit by the same author. There is, for example, a problem with sweep rates if one is interested in the superconducting energy gap region of the tunneling characteristic. The problem is illustrated in Fig. A1.

A standard load-line problem considers a non-linear element in series with a load resistance R_L as in Fig. A1a. The intersection point of the load line and the I(V) characteristic of the element is the value of I and V which the circuit will adopt. If V_{bb} is swept linearly in time the load line will propagate parallel to itself at a uniform rate. One may choose the slope of the load line to be anywhere from horizontal to vertical. A horizontal load line will obviously trace out the flat portion of the I-V characteristic at a very high rate relative to the remaining portions, while a vertical load line will be too fast on the vertical part of the characteristic. The optimum

Fig. A1

Standard load-line problem

(a) A non-linear element in series with a load resistance R_L

(b) I-V characteristic

(c) dI/dV characteristic

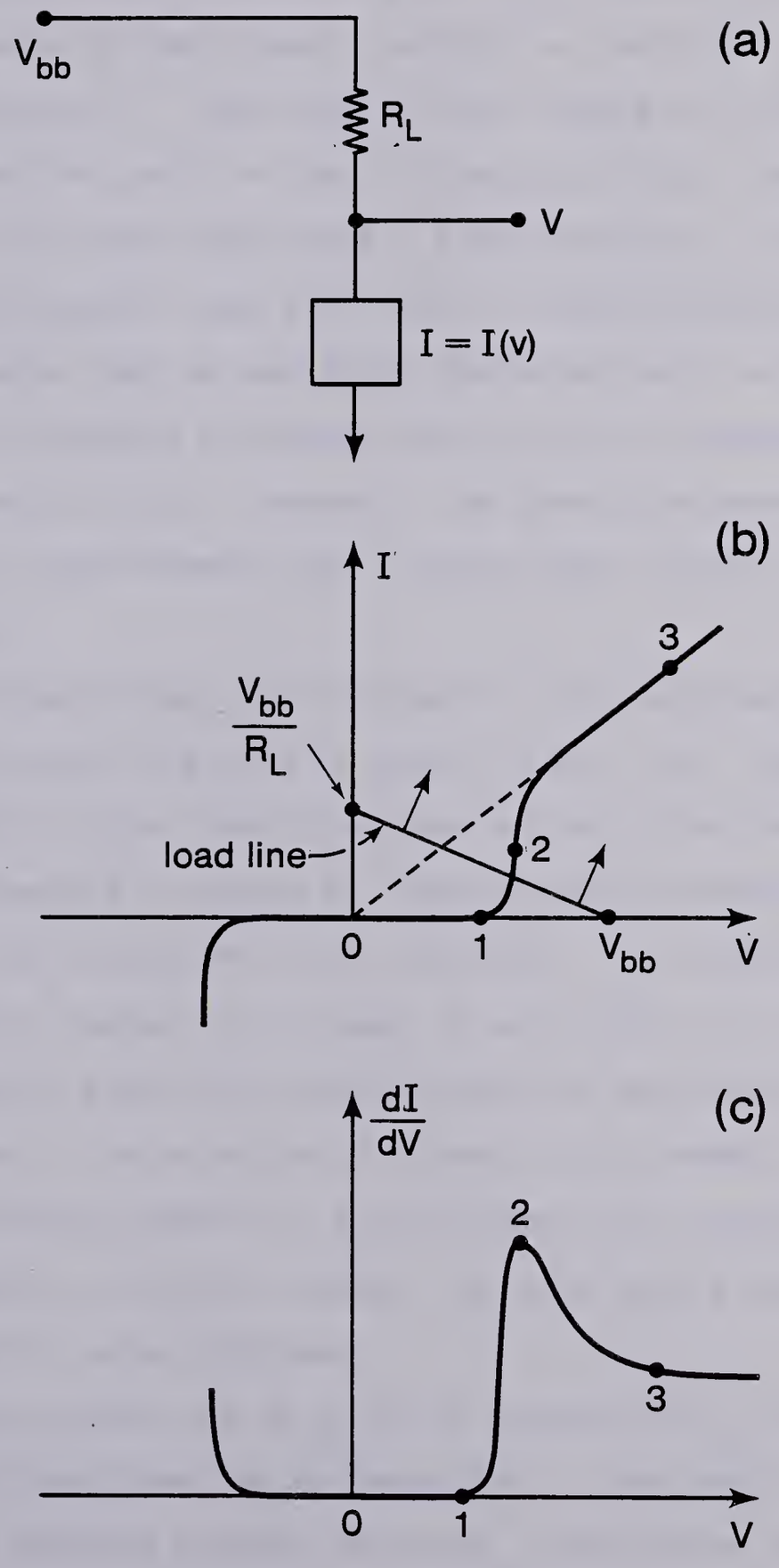
(a)
V_{bb}
R_L
V
I = I(v)
(b)
I
3
$\frac{V_{bb}}{R_L}$
load line
2
0
1
V_{bb}
V
(c)
$\frac{dI}{dV}$
2
3
0
1
V

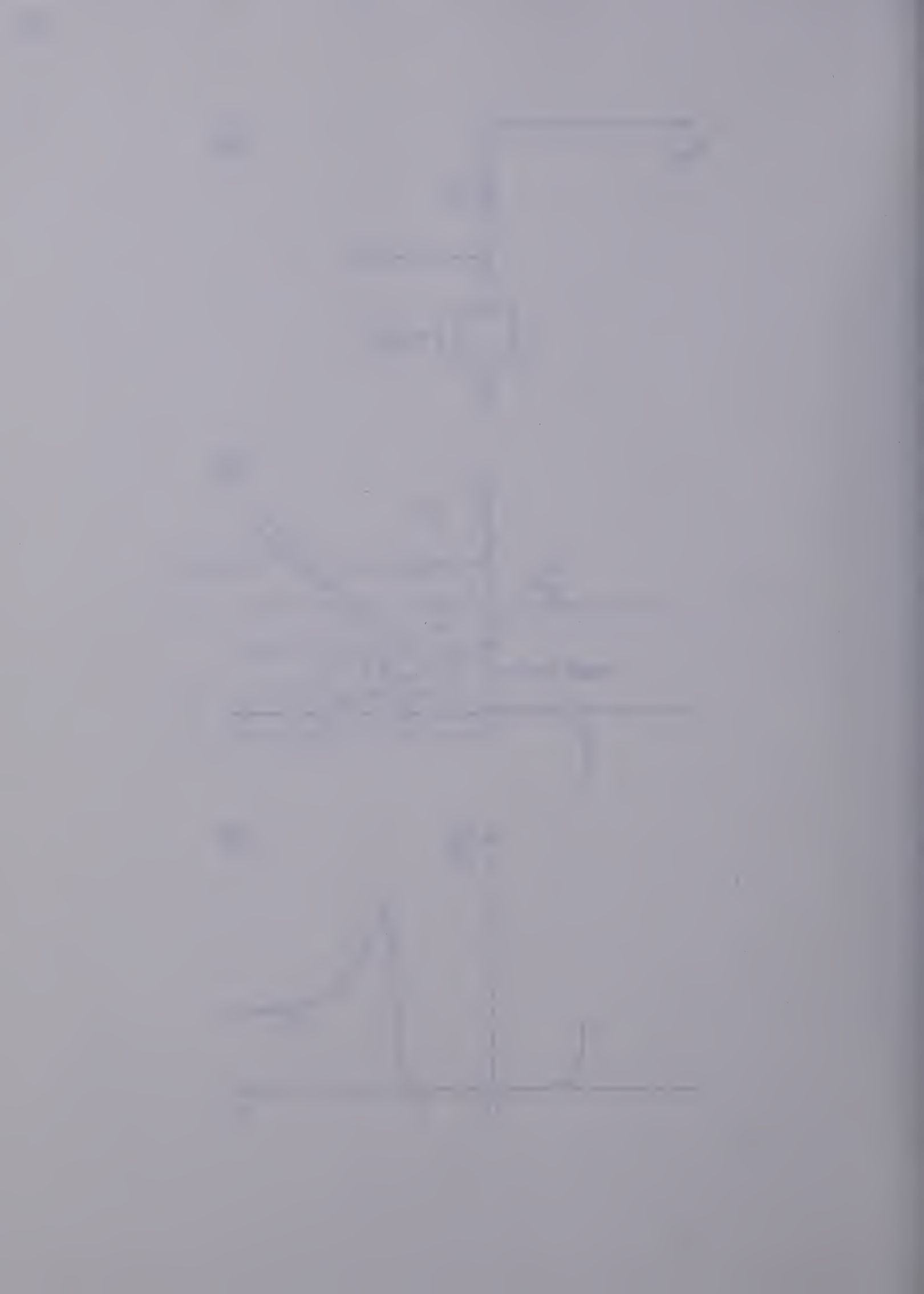

choice for the load line is $R_L = R_x$, where R_x is the resistance of the tunnel junction in the ohmic region beyond point 3. This choice only sweeps the horizontal and vertical parts of the I-V characteristic about 40% faster than the ohmic part. Unfortunately, the region between points 1 and 2 of the I-V characteristic corresponds to a large jump on the dI/dV characteristic, so that some manual attention to sweep rates is still necessary with this choice of R_L. However, the idea does seem in practice to be an improvement over systems which ignore the problem entirely.

A simplified illustration of the conductance bridge circuit which was used is shown in Fig. A2. The subscript x refers to the tunnel junction and s to the reference (or "standard") elements. The secondary windings S_1 and S_2 of the transformer are identical. The operational amplifier slaves the voltage at a to that at a' quite accurately since the configuration is basically a voltage follower. The capacitor C blocks the dc sweep voltage, so this voltage appears at a and causes a dc current to flow through R_x and R_s to common. R_s acts as the load resistor for the dc sweep problem.

The bottom end of S_1 is ac coupled to R_x through C and isolated from the dc sweep by R. The modulation signal at S_1 therefore appears across R_x, and the ac current through R_x flows to common through R_s. Since the modulation voltage at the sample is maintained constant, the ac

Fig. A2

Simplified Schematic of the Conductance Bridge

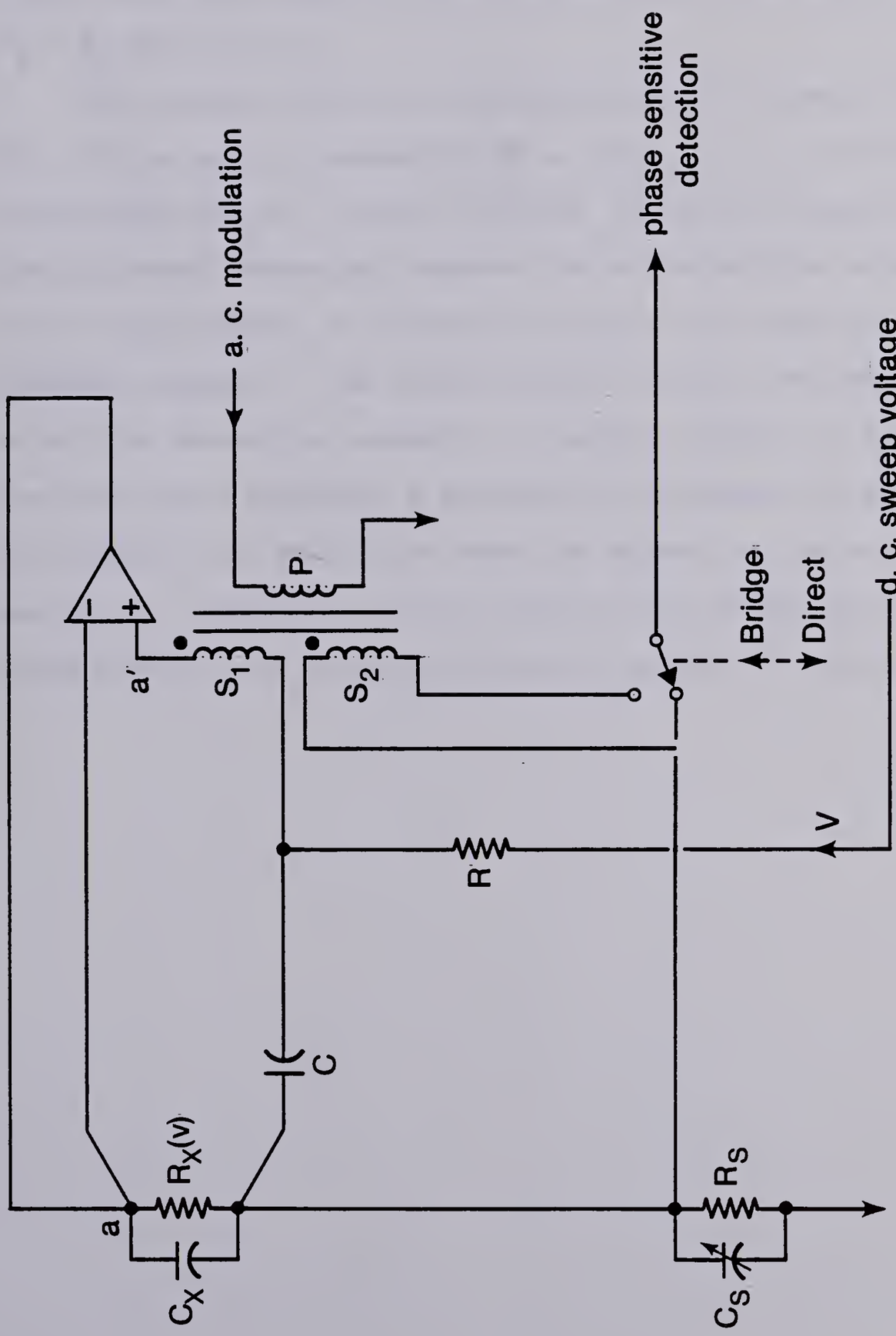
phase sensitive detection
a. c. modulation
d. c. sweep voltage
Bridge
Direct
P
a'
S_1
S_2
R
V
C
$R_X(v)$
a
C_X
R_S
C_S

voltage across R_s is proportional to dI/dV. In the bridge mode, the error signal to the detector will be zero when $R_s = R_x$ and $C_s = C_x$.

The reader should be cautioned that the circuit of Fig. A2 is only illustrative of an idea. If it is actually constructed as is, it will be found to have an unsatisfactory sweep behaviour because the RC decoupling network is too approximate in relation to the strong negative feedback present. The circuit which finally evolved uses an active decoupling network, a current booster to handle low resistance samples, a switching arrangement to protect the sample from transients when the system is turned on, and so on. Detailed circuit diagrams and performance documentation are available from Dr. Rogers on request.

APPENDIX B

Spin Polarization Papers

Solid State Communications, Vol. 28, pp. 397–399. 0038–1098/78/1101–0397 $02.00/0
© Pergamon Press Ltd. 1978. Printed in Great Britain.

ANALYSIS OF SPIN POLARIZED TUNNELING RESULTS*

J.S. Rogers and P.C. Sullivan

Department of Physics, University of Alberta, Edmonton, Alberta, Canada T6G 2J1

(*Received* 13 *July* 1978 *by R. Barrie*)

We report spin polarized tunneling results for Fe which confirm the original work of Tedrow *et al.* at MIT, and also use the data to illustrate an analysis which determines, with only qualitative reference to theoretical calculations, the true polarization index of the sample, provided the polarization is not too small.

THE SPIN POLARIZED tunneling experiments of Tedrow and Meservey *et al.* [1–3] at the Massachusetts Institute of Technology (MIT) are interesting thin film electron tunneling experiments which may prove to be an important contribution towards a complete understanding of ferromagnetism, but as yet there has been no independent confirmation of their results that we are aware of. We report here a confirmation of results for the case of Fe, and also illustrate a method of analysing the experimental data which is different from the MIT procedures in that only a qualitative reference to theoretical results is needed in order to extract a true polarization index for the sample.

Our experimental arrangement uses analog electronics to present sample conductance as a function of bias voltage on an X–Y recorder. We have manually digitized one such record and fed the results into a computer for analysis. This procedure introduced noise into the data since the original record was relatively free of noise. All of the curves shown here were then drawn by the computer with smoothing intentionally not employed as an illustration of analysis in the presence of noise.

The solid line of Fig. 1 is accordingly the conductance result for an Al–Al_2O_3–Fe tunnel junction in a magnetic field at low temperature. If A is the normalized conductance at, or nearly at, the peak labelled A in Fig. 1, and so on for the remaining peaks, then the apparent polarization index for the sample is defined as [2]

$$p_a = \frac{(A-C)-(D-B)}{(A-C)+(D-B)}.$$

For the sample shown, we find $p_a = 0.437 \pm 0.005$, which is in good agreement with the MIT value [2] of 0.44. A second sample preparation yielded much the same result.

* Work supported in part by the National Research Council of Canada.

The dashed lines of Fig. 1 show the sample conductance decomposed into spin-up and spin-down parts, where spin-up is the majority spin direction in the saturated ferromagnet. The decomposition assumes that the normalized sample conductance $G(V)$ may be written in terms of a single basis function $B(V)$ as

$$G(V) = (1+p)B(V) + (1-p)B(-V),$$

where p is the true polarization index for the sample. What we are calling a basis function is in reality the spin-up part of the superconducting modification of the density of states in the Al film in the presence of a magnetic field, as seen by tunneling with a normal-metal counter-electrode [2]. We take $B(V)$ to have an amplitude of 0.5 at high bias voltage. At the temperature of our experiment, $B(V)$ should be qualitatively similar to the density of states functions calculated by Engler and Fulde [4] for the case of spin-orbit scattering, and Bruno and Schwartz [5] for the case of spin–flip scattering.

Solving the above equation for $B(V)$ yields

$$B(V) = \frac{1+p}{4p}G(V) - \frac{1-p}{4p}G(-V).$$

While any value of p (other than $p = 0$) will generate a basis function through this equation, we find that only a very limited range of p values will generate a result which is in qualitative agreement with theory. An example of an incorrect basis function is shown in Fig. 2, where we have used $p = p_a$ as a trial value for p. The basis function is shown folded over on itself as in the theoretical presentations. The two main peaks which result in this case are of equal amplitude as a consequence of the definitions of p_a and $B(V)$, while the sub-peaks P1 and P2 are a consequence of partial cancellation of peaks in the input data.

Reference to the theoretical curves shows that the basis function of Fig. 2 cannot be correct. The main effect of small amounts of spin–orbit or spin–flip

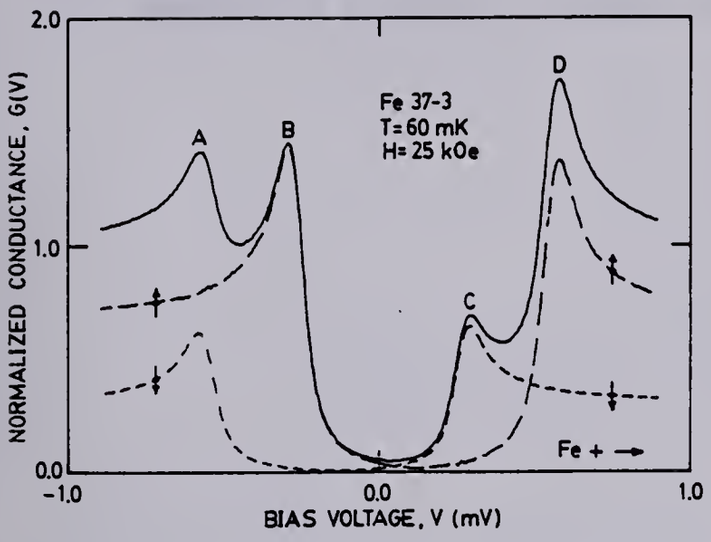

Fig. 1. Spin polarized tunneling result for an Al–Al_2O_3–Fe sample (solid line) shown decomposed into spin-up and spin-down parts (dashed lines).

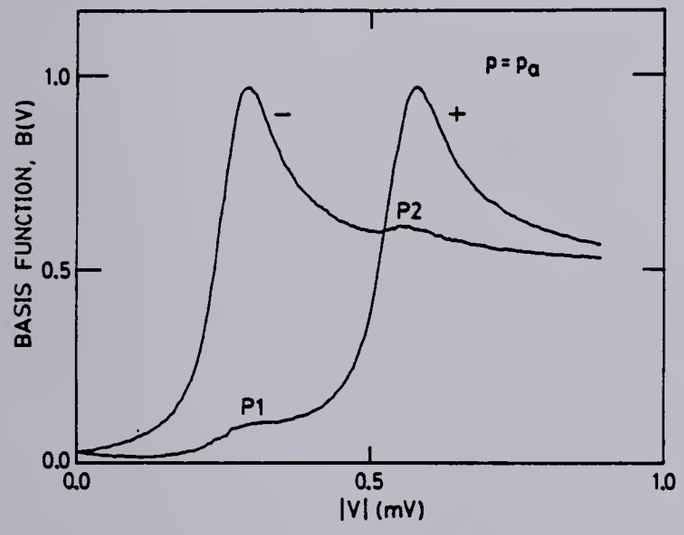

Fig. 2. Illustration of an incorrect basis function (see text). The (+) and (−) signs refer to the bias voltage polarities of Fig. 1.

scattering is to transfer spin states from the high energy main peak into a small, spread-out sub-peak just above the energy gap. This spin state mixing also occurs in the reverse direction, but to a much smaller extent. The density of states result of Engler and Fulde for a spin–orbit scattering parameter of $b = 0.2$ is a particularly good illustration of a much reduced high energy main peak, a clearly visible low energy sub-peak, and a barely visible high energy sub-peak which does not peak up at quite the same energy as the corresponding main peak.

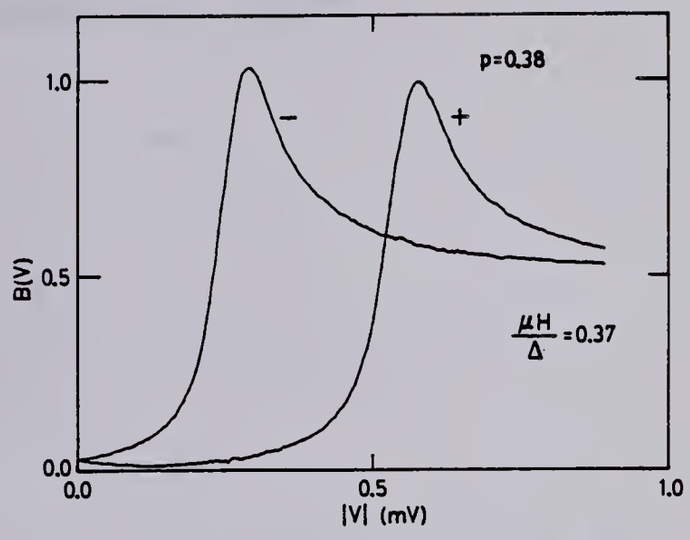

Fig. 3. Correct basis function for the tunneling result of Fig. 1.

We therefore take the true polarization index of the sample to be that which causes the sub-peak P2 of Fig. 2 to vanish, as shown in Fig. 3. The main peaks of $B(V)$ are then unequal, so that the main effect of spin–orbit and spin–flip scattering shows up. The next highest order effect of a small, low voltage sub-peak is not resolved by our data. The still smaller high voltage sub-peak should then be totally unresolved, and our criterion for the true polarization index valid.

The high bias voltage peak cancellation of Fig. 3 has occurred along the sides of peaks in the input data as well as at the tops, so that a number of data points are involved. This makes the peak cancellation surprisingly sensitive to the assumed value for p, even though the analysis amplifies noise as $|p|$ is decreased from unity. It also makes the true voltage origin for the input data well defined. For the data shown, we obtain $p = 0.380 \pm 0.005$, and a true voltage origin uncertainty of less than 1 μV.

An attempt to compare our true polarization value with the MIT results reduces to a comparison of values for the spin–orbit scattering parameter b, which in turn varies with sample preparation [3]. The model calculation of Paraskevopoulos *et al.* [3] indicates that our polarization ratio of $p/p_a = 0.87$ corresponds to $b = 0.08$, which is just inside the range of values obtained at MIT [3, 6].

REFERENCES

1. TEDROW P.M. & MESERVEY R., *Phys. Rev. Lett.* **26**, 192 (1971).
2. TEDROW P.M. & MESERVEY R., *Phys. Rev.* **B7**, 318 (1973).
3. PARASKEVOPOULOS D., MESERVEY R. & TEDROW P.M., *Phys. Rev.* **B16**, 4907 (1977).
4. ENGLER H. & FULDE P., *Z. Phys.* **247**, 1 (1971).

5. BRUNO R.C. & SCHWARTZ B.B., *Phys. Rev.* **B8**, 3161 (1973).
6. MESERVEY R., TEDROW P.M. & BRUNO R.C., *Phys. Rev.* **B11**, 4224 (1975).

Solid State Communications, Vol. 45, No. 11, pp. 977–978, 1983. 0038–1098/83/110977–02$03.00/0
Printed in Great Britain. Pergamon Press Ltd.

SPIN POLARIZATION FOR ELECTRONS TUNNELING FROM Mn_xSb_{1-x}*

P.C. Sullivan and J.S. Rogers

Department of Physics, University of Alberta, Edmonton, Alberta, Canada T6G 2J1

(*Received* 29 *October* 1982 *by R. Barrie*)

The spin polarization of electrons tunneling from Mn_xSb_{1-x} was measured over the full Mn concentration range $0 \leqslant x \leqslant 1$. The polarization is positive and qualitatively similar to the magnetization per Mn atom of bulk material; for MnSb ($x = 0.5$) it is + 25%.

TEDROW AND MESERVEY *et al.* [1, 2] at the Francis Bitter National Magnet Laboratory (NML) have reported on spin polarized tunneling measurements from the 3*d* ferromagnetic metals. They have also published results on binary ferromagnetic alloy films [3, 4] where at least one of the components was by itself a ferromagnet. Their work shows that for the ferromagnetic alloys studied the spin polarization of tunneling electrons is approximately proportional to the saturation magnetic moment per atom of alloy.

In this paper we present tunneling results for the binary alloy system Mn_xSb_{1-x}, which is ferromagnetic at all compositions except those very close to pure Mn or Sb [5]. Neither of the components is ferromagnetic by itself. Mn is an antiferromagnet and Sb is non-magnetic. The Mn–Sb system and other alloy systems containing Mn were first studied by Heusler in 1903 [6].

Our procedures for spin polarized tunneling are much the same as those for the NML group, the latter being the originators of this type of experiment. As two independent groups we appear to be obtaining excellent agreement whenever we attempt to duplicate each other's results. In the present case the tunnel junctions were of the form $Al–Al_2O_3–Mn_xSb_{1-x}$, with the ultra-thin Al film deposited on a glass substrate at 80 K and the oxide formed in an O_2 glow discharge at room temperature. The binary alloy films were prepared by simultaneous evaporation of the two elements from two separate boat sources. Two quartz crystal oscillator gauges were used to determine the mass deposited from each vapour stream and hence the Mn concentration of the alloy film. The Mn concentration of two of the films was verified by X-ray fluorescence and agreement was found to within ± 1 at. % Mn. The tunnel junctions were measured in an adiabatic demagnetization cryostat which permitted parallel magnetic fields at the sample of up to 40 kOe at temperatures of approximately 50 mK.

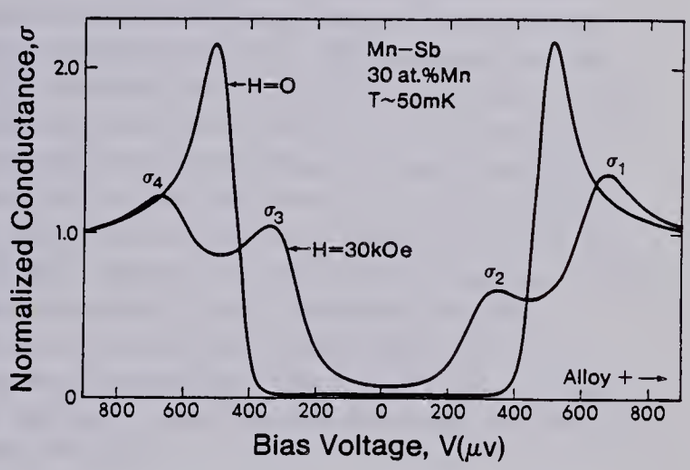

Fig. 1. Typical conductance characteristic for an $Al–Al_2O_3–Mn_xSb_{1-x}$ tunnel junction.

Temperature drift during the measurement process had no detectable effect on the tunneling characteristics.

Figure 1 shows a typical conductance vs voltage record. The $H = 0$ trace shows the superconducting energy gap of the Al film, and the $H = 30$ kOe trace shows the Zeeman splitting. The amplitude of the conductance peaks gives the apparent polarization [2],

$$P = \frac{(\sigma_4 - \sigma_2) - (\sigma_1 - \sigma_3)}{(\sigma_4 - \sigma_2) + (\sigma_1 - \sigma_3)}.$$

The polarization obtained in this way may be corrected for the effects of spin–orbit scattering in the Al film by multiplying by a nearly constant factor of 0.90 [4, 7].

The uncorrected polarization results are shown in Fig. 2 along with the bulk magnetization data. The latter data is that published by Guillaud [8] and is for well annealed samples. No magnetization data is available for Mn concentrations below 45 at. % or above 75 at. %. Two stoichiometric compositions exist for these alloys – MnSb ($x = 0.5$), and Mn_2Sb ($x = 0.67$). MnSb is present in alloys from about 0–60 at. % Mn and carries a magnetic moment of 3.53 μ_B/Mn atom. Mn_2Sb is present over the remaining range and carries 0.94 μ_B/Mn atom. On the Mn rich side of MnSb the excess Mn atoms

* Work supported in part by the Natural Sciences and Engineering Research Council of Canada.

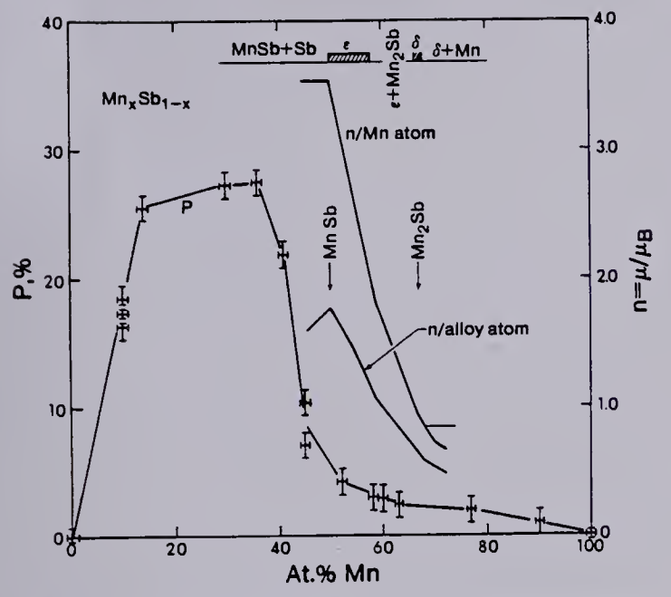

Fig. 2. Spin polarization results compared to bulk magnetization data of Guillaud [8].

occupy interstitial sites at random and have no magnetic moment amongst themselves, although they do cause some reduction of magnetization per formula unit [9]. In this ϵ phase the magnetic moment/Mn atom then decreases linearly with Mn concentration.

On comparing the polarization result to the magnetization results it is clear that the polarization tends to follow the magnetic moment per Mn atom rather than per alloy atom, and that there is a systematic error in our concentration values of about 10 at. % in the central region of concentration. An error with respect to concentration is to be expected from the sample fabrication sequence which we have used and the nature of the growth of thin alloy films. When electrons tunnel into a ferromagnet the sampling depth is of the order of 10 Å or less [10], so that in the present case it is material deposited during the nucleation and growth stage of alloy film formation which is being sampled.

Anton *et al.* [11] have shown that even for elements as similar as Ag and Au and which are mutually soluble in all proportions, small differences in adsorption and diffusion energies can lead to compositions for this part of the film which are quite different from the bulk of the film. For elements as dissimilar as Mn and Sb and which have a complicated alloy phase diagram, we do not know what to expect for the microstructure and composition of this part of the film.

The tunneling results themselves would seem to indicate that at approximately 40 at. % Mn indicated concentration, the alloy composition at the interface is MnSb, and at indicated concentrations down to 15 at. % Mn, regions of MnSb still occur at the interface and tunneling is predominantly into these regions. This last conclusion follows from the definition of polarization, $P = (\eta\uparrow - \eta\downarrow)/(\eta\uparrow + \eta\downarrow)$, where η is tunneling electron number. Anything which contributes unpolarized electrons to the tunnel current will reduce the measured polarization. The rapid decrease of polarization beyond 40% Mn evidently corresponds to the bulk ϵ phase, but the narrowness of this phase relative to the uncertainty of the composition being sampled by tunneling does not permit any quantitative conclusions.

Thus the only quantitative result that emerges is that the spin polarization of electrons tunneling from MnSb is approximately 25% after correcting for spin–orbit scattering in the Al film. This yields $P/n_{Mn} \simeq 7\%$, where n_{Mn} is magneton number per Mn atom. The corresponding ratio for the Fe-group elements and their alloys is $P/n \simeq 20\%$ [4], where n is per alloy atom for the alloys, and for the heavy rare earth metals $P/n_{CE} \simeq 20\%$ [12], where n_{CE} is per conduction electron. In this last case the atoms carry a considerable localized moment. For Gd, $P/n_{Gd} \simeq 2\%$. MnSb appears to be somewhat intermediate between the Fe group elements and the heavy rare earth metals in its spin polarized tunneling behaviour.

REFERENCES

1. P.M. Tedrow & R. Meservey, *Phys. Rev. Lett.* **26**, 192 (1971).
2. P.M. Tedrow & R. Meservey, *Phys. Rev.* **B7**, 318 (1973).
3. D. Paraskevopoulos, R. Meservey & P.M. Tedrow, *Physica* **86–88B**, 1201 (1977).
4. D. Paraskevopoulos, R. Meservey & P.M. Tedrow, *Phys. Rev.* **B16**, 4907 (1977).
5. R.M. Bozorth, *Ferromagnetism*, p. 334 and references therein. Van Nostrand, New York (1951).
6. F. Heusler, *Verhandl. Deut. Physik. Ges.* **5**, 219 (1903).
7. J.S. Rogers & P.C. Sullivan, *Solid State Commun.* **28**, 397 (1978).
8. C. Guillaud, *Ann. Physique [12]*, **4**, 671 (1949).
9. Y. Yamaguchi, H. Watanabe & T. Suzuki, *J. Phys. Soc. Japan* **41**, 703 (1978).
10. P.M. Tedrow & R. Meservey, *Solid State Commun.* **16**, 71 (1975).
11. R. Anton, M. Harsdorff & Th. Martens, *Thin Solid Films* **57**, 233 (1979).
12. R. Meservey, D. Paraskevopoulos & P.M. Tedrow, *Phys. Rev.* **B22**, 1331 (1980).

B30396